A DECAY DETECTION SYSTEM AND ITS APPLICATION TO THE OMEGA MESON

by

MICHAEL ERNEST KAY

A Thesis submitted for the Degree of

DOCTOR OF PHILOSOPHY

in the

UNIVERSITY OF LONDON

Physics Department,
Imperial College of Science & Technology,
LONDON, S.W.7.

JUNE 1972

ABSTRACT

An account is presented of the design of a decay detection system used for the detection of pions and gammas produced in reactions of the type

$$\pi^- + p \rightarrow n + X^0$$
$$\pi^- + p \rightarrow p + X^-$$

where X^0 and X^- subsequently decayed in very short times.

The system was designed to cover as much as possible of the area surrounding the hydrogen target by means of counters arranged with cylindrical geometry and capable of detecting both pions and gammas.

The extensive study of the behaviour of the gamma counters in response to the passage of a gamma ray is discussed as well as the performance of the system as a whole under experimental conditions in subsequent data collection, and its simultation by a Monte Carlo program.

The design and analysis of the behaviour of the system was put to test by a measurement of the branching ratios of the omega decay modes, including a search for the rare decay mode, $\omega \rightarrow \pi^0 \pi^0 \gamma$. The upper limit for this latter mode was found to be 1.0%. A measurement of the main neutral mode, $\pi^0\gamma$, was made by identifying the gammas present, at the same momentum. The branching ratios were measured as follows, (assuming only the two modes to exist):

$\pi^+ \pi^- \pi^0$	$90.8 \pm 7.7\%$
$\pi^0 \gamma$	$9.2 \pm 2.9\%$

CONTENTS

PREFACE

The experimental work described in this thesis was carried out at the Rutherford Laboratory proton synchrotron 'Nimrod' by the Imperial College Counter Group in collaboration with a team from the Physics Department, Southampton University and a small team from the Rutherford Laboratory. As the experiment as a whole involved the work of many people, the emphasis in this thesis is laid upon the work for which the author was most concerned. Consequently, brief consideration only is given to the beam design, the electronic logic system and related problems of the main experiment.

CHAPTER I

THE NARROW BOSONS EXPERIMENT

1.1 Experimental Aims

This thesis describes a decay detection system, a detailed study of its performance and its introduction into a large experiment whose purpose was to study interactions of the type

$$\pi^- + p \rightarrow n + X^0$$
$$\pi^- + p \rightarrow p + X^-$$

The neutron or proton produced was detected by a counter array, identified as either a neutron or proton and timed. The boson produced along with the timing particle rapidly decayed, the final decay products being either pions or gammas. It was these particles which were detected by the decay detecting system. Either neutral or negatively charged bosons could be examined in this way.

In addition to specific tasks, such as a study of η and ω mesons in order to examine the performance of the apparatus, an investigation of the suspected A2 split and a study of R mesons, a scan of the whole momentum range possible up to a beam momentum of about 3 GeV/c was to be carried out to search for new neutral and negatively charged bosons, should they exist.

1.2 The Experiment

The narrow bosons experiment was carried out at Nimrod, the 7 GeV proton synchrotron at the Rutherford Laboratory. Bursts of circulating protons in the machine were made to interact with an internal target in order to spray out particles into a beam line, which transported them to the experimental area. Here negatively charged pions were selected and fired into a second target, surrounded by the decay detection system.

Further downstream, an array of neutron and anti-counters detected the timing particle. A complicated system of electronic logic sorted out the events and fed the information into a computer where preliminary analysis was performed and data placed on magnetic tape.

The experiment used the 'time of flight' technique to identify the effective mass of the other interaction products. By timing the passage of the timing particle, either a neutron or a proton, over a fixed distance, its velocity could be found. Then, with a knowledge of the beam momentum, the mass of the other interaction products, the 'missing mass' could be evaluated. This method did not depend upon the actual measurement of decay products and so the $\pi^0\gamma$ decay mode of the omega meson would have the same shape as that of the $\pi^+ \pi^- \pi^0$ mode. The method also led to a narrow mass resolution which permitted the more accurate study of narrow mesons such as the omega.

The timing of an event depended upon timing the arrival of a beam pion at the hydrogen target, which was found to react, together with the timing of the arrival of the neutron or proton from the interaction at the neutron counter.

The decay counters were used to indicate the passage of the other interaction particles through them. In practice, an event could be read about once every 100 nanoseconds, compared with the cycling times of spark chambers and bubble chambers which were measured in milliseconds. The disadvantage of the counting system was the spatial resolution of a counter which was defined by its area. Because of the short cycling time of counters, fast electronic logic and an on-line computer, very large statistics could be accumulated. Approximately sixteen omegas were expected every million beam pions, that is, every 12 seconds.

1.3 The Beam Line

In addition to transporting charged particles to the experimental areas, the beam line was used to focus the beam and select from it pions of a specific

momentum. This was done by a series of magnetic quadrupole lenses and bending magnets, as shown in Fig.(1.1).

The beam was taken from Nimrod at an angle of 17^{o} to the circular axis of the machine. The magnetic quadrupole lenses, Q_1 and Q_2, focused the beam on to the G hodroscope after a horizontal deflection of $7\frac{1}{4}^{o}$ in the bending magnet, BM1. Then BM2, a second bending magnet, deflected the beam horizontally by a further $9\frac{3}{4}^{o}$ into the magnetic quadrupoles Q_3 and Q_4 which, this time, focused the beam on to the H hodoscope. The two hodoscopes, G and H, were at the conjugate foci of the magnetic quadrupole lenses, Q_3 and Q_4.

A Cerenkov counter was placed near to the focus at the G hodoscope but a little upstream of it and used to veto the electrons. There were two collimators, one just upstream of the Cerekov counter and one just upstream of the H hodoscope. The upstream collimator limited the momentum of the beam, as did the G hodoscope. The 100 mm square hole in the downstream collimator was used to cut out stray particles.

A floating wire experiment was carried out on the beam magnets. The bending magnets were examined with a long search coil and abnormalities detected to one part in 10^4 and metal shims used to remove them. The bending angle was measured to one part in 10^3.

The G hodoscope consisted of eleven fingers of scintillator 60 mm high, 6.8 mm wide and 5 mm thick. The H hodoscope consisted of seven fingers 60 mm high, 7.5 mm wide and 3 mm thick. Only nine and five fingers were used respectively. The five fingers used in the H hodoscope chose a central momentum of p_0 and four other channels which were p_0 - 1%, p_0 - $\frac{1}{2}$%, p_0+ $\frac{1}{2}$% and p_0 + 1%.

The beam consisted of approximately 80 - 90% of negative pions, less than 1% of negative kaons, about 10% of electrons and the rest muons. At the focus, the horizontal beam size was about 40 mm for all five channels,

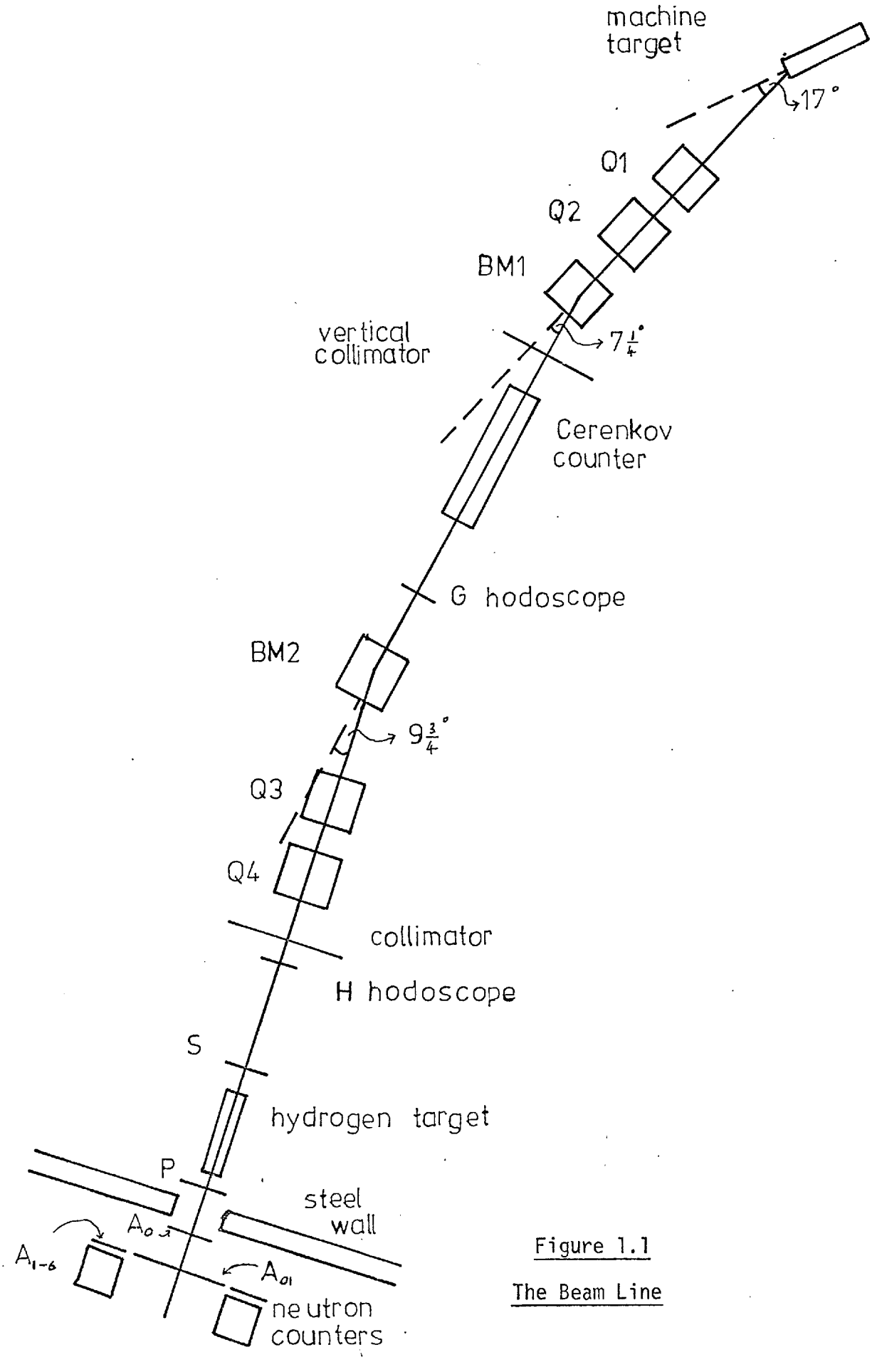

Figure 1.1

The Beam Line

whilst 4.50 metres upstream of the focus, it was about 45 mm. The beam spread was approximately symmetric upstream and downstream of the focus. The vertical beam size, defined by the internal machine target, was between 6 and 10 mm.

The momentum telesope selected a pion of the correct momentum and this telescope was completed by the H hodoscope 450 mm upstream of the centre of the hydrogen target. Downstream of this hodoscope was counter S , 43 mm by 50 mm by 2 mm, which, together with the G, H and Cerenkov counters, defined a pion entering the hydrogen target.

1.4 The Hydrogen Target

The beam transported negatively charged pions of a well defined momentum to the hydrogen target, shown in Fig. (1.2). A beam pion could then interact with a proton in the target and produce a resonance which rapidly decayed into pions and gammas. The target was designed to present a large number of protons to the beam pions whilst permitting the decay products to escape with minimum interference. To do this, a large thin target was required. A limiting factor on length was the loss of momentum of a beam pion in traversing the target length. For this target, which was sausage shaped, 323 mm long and 65 mm in diameter, the loss would have been about 8½ MeV/c. This amounted to about ¾ % of the typical beam momentum compared with a momentum bite in the hodoscope telescope of ½%.

The target was narrow to allow the pions and gammas to pass out sideways towards the decay counting system without affecting them. The sausage was thus made of mylar 0.254 mm thick and contained in a vacuum jacket made from aluminium, which is a low density metal. The jacket was in the form of a cylinder 0.64 mm thick and fitted with mylar windows at each end, only 0.13 mm thick, in order to present as little non-hydrogen material in the way of the beam as possible. The sausage was filled with liquid hydrogen which was being constantly circulated in order to maintain

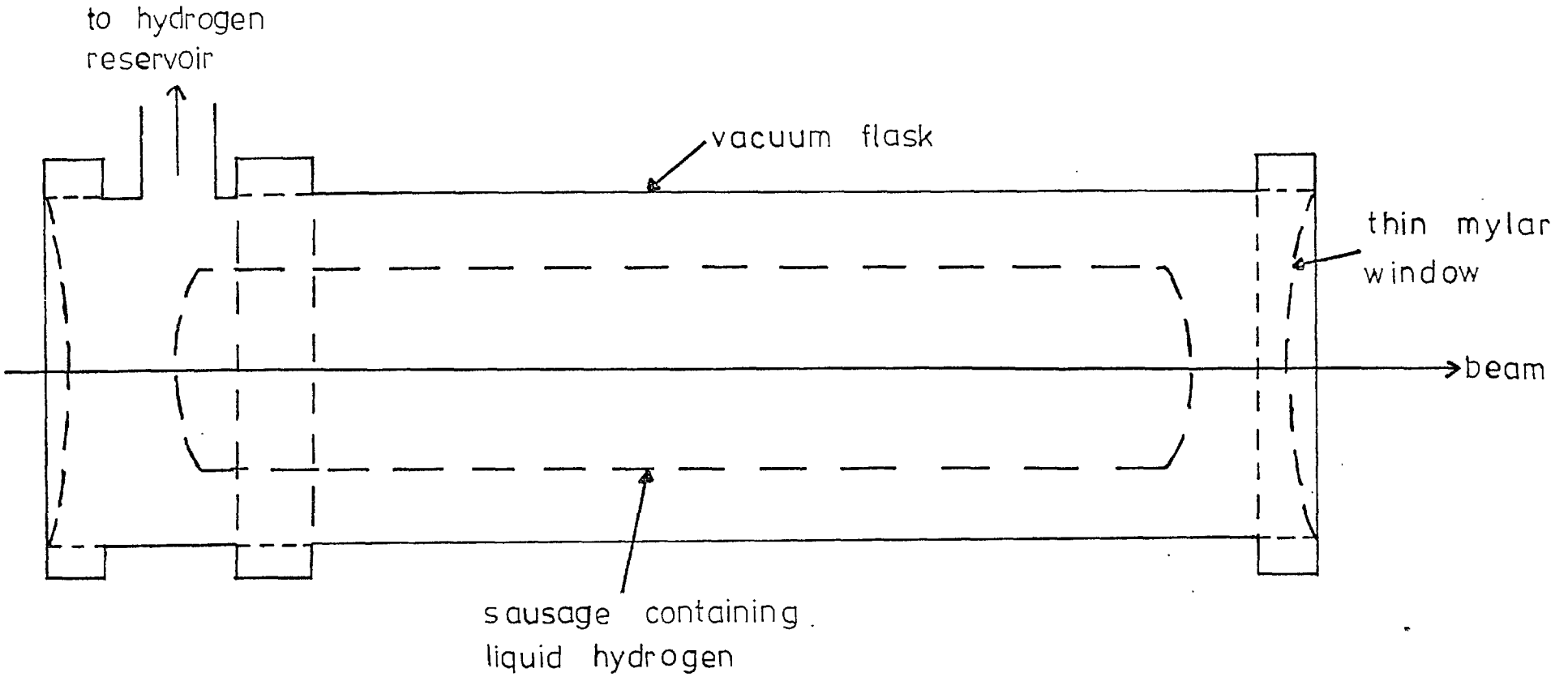

Figure 1.2 The Hydrogen Target

it at a fixed temperature. The target was aligned to about half a millimetre.

In the data analysis, effects were observed which were caused by a decay pion interacting with the target on its way out, as discussed in Section (5.5). For example, a secondary pion passing outwards through the hydrogen would have a 1.5% probability of producing a delta ray. Such a pion passing through the aluminium jacket would have a probability of 1.9% for the same effect. These probabilities were estimated for the decay of the omega meson at 1153 MeV/c.

1.5 The Detection of the Timing Particle

The decay counter array occupied a region surrounding the hydrogen target from the H hodoscope to another counter, P, situated 650 mm downstream from the centre of the target. This latter counter was circular with a diameter of 175 mm and 2 mm thick. For proton time of flight, it was used to ensure that the charged timing particle had come from the hydrogen target and not scattered from somewhere else. It did not distinguish between charged particles and it was not used in the decision as to whether the timing particle was a neutron or a proton. The P counter also helped to reduce stray particles entering the neutron counters from the target region and giving accidental events.

Downstream from the decay system was a large thick steel wall whose purpose was to shield the following neutron counters from decay products interacting in the decay system. Immediately following the steel wall was A_0, 2½ metres from P. The neutron counter array could be varied in distance from the target, between 1.8 and 7.5 metres. In the centre of this array was the counter A_{01}, 320 mm in diameter and 5 mm thick. The purpose of A_0 and A_{01} was either to identify beam particles which had not interacted in the target or to identify timing particles which did not enter the neutron counters by the front face, thus affecting the response.

The neutron counters were placed in two rings of six counters each. Each counter was 300 mm long and 300 mm in diameter. There were twelve anti-counters,

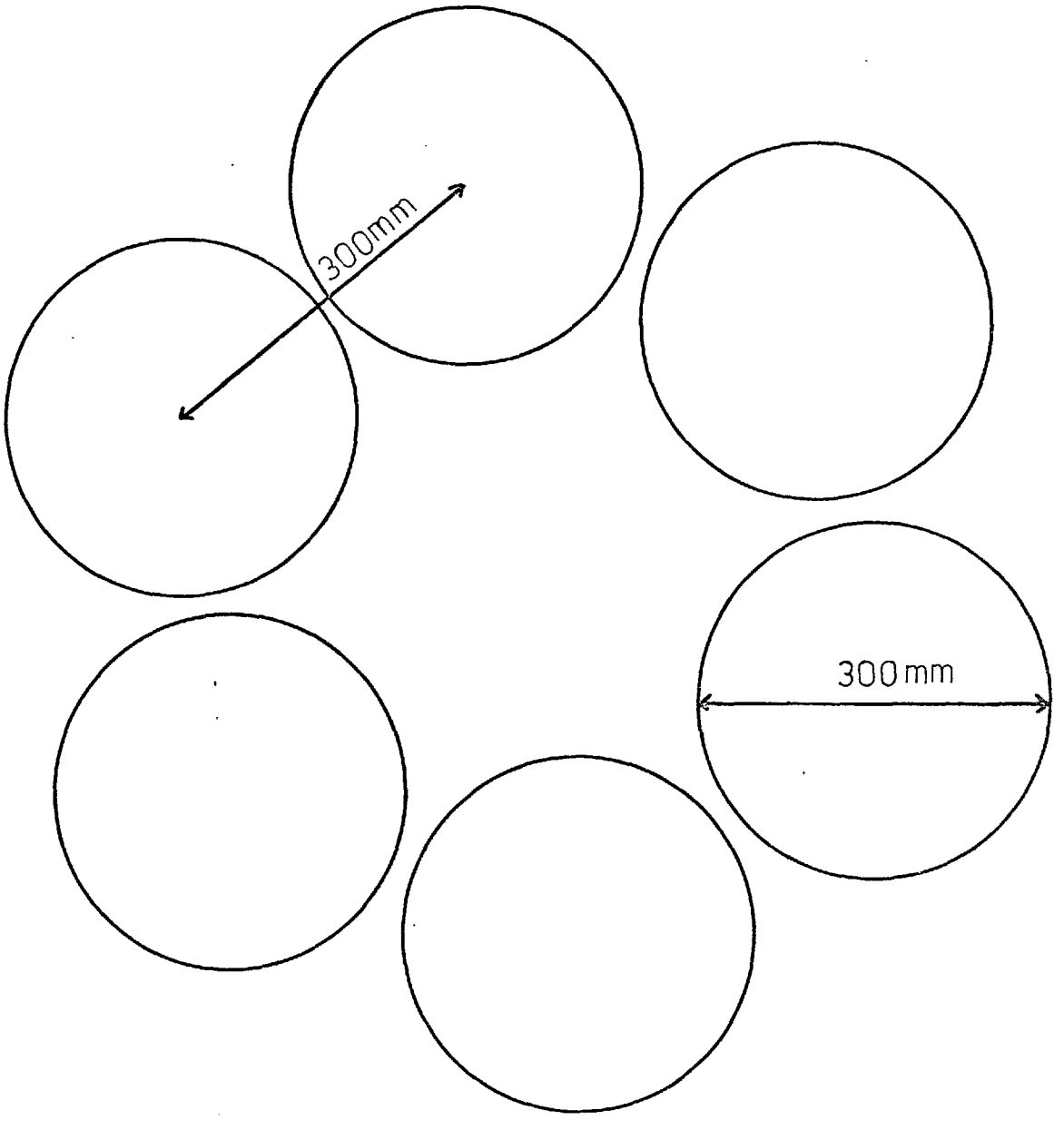

Figure 1.3

The Neutron Counter Array (Inner Six Only)

one in front of each of the neutron counters, which were used to indicate whether a particle entering the neutron counters was charged or neutral. To identify a neutron, they were in anti-coincidence, whereas, to select a proton, they were placed in coincidence. The neutron counters subtended only a small angle at the target. For the inner six only, which were the ones normally in use, at a distance of 5 metres, the angle subtended was typically $3\frac{1}{2}$%. The inner six gave better coplanarity information which was extremely useful in identifying two body decay modes.

1.6 Event Selection

The entry of a pion into the hydrogen target was registered by a count in S. For an interaction to have taken place, the pion must not have been detected coming out of the target by A_0 and A_{01}. Consequently, an event was identified by S. $\overline{A}_0$. $\overline{A}_{01}$, using a wide timing gate.

The analysis by computer then further identified events from the information read out of the entire logic system by classifying them as proton or neutron events (P. A_i. N_i or $\overline{P}$. $\overline{A}_{1-6}$. N_i, respectively) and by classifying the decay counter signature for each.

1.7 The Decay Counter System

The design of the decay counter system, Fig. (1.4) evolved from a desire to use scintillation counters to detect the pions and gammas from the decays of resonances with some spatial information. The most important factor was to have a symmetrical system which would, therefore, not distort the response of the system to a particular decay. As the target was cylindrical in shape this suggested a cylindrical geometry for the decay array. The resulting configuration then depended on various conflicting requirements.

In order to detect decay modes as cleanly as possible, especially those with numerous decay products, a large number of counters in the array were needed, thus minimising the possibility of two particles entering the same

Fig. 1.4 The Decay Counter System

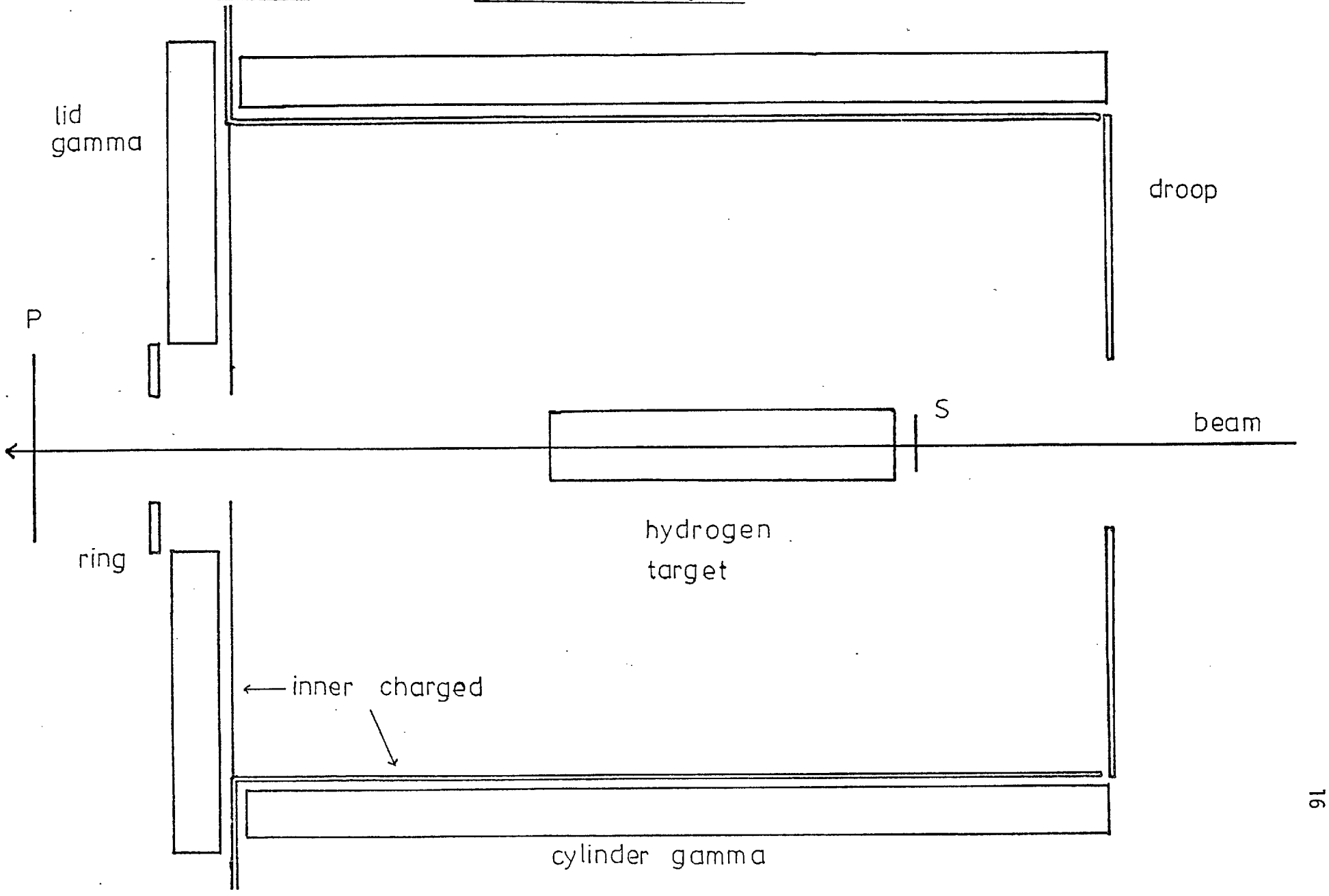

counter. This argument implied that the solid angle subtended by the counter at the target should be as small as possible. However, to reduce the effect of the particles initiating a signal in one counter which then passed into its neighbouring counter, lead was placed along the sides of the counter. The tape used to light tight the counters and practical air gaps introduced a counter separation with a possible loss of particles in the gap. Consequently, the greater the counter width compared to the gaps, the better.

The consequence of these arguments was to design a system with a large number of very wide counters but this was, of course, restricted by practical size and mechanical construction with its subsequent weight problems. Also, a moveable decay array was required to give access to the target and counters, and also to use the geometrical properties of the array to advantage. There was a practical limit to the length of scintillator possible in a strip in order that it would not craze under the strain of its own weight and impair the uniformity of response both along the scintillator and from counter to counter.

A guide to the practical counter size required was to consider the decay of a π^0 of mass m and momentum $\vec{p}_0$. It decays into two gammas with momenta $\vec{p}_1$, $\vec{p}_2$, making angles θ_1, θ_2 with $\vec{p}_0$. Writing the total energy as E, where $E = \gamma m$ for units with velocity of light equal to 1, then $E^2 = m^2 + p_0^2$, and $p_0 = \beta\gamma m$.

To conserve energy,

$$p_1 + p_2 = \gamma m \quad . \qquad (1)$$

To conserve momentum,

$$\vec{p}_1 + \vec{p}_2 = \vec{p}_0 \quad . \qquad (2)$$

Therefore, parallel to $\vec{p}_0$, $p_1 \cos\theta_1 + p_2 \cos\theta_2 = p_0$, (3)

and, perpendicular to $\vec{p}_0$, $p_1 \sin\theta_1 - p_2 \sin\theta_2 = 0$. (4)

The opening angle is θ where $\theta = \theta_1 + \theta_2$ and this is minimumwhere $\theta_1 = \theta_2 = \theta_0$ and $p_1 = p_2$.

From Equation (1), then, $p_1 = p_2 = \frac{\gamma m}{2} = p$.

Therefore $2p \cos \theta_o = p_o$,

and $\cos \theta_o = \frac{p_o}{2p} = \frac{\beta\gamma m}{\gamma m} = \beta$,

and $\sin \theta_o = (1 - \cos^2 \theta_o)^{\frac{1}{2}} = (1 - \beta^2)^{\frac{1}{2}}$

therefore $\sin \theta_o = \frac{1}{\gamma}$, $\cos \theta_o = \beta$.

The gammas, therefore, are on opposite sides of a cone, radius r. If the π^o was heading for a junction between two counters, the probability of getting two gammas in the same counter would be zero. If the probability of getting two gammas in the same counter from a pion heading for the centre of a counter was p, then the total probability would have been $\frac{p}{2}$, to a first order approximation.

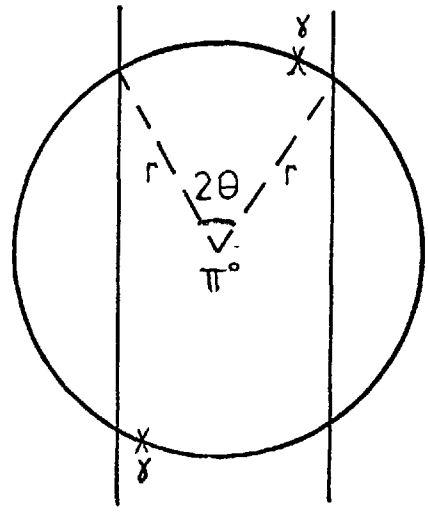

p is equal to the fraction of the circumference of the cone which lies within the central counter.

The cone circumference lying within the centre counter was 2 x r (2θ) for a central pion. Where the counter thickness was t cms,

$t = 2r \sin \theta$,

therefore $\theta = \sin^{-1} \frac{t}{2r}$.

As a result, the probability of getting the two gammas in one counter was

$\frac{1}{2} \times 4r \sin^{-1}(\frac{t}{2r}) / 2\pi r,$

$$= \frac{1}{\pi} \sin^{-1} \frac{t}{2r} \quad .$$

At about 600 MeV, a pion had an opening angle of about 32^{o}[1]. The shortest distance to the middle of a gamma counter was made, in fact, about 37 cms, and so the cone radius was 37 tan 16^{o} = 10.6 cms. This was the width chosen for the counter, approximately, and so r = t, whence the probability was $\frac{1}{\pi} \sin^{-1}(\frac{1}{2}) = \frac{1}{6}$ or about 17%. These chosen measurements, therefore, as well as being about the largest practical construction for the situation, gave a probability of about 17% for obtaining two gammas from a pion in one counter at this energy. In fact, twenty counters were used subtending an angle of 18^{o} each at the hydrogen target. The gamma energy spectrum for relativistic π^{o}'s is approximately uniform up to the pion energy. Consequently, if it is assumed that all gammas less than some minimum energy were undetected whilst those above were detected with 100% efficiency, the fraction of gammas lost was $2E_{min}/E_{\pi}$. The factor 2 compensated for the two gammas from each pion. The energy cut off was approximately 50 MeV and so about $\frac{1}{6}$ or 17% of the gammas were lost. There was thus an approximate balance between the two effects.

The loss of a gamma between counters was given by the size of the gap compared with the counter width and was about 5%.

These order of magnitude arguments lead to a width for each counter in the cylinder array. There was still the question of the length of the scintillator to be used. In addition to the cylinder array, the downstream end of the cylinder was designed to include a lid of counters fitting into a disc shape and aligning with the cylinder gamma counters. Both cylinder and lid were to consist of counters able to detect pions and counters to detect gammas. The upstream end was to be treated differently due to the small number of decay products in this region. The design was to permit the cylinder and lid

counters to each detect reasonable amounts of the decay products, thus doubling the ability to detect individual particles without two particles entering the same counter and remembering the inner part of the lid disc counters were narrow. To simplify the design, the upstream region of the cylinder was filled only with charged particle detector and this was without the spatial definition of the cylinder and lid system. Consequently, the cylinder was extended upstream of the target as far as was reasonable to give the added detection information over as much solid angle as possible. Consideration of all the factors involved led to the selection of a cylinder counter length of 800 mms. The typical arrangement was then to have a downstream overhang of about 300 mms and the extension past the target upstream was 200 mms.

For the $\pi^+ \pi^- \pi^0$ decay mode of omega at 1153 MeV/c, this led to a ratio of two pions in the cylinder : two pions in the lid : one particle in each of approximately 50: 4: 40. For the two gammas from the π^0, this ratio was approximately 50: 6: 30.

As a result of this configuration, about 7% of such omega events had a gamma entering the upstream disc and being lost as against about 13% for an upstream extension of only 100 mms. The same figures in the R meson region were 3% and 4%.

The design was simplified by having only an upstream disc of charged detector as to have had gamma ray detectors in this region would have introduced accidental effects from stray beam particles with so much lead in the region with little return in events saved. The number of pions entering the upstream disc was about 5% for omega as against about 2½% for the R region. If a charged detector was placed here, with a hole of 100 mms to permit the beam to pass through undetected, there would have been 2% of decay pions lost. In fact, a hole of 80 mms was used, being a compromise between pion loss and possible beam detection.

There was a similar hole in the downstream disc or lid, as it was called. The difficulty was to cover as large a solid angle as possible especially in this crucial forward region without detecting or interfering with the escape of the timing particle. As a result of these considerations the hole in the nearer charged detectors was 50 mm in radius, whilst that in the gamma counters was 100 mm. The latter gave rise to a loss of gammas varying between 8% and 14% for a three pion decay mode, whilst the former was responsible for a loss of between 3% and 4% of pions.

In order to assist in the analysis of events, a special charged particle detector, called the 'ring counter' was introduced in the region between the 50 mm and 100 mm radii. This served as extra evidence that a charge particle had passed through the lid system and also assisted in identifying it as passing through the region where the gamma detector was not also present. Pions passing within a radius of 100 mm constituted between 12% and 16% of events and so the number of events with pions in the ring counter region was between 9% and 12%.

The remaining design difficulty at this stage was the overlap region where cylinder and lid counters met. The two extreme alternatives were to lose all the gammas in this region or to count them twice and hence give the indication of the presence of π^0. The problem was not crucial for pions as the number present was decided by the time of flight in that, for a neutron, only even numbers of charged pions could be present whilst for a proton, only odd numbers of charge pions were allowed. The problem, then, for pions was much simplified. Care was taken with the gamma counters to ensure that both effects were reduced to a minimum by careful positioning. Only a small percentage of gammas were affected by this, probably less than 5% and so the actual loss or duplicity of signal in this region was quite small.

1.8 The Mounting of the Decay Counter System

A light but strong 'core' of aluminium alloy was used to support the cylinder counters, which were of two types. One type, the inner charged counters are described in Section (1.9) whilst the other, the cylinder gamma counters are described in Section (1.10). There were twenty counters of each type, the former being mounted on the inside of the cylindrical core whilst the latter were mounted around the outside. The core was 9.5 mm thick with an outside radius of 330.0 ± 0.4 mm. The inner charged counters were held in place by the mounting of the photomultiplier base and a retaining ring whilst the cylinder gamma counters were supported by a lip on the core with clamping screws.

There was an asymmetry in the system in that, at the very top of the array, the feed pipe from a resevoir of hydrogen to the target had to enter through the system. A slot in the core permitted this to happen but the presence of the pipe necessitated the construction of a shorter inner charged counter and the design of a special gamma counter to fit into this much shortened region. These are described later.

In addition, a disc of aluminium 19 mm thick with inner and outer diameters of 219 mm and 1028 mm respectively, was used to support the lid gamma counters, described in Section (1.12). These counters were mounted on the upstream side of this disc which was itself mounted just downstream of the cylindrical core.

1.9 The Inner Charged Counters

These counters are shown in Fig. (1.5). Each counter consisted of scintillator 800 mm long, 100 mm wide and 10 mm thick, together with a second piece of scintillator, 5 mm thick with sides at an angle of 18^{o} to each other covering a circular region from a radius of 50 mm to approximately 320 mm at a distance of about 450 mm downstream of the target. The two pieces were

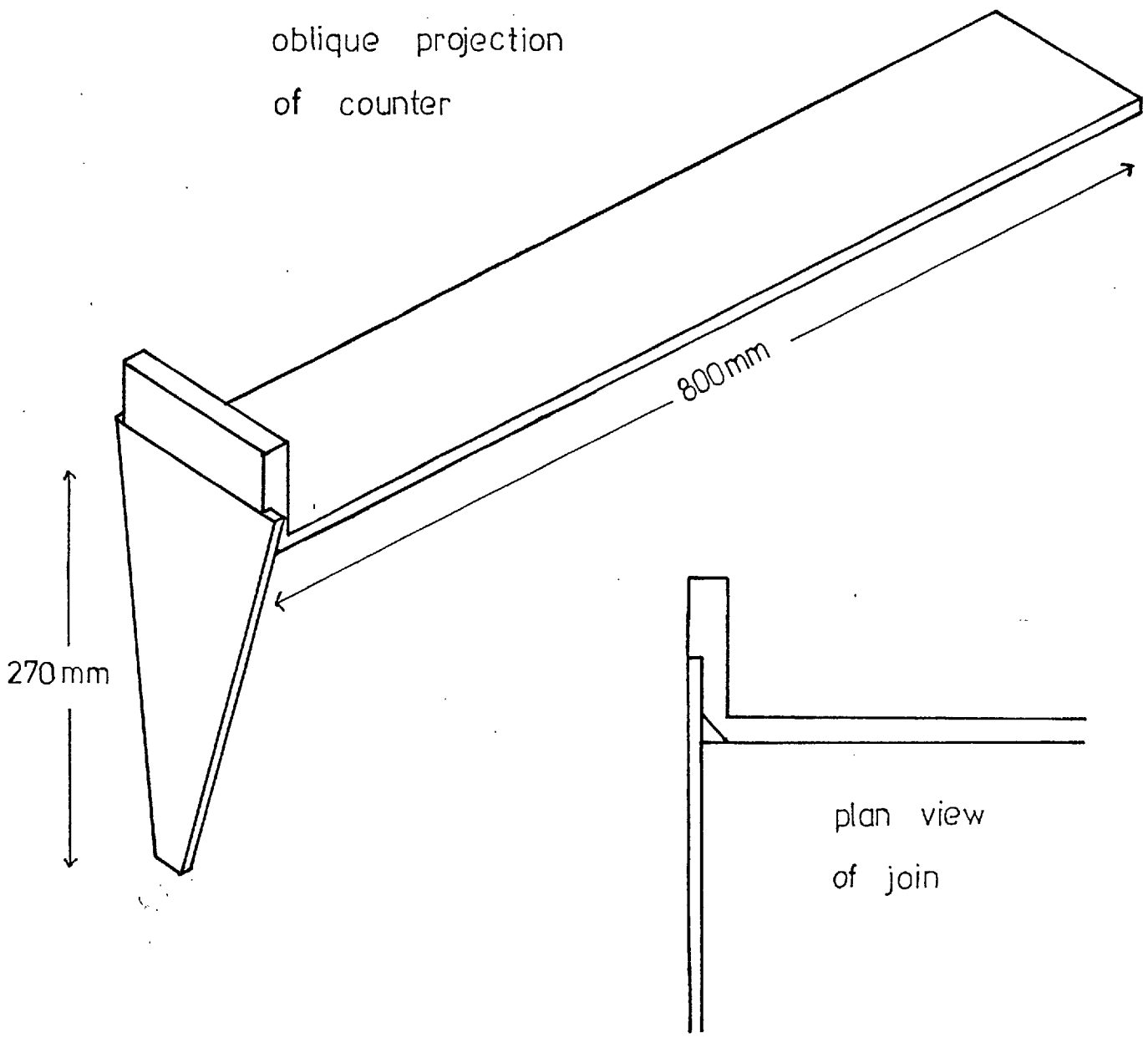

Figure 1.5. The Inner Charged Counter

joined together at right angles with an elongated highly polished reflecting prism of duralumin.

The original design consisted of two perspex light guides attached to a perspex block to which the pieces of scintillator were fixed. There was a small gap between the light guides which allowed them to be bent to eventually lie on top of one another, and then to be attached to a perspex cylinder. This was then fitted to a 56 AVP photomultiplier. Contact was made with a narrow air gap, as the base was held on to the light guide by tape and the photomultiplier was spring loaded. The counter was completely wrapped in aluminium foil and then with black PVC tape to make it light tight. A great deal of care was needed at this stage and the counter was carefully checked for light leaks.

When the counters were placed in their final positions for the main experiment, it soon became evident that the light guides themselves were detecting particles due to the emission of Cerenkov light. This radiation, which was visible, could be produced by a fast electron passing through a transparent material such as a light guide if its speed were greater than the velocity of light in the material[(2)]. As the light guides of the inner charged counters were external to the gamma counters, they could in fact detect a gamma as a pion from an electron produced in the gamma counters reaching the light guides. Consequently, the perspex light guides were replaced by air light guides.

A copper 'shovel' (shown in Fig. (1.6)), which was 1 mm thick, was used to attach the photomultiplier tube to the counter and to keep the system light tight. The shovel was lined with mylar attached by double-sided tape. One end fitted over the top of the photomultiplier whilst the other end fitted on the perspex which was used to join the two parts of the inner charged counter together. The bases in which the photomultipliers were held, were

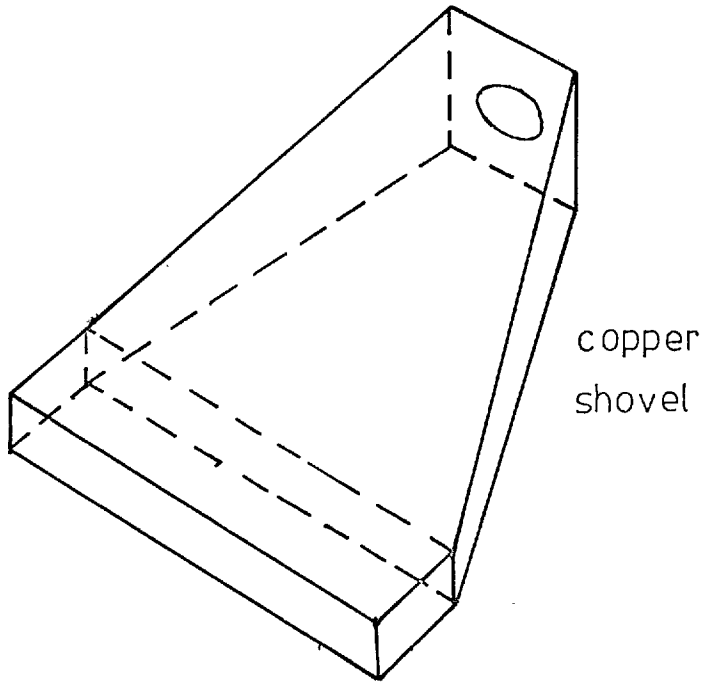

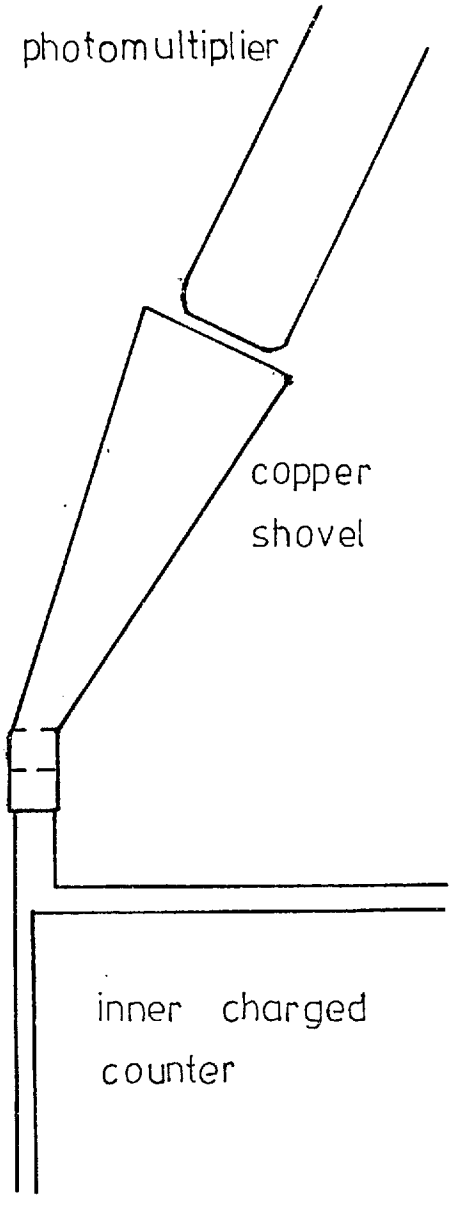

Figure 1.6

The "Copper Shovel" Light Guide to an Inner Charged Counter

mounted on to an extension of the collar of the core.

There were nineteen counters constructed to this design, whilst the twentieth was only 500 mm long to make room for the hydrogen pipe to enter the decay system.

1.10 The Cylinder Gamma Counters

There were nineteen standard counters of this type (shown in Fig. (1.7)), and one special counter described in the next section. Each counter subtended an angle of 18^0 at the centre of the hydrogen target and so the counter itself was tapered to this angle. The opening angle of the gammas from a $\pi^+ \pi^- \pi^0$ or $\omega \to \pi^0 \gamma$ at 1153 MeV/c was a little less than twice the angle subtended at the beam axis by one counter.

The counters consisted of alternate layers of scintillator and lead placed alternately on top of each other with a layer of lead at the bottom, that is, innermost to the target. A Monte Carlo program was written by Dr. D.M. Binnie to simulate the passage of an electron through such a sandwich of scintillator and lead. The efficiency of the counter was investigated for various numbers of layers of lead and for various thicknesses of lead. A flat plateau of high efficiency was required with a rapid rise to the plateau value. The counters were required to be as efficient as possible over as large an energy range as possible. In the decay modes of resonances such as omega, there were many low energy gammas produced. The curves in Fig. (1.8) indicated that an optimum design was probably six layers of lead, each of 0.7 radiation lengths thickness. With this configuration, as approximately 45% [3-9] of the gammas passing through a layer were expected to produce a pair of electrons, an efficiency of about 98% was expected. The addition of extra layers made only a slight improvement on the efficiency whilst reducing the collection area available for earlier layers at the photomultiplier. Fewer layers of lead of greater thickness increased the collection area available per layer of scintillator as fewer

Figure 1.7(a). The Cylinder Gamma Counter

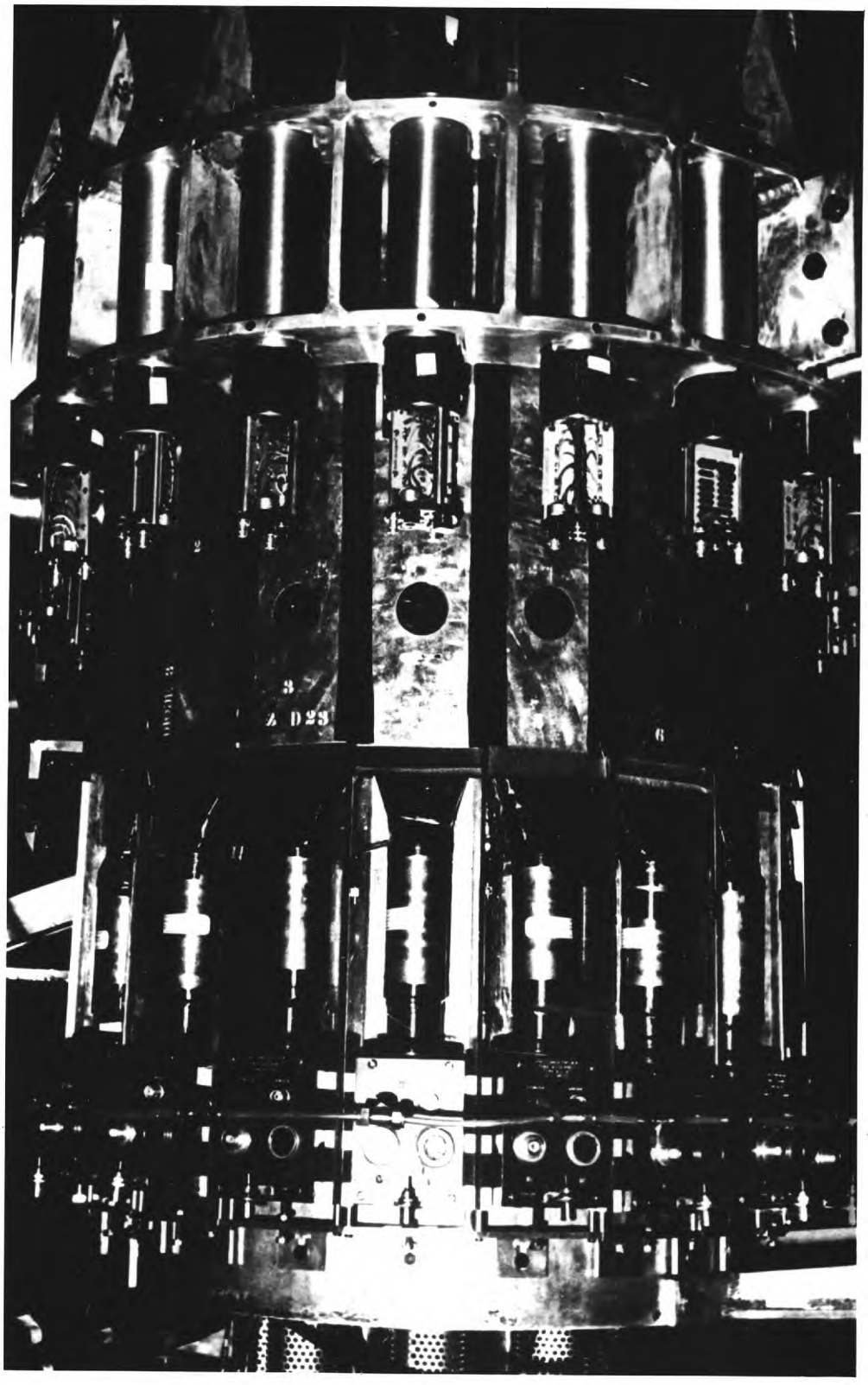

Figure 1.7(b). The Cylinder Gammas in Situ

Figure 1.8. The Response Curves for Various Types of Sandwich Counter

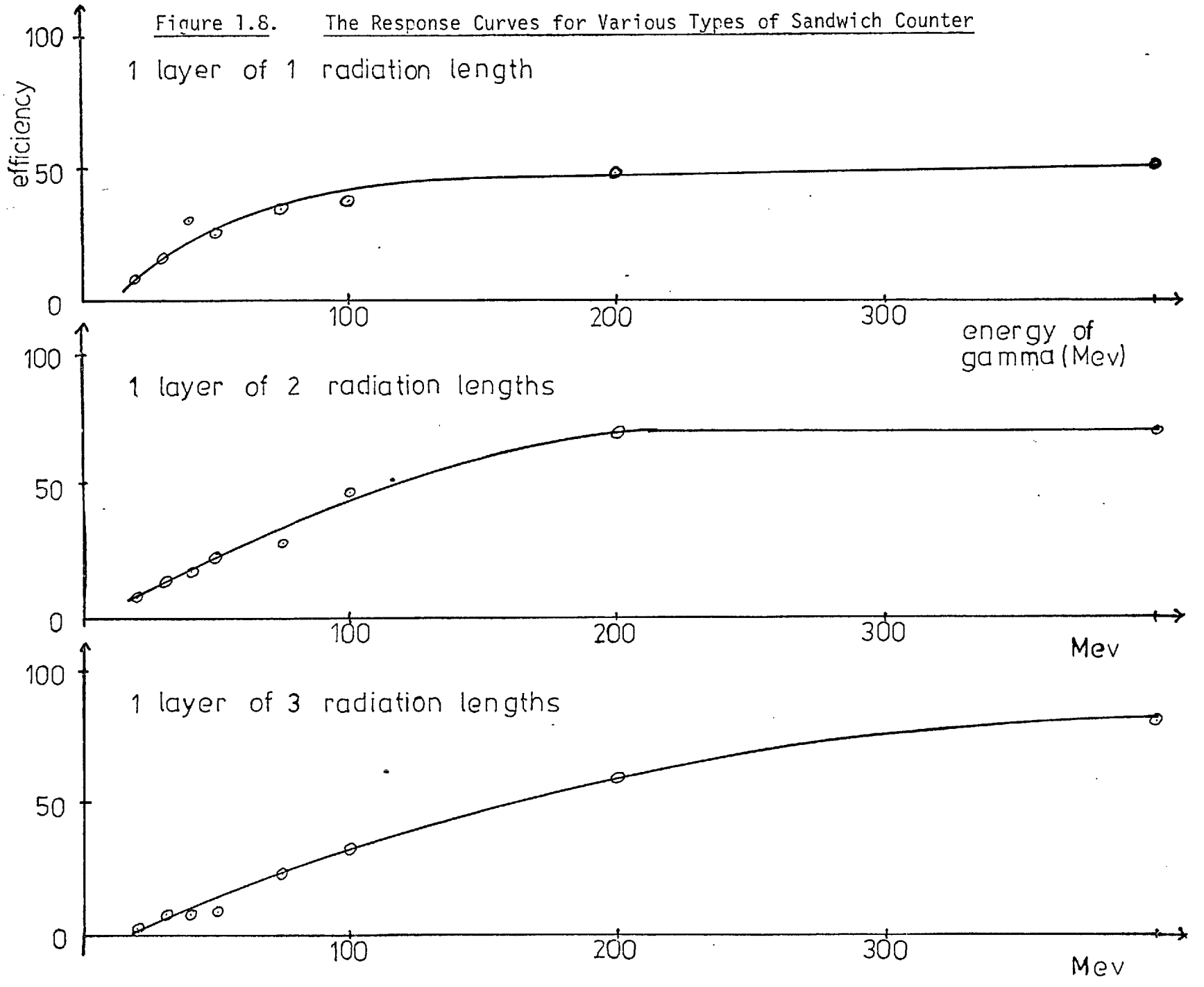

were needed, but the rise of the efficiency curve to the plateau was slower.

With this chosen configuration for the sandwich, each layer of lead was, in fact, 3.97 mm thick and their widths were 102.4, 103.0, 106.2, 109.4, 112.5 and 115.7 mm. Each layer of scintillator used in the sandwich was 4.75 mm thick and made of scintillator of the type NE 102 A. The widths of these layers were 102.0, 103.5, 106.5, 109.5, 112.5 and 115.5 mm. Each layer of lead and scintillator was 800 mm long.

The scintillator was joined to six 'fish tail' light guides 150 mm long and these were set in a perspex cup with bakelite epoxide resin R 18774/1. Their widths at the narrow end were 50 mm. The same resin was used to join the light guides to the scintillator. Each cup had a light diode set into it, so that in tests and in situ in the experiment, it was possible to check the performance of the photomultiplier without having to dismantle the apparatus.

Each layer of lead used was wrapped in aluminium foil and then the complete sandwich was similarly wrapped. The purpose of this was to reflect the scintillator light back inside the scintillator until it travelled as far as the light guide and on to the photomultiplier. The counter was then wrapped in black PVC and made light tight. Then, it was placed into a can of tin plate 1.2 mm thick. Along one side of the sandwich inside the tin was placed a layer of lead 3.25 mm thick with the purpose of stopping electron showers in one counter spreading to the next and thus indicating two adjacent gammas where there was only one. A similar piece of lead was placed at the end of the counter. A layer of foam rubber was then placed on top of the counter and held under compression by the lid of the can in order to prevent any movement of the sandwich inside.

Fitted into the can was a 56 AVP photomultiplier contained within a cylinder of mumetal magnetic shielding and mounted on a 2 ma base made at

the Rutherford Laboratory. The base was firmly held with the photomultiplier spring loaded so that the latter was in close contact with the counter. The counter was then made light tight and the light diode wires connected to a junction on the inside of the can so that no mechanical strain would be put on the light diode itself.

A slit 19 mm long and 9.75 mm wide was cut into one of the layers of lead at the end furthest from the photomultiplier, so that a small radioactive beta source could be inserted into the counter for testing purposes. This slit was placed in the outermost layer of lead, which was the one nearest the top of the can. The way in which these tests were carried out is described in Section (3.10).

1.11 The Twentieth Cylinder Gamma Counter

This special counter was constructed in an entirely different manner, as shown in Fig. (1.9). In order not to take up the restricted detection area with light guides and photomultiplier, the light guides were attached at right angles, using highly polished elongated reflecting prisms of duralumin. In order not to complicate the design too much, only two layers of scintillator were used, 435 mm long and 12.7 mm thick, together with two layers of lead 6.4 mm thick. The light guides were fish tailed to a perspex button, fitting on to a 56 AVP photomultiplier, held by its base to the extension of the collar to the core, along with the twentieth inner charged counter.

This counter was placed in a thinner can, only 0.76 mm thick. Lead was placed along one side of the can as in the other cylinder gamma counters.

1.12 The Lid Gamma Counters

These counters were constructed in a similar manner to the cylinder counters, as shown in Fig.(1.10). Each counter was constructed so as to form an 18^{0} sector and was mounted on to the disc support. The six layers

Special cylinder gamma counter

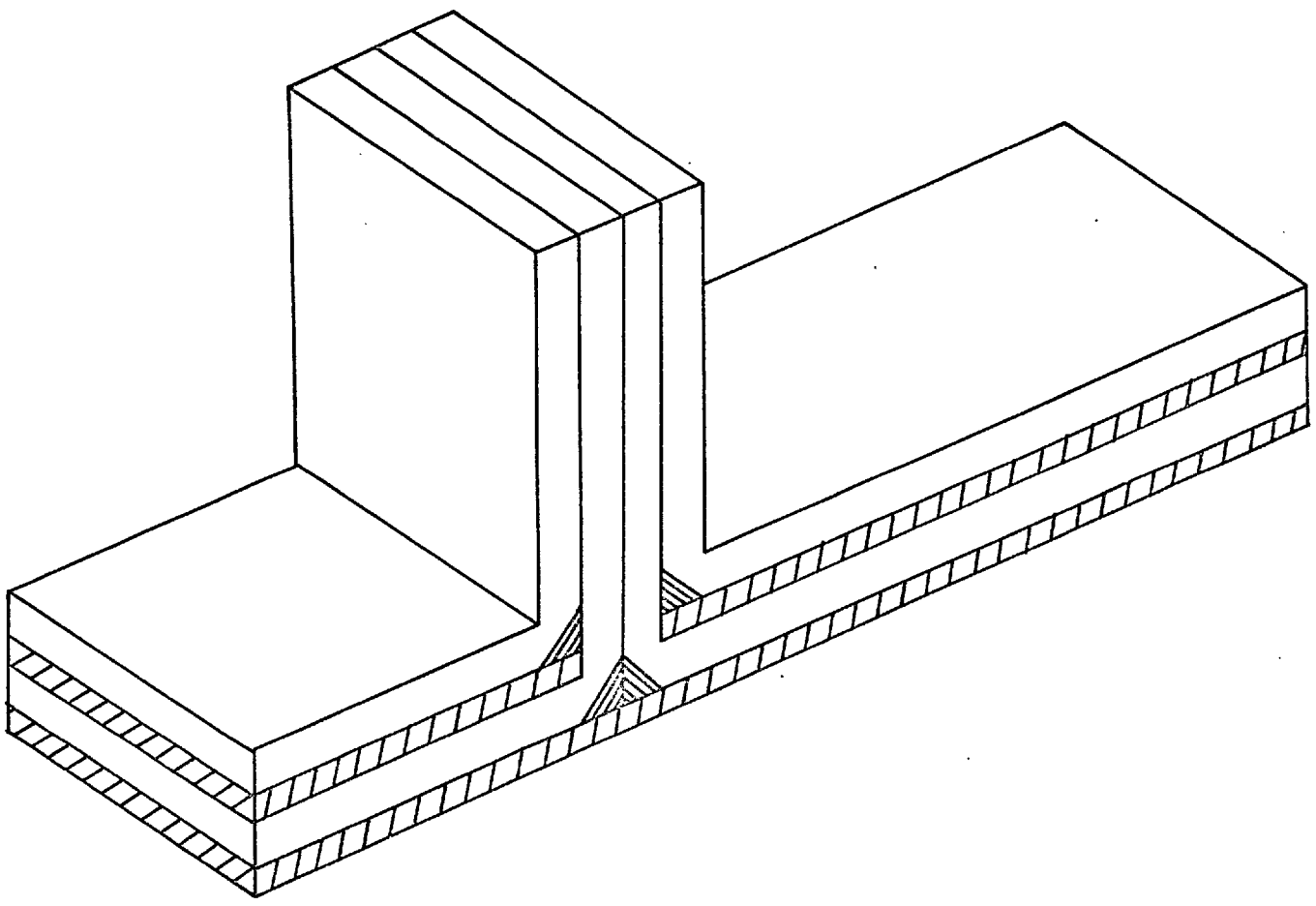

Figure 1.9

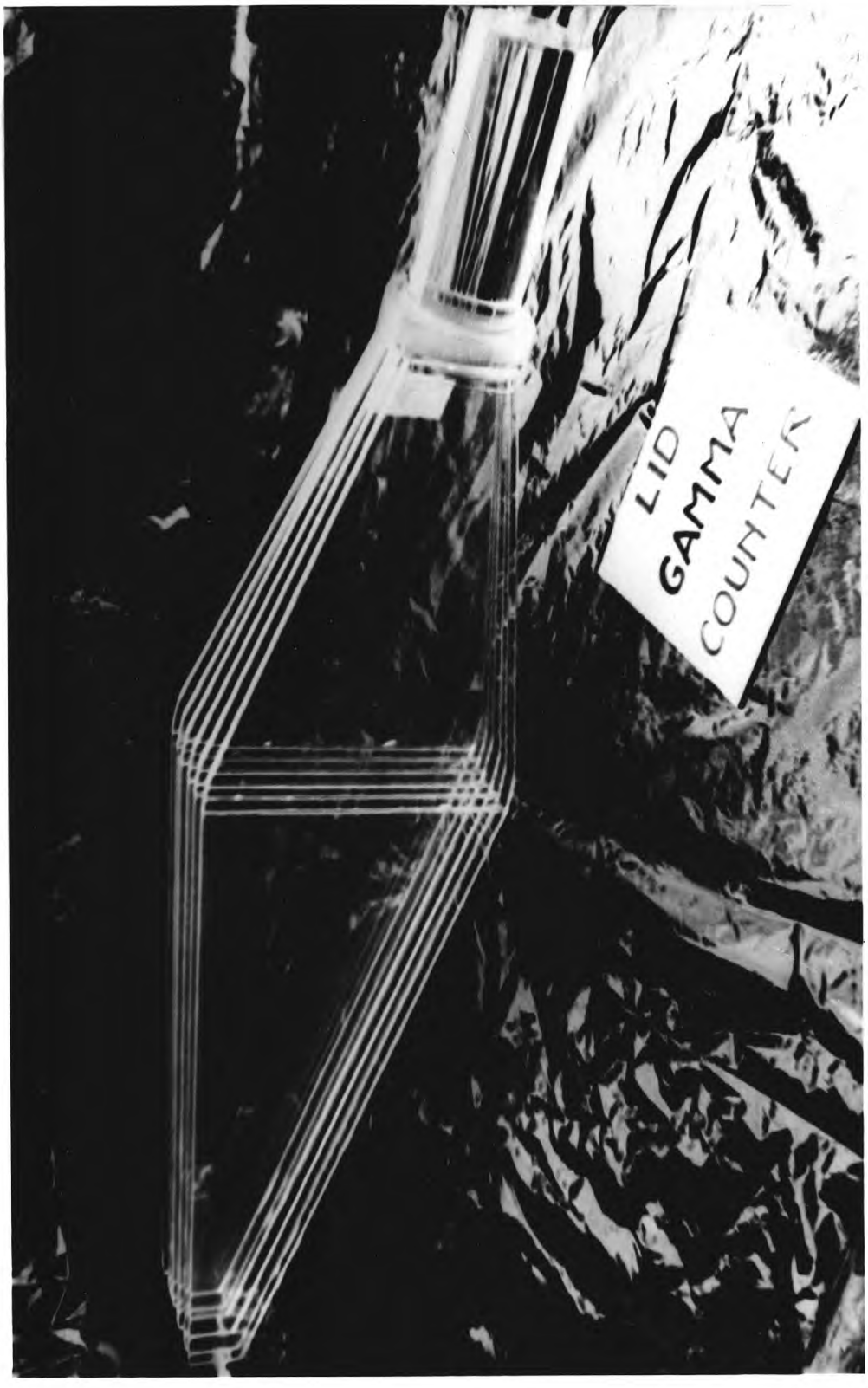

Figure 1.10(a) The Lid Gamma Counter

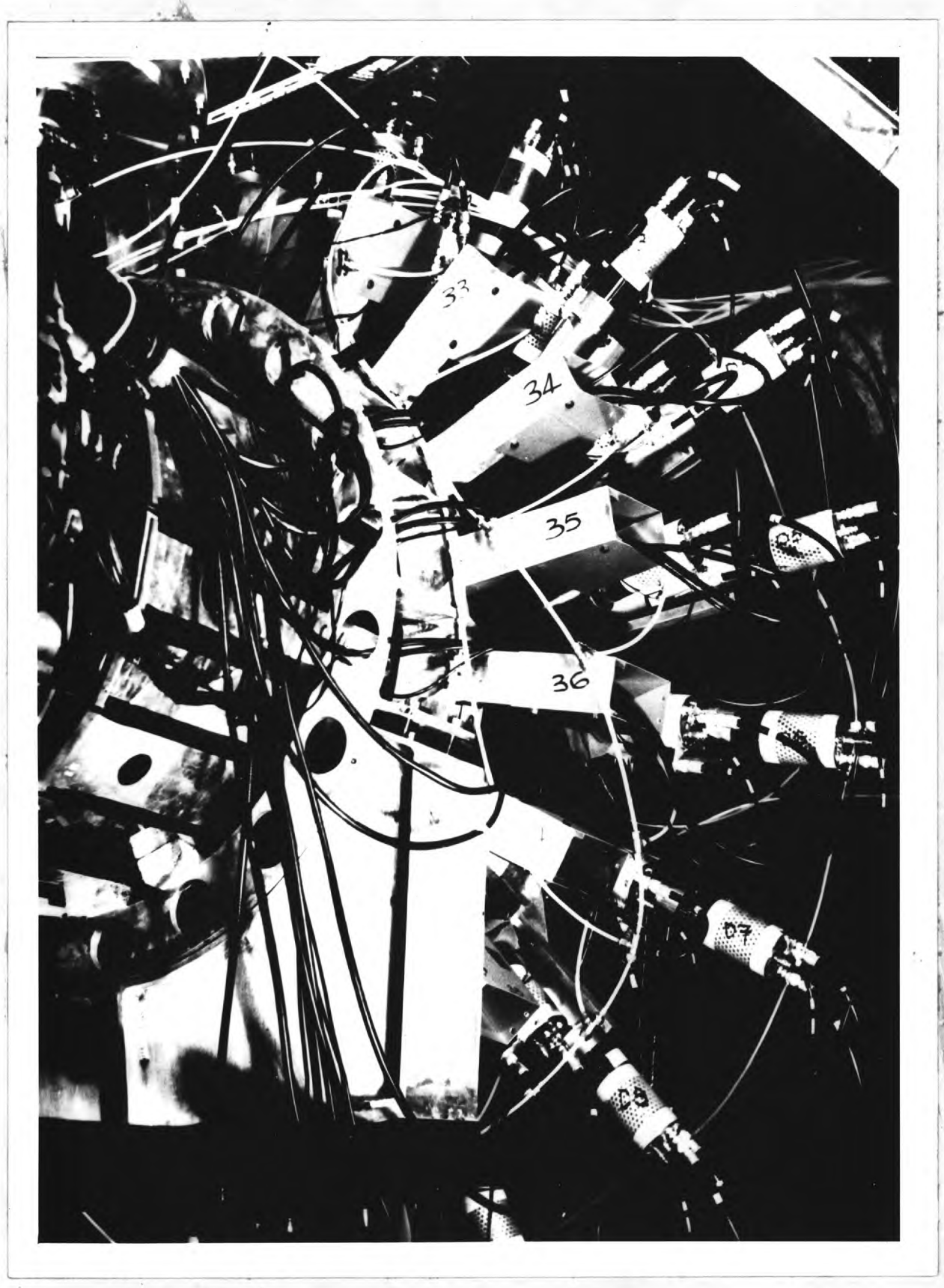

Figure 1.10(b). The Lid Gammas in Situ

of scintillator were the same size and shape, varying in width from 120 mm to 25 mm and were 300 mm long. Each layer of scintillator was 5 mm thick whereas each layer of lead was $^{5}/_{32}$ inch thick. The alternating layers of lead and scintillator were arranged so that the uppermost layer was of lead as this was the first layer encountered by particles from the target. For cylinder gamma counters, it was the bottom layer which was first encountered.

The counters were wrapped in the same way as the cylinder gamma counters and also mounted in a metal can. However, a layer of lead 1.63 mm thick was placed along both sides with no lead at the end furthest from the photomultiplier. This narrow end of the can was also open ended. To have metal here more than necessary introduced the possibility of causing the timing particle to interact and so give a spurious signal.

Fan tail light guides were used to connect the scintillator to a perspex button 38 mm in diameter. A 56 AVP photomuliplier was placed in contact with this button under spring pressure. A light diode was attached to the button as before.

The slit for insertion of the beta source was made in the two first encountered layers of lead which were the nearest to the top of the can. The top layer of the counter sandwich was, in fact, a layer of lead and so two slits were necessary, one for the beta source and the other to allow the beta rays to escape from the counter.

1.13 The Remaining Counters

The upstream end of the decay counter system was filled only with a charged particle detector called 'droop.' This counter consisted of two semi-circular sectors of scintillator 10 mm thick. Each sector was in two equal parts joined together by a highly polished elongated reflecting prism of duralumin. Four 50 mm wide light guides were attached at right angles to the quadrants at the junction. The set of four light guides was then shaped to come together to meet in a rectangle and was then fixed

to a perspex button and held in spring contact with a photomultiplier, which was mounted on the upstream side of each of the two sectors. The counters had an inner radius of 80 mm and an outer radius of 300 mm.

The ring counter was designed in the form of a split washer of diameter 201.6 mm and with a width of 50 mm. It was attached to a photomultiplier in the usual way and placed in the region described in Section (1.7).

1.14 Preliminary Tests

Before any of the counters were mounted in position, each one was thoroughly checked to see if it was light tight, that the noise rate was sufficiently low and that each layer was giving a comparable response. This latter test was approximate only but was capable of picking out broken or badly crazed layers of scintillator damaged in transportation. In addition, the response of the light diode was measured. Extensive tests were carried out on the gamma counters, as described in Chapter (IV).

The charged particle counters were examined so as to set their EHT comfortably above the knee of the curve of efficiency versus EHT, so that they were very efficient and very stable. The long air guide on these counters made the compromise between the high EHT required and the photomultiplier noise difficult. The tubes were used at their limit as there were only a few photons detected by them. Consequently, the EHT of the counter was set high first and tubes specially selected to give low noise.

CHAPTER II

THE DECAY SIMULATION PROGRAM

2.1 Introduction

In order to be able to analyse the data to be obtained from the experiment, it was essential to have a program capable of simulating the production and decay of a resonance, and its subsequent detection in the decay counter system.

A program written by Dr. W.G. Jones already existed, which was able to simulate the production and decay of the eta meson. This program had been updated by Dr. D. Mason and used to simulate the production of the phi meson and its decay into two kaons.

As it then stood, the program generated random numbers and used a Monte Carlo method to obtain values for variables in the production and decay processes. The natural shape of the beam was simulated using a triangular beam spread which was a reasonable first order approximation. The beam was assumed to have no real width, compared to the real width of 45 mm and was coincident with the axis of the hydrogen target, which itself was taken to be only a line of finite length. The probability of a pion interacting with the target was uniform along the length of the target and the pions energy loss was allowed for. As the density of final states was proportional to the centre of mass momentum, the probability of production of a resonance was also taken to be proportional to p*. The mass was chosen from a Breit Wigner distribution[10] and its width on an effective mass plot was specified by experimental or theoretical information already known.

The resonance was then allowed to decay instantaneously into two particles of equal mass produced isotropically in the centre of mass system. The interaction thus allowed was, typically,

$$\pi^- p \rightarrow n \phi \quad , \quad \phi \rightarrow K^+ K^- \quad .$$

The timing particle, in this case, the neutron, was then inspected to see if it entered a ring of six neutron counters placed symmetrically around the axis at a specified distance downstream of the target. If the neutron entered the neutron counters, the event was selected and the time of flight of the neutron calculated. Various timing errors of the order of magnitude expected in the experiment were allowed in this calculation and histograms plotted of the time of flight spectra with these errors.

The subsequent detection process was designed for two charged particles passing through spark chambers and was not relevent to the geometry of the detection system in this experiment.

2.2 The New Program

The production side of the existing program was only modified in small ways. Firstly, a beam pion was allowed to have a small angle, 10 mr, to the beam axis. The value used here was specified by the divergence of the beam between its last focus, which was the H hydoscope, and the centre of the hydrogen target. The beam pion was then given a uniform probability of interacting anywhere within a cylindrical volume of specified dimensions, representing the target. This was important as it made allowance for off axis decays to two particles which would not be exactly coplanar.

The fundamental changes to the program were in the decay processes written into the program, the decay detection system and its responses. The resonance produced was allowed to decay into two or three particles. The program made the decision as to which by investigating the mass of the third particle. If this was exactly zero, a two body decay took place. Decay modes were permitted in which one or more particles were able to decay further. At each level, the program made the same inspection to decide the number of particles in that level. The program was written in such a way that other decay modes could easily have been added if required. The modes written into the program already are shown in the table in Fig. (2.1), which shows how the two parameters

Figure 2.1

Control Parameters for Different Decay Modes

L1	L4	Type of Decay
6	0,1	R → 1 + 2 + 3
7	0,1	R → 1 + 2 + 3 └→ 4 + 5 + 6
8	0	R → 1 + 2 + 3 └→ 4 + 5 + 6 └→ 7 + 8 + 9
8	1	R → 1 + 2 + 3 └→ 10 +11 +12 └→ 4 + 5 + 6
9	0	R → 1 + 2 + 3 └→ 10 +11 +12 └→ 4 + 5 + 6 └→ 7 + 8 + 9
9	1	R → 1 + 2 + 3 └→ 4 + 5 + 6 └→ 13 +14 +15 └→ 10 +11 +12 └→ 7 + 8 + 9
10	2	R → 1 + 2 + 3 └→ 13 +14 +15
11	2	R → 1 + 2 + 3 └→ 13 +14 +15 └→ 10 +11 +12 └→ 4 + 5 + 6

L1 and L4 were used to produce them.

All decays into three particles were isotropic in the centre of mass, as were all two body decays except where the resonance itself decayed into only two particles. Fig. (2.2) shows how the parameter L5 was used to decide the angular distribution of the two decay products in this particular case.

In addition to resonant decays, the parameter L1 was used to allow the generation of three body non-resonant background.

An example of one of the multi-level decay modes possible is given below, selected by L1 = 9, L4 = 1.

$$\omega \rightarrow \eta + \gamma$$

$$\downarrow$$

$$\pi^0 + \pi^0 + \pi^0$$

$$\downarrow \qquad \downarrow \qquad \downarrow$$

$$\gamma+\gamma \qquad \gamma+\gamma \qquad \gamma+\gamma$$

Each level of decay was considered in the frame of its parent particle and instead of carrying out a Lorentz transformation immediately into the laboratory system, a more accurate procedure was adopted. Each decay level was transformed back to its parent frame. In the example above, the properties of each γ, calculated in its own centre of mass frame, would be transformed to the frame of its parent π^0, then to the centre of mass frame of the η, then to the centre of mass of the ω, and finally to the laboratory system.

The program was modified to allow both neutral resonances with a neutron as the timing particle and negative resonances with a proton as the timing particle, to be produced. The timing particle was detected by twelve neutron counters, placed in two rings symmetrical with the axis as described in Section (1.5), with one ring outside the other. A parameter, L2, was used to instruct the program as to whether the inner six only, the

Figure 2.2

Angular Distribution of the Decay Products of a Resonance

L5	
0	Isotropic
1	$A + B \cos^2\theta$
2	$A + B \cos^2\theta + C \cos^4\theta$
3	$A + B \cos^2\theta + C \cos^4\theta + D \cos^6\theta$
4	$A + B \cos^2\theta + C \cos^4\theta + D \cos^6\theta + E \cos^8\theta$
5	$A + B \cos^2\theta + C \cos^4\theta + D \cos^6\theta + E \cos^8\theta + F \cos^{10}\theta$
6	$1 - \cos^2\theta$

The values of the coefficients A, B, C, D, E, F were read in from a DATA statement in the DECAY subroutine.

outer six only or all twelve neutron counters were to be used, as shown in the table in Fig. (2.4). The distance of the neutron counter array from the target could also be specified.

The decay detection system was carefully written into the program, to include both cylinder and lid gamma counters, inner charged counters, special twentieth counters and droop counters. As well as the geometric data, the different performances of the different types of counter were included in detail from the lengthy tests that were carried out. The actual physical position of the decay counter array was moveable and so this was also written into the program.

Various aspects of the program are discussed below in more detail.

2.3 The Production of a Resonance

The production of a resonance was simulated in the main part of the program,called MCARLO. The following assumptions were made :

(i) The momentum spectrum of the pions incident on the hydrogen target was taken to be triangular, centred upon a specified value and with a specified full width at half height. The momentum chosen from this spectrum was then corrected for energy loss in the hydrogen target.

(ii) The beam pion was assumed to be incident upon the target within a cone of half angle 10 mr, or approximately half a degree. It was then assumed to interact within a cylindrical volume of specified length and radius, whereas the actual target was sausage shaped.

(iii) No allowance was made for the attenuation of the intensity of the beam in traversing the hydrogen target.

(iv) An event was regarded as detected if the trajectory of the timing particle intersected a section through the centre of

the neutron counter perpendicular to the beam axis. The efficiency of the neutron counter was taken to be constant for all timing particle energies and to be uniform over the face of the counter.

(v) The resonance was assummed to be produced isotropically in the centre of mass system.

(vi) The mass was chosen as a random number satisfying a Breit Wigner distribution. If N was a random number between 0 and 1, M was the mass, ΔM was the deviation from the central mass and Γ was the width, then the Breit Wigner distribution had the form :

$$\frac{dN}{dM} = \frac{A}{(\Delta M)^2 + (\tfrac{1}{2}\Gamma)^2} \quad \text{or} \quad N = \frac{2A}{\Gamma} \tan^{-1}\left(\frac{2\Delta M}{\Gamma}\right) + B \,,$$

where A and B were two constants to be determined by the boundary conditions. ΔM was taken to equal $+\infty$ when N = 1 and $-\infty$ when N = 0, and so $B = \pi/2$ and $\Gamma/2A = \pi$. Therefore, $\Delta M = \frac{1}{2}\Gamma \tan(\pi N - \pi/2)$ or $\frac{1}{2}\Gamma \tan\theta$ where θ was a random angle uniformly distributed between $+\frac{\pi}{2}$ and $-\frac{\pi}{2}$.

(vii) The program assumed that the cross section for production of a resonance was proportional to p* up to some limit, p^*_{max}, representing the maximum number of final states possible, after which the cross section was assumed constant. The probability of production of a resonance was taken as p^*/p_{max} and p_{max} was calculated in a way that few events would have $p^* > p_{max}$. It was calculated as the centre of mass momentum of an event produced with a pion of the highest momentum in the beam distribution and with a mass lower than the central mass value by about four Breit Wigner widths.

(viii) The output of the program was not normalised, but the

equivalent number of pions was calculated.

(ix) For the time of flight spectra specified, timing errors were assumed in accordance with a Gaussian distribution and added to the time of flight.

The production of resonance was governed by the parameter L1 as shown in the table in Fig. (23).

2.4 The Decay of the Resonance

The subroutine that organised and controlled the decay of the resonance was called TRIXIE.

After selecting the direction cosines of the resonance in the π^-p centre of mass frame, the resonance was allowed to decay and the relevant physical properties of its decay products were found in the centre of mass frame of the resonance. Then these values were transformed into the laboratory frame. There then followed a complicated section of the program which selected the chosen decay modes of the decay products at successive levels. The scope of this part of the program was virtually unlimited. Each particle that was to decay was passed through a subroutine called DECAY described in Section (2.5). All decays were instantaneous in time and space and all decay products, whether stable or otherwise, were labelled and the relevant properties calculated.

All stable decay products were labelled with the parameter ND(I) = 1, whereas unstable particles had a zero value. As the final decay products were either pions or gammas, one other parameter, NG(I) was used to label the particle. A value of unity indicated a gamma, whereas a zero value indicated a pion. If required, other values could have been given to this parameter to examine other final products of other decay modes if they were of interest.

Finally, the subroutine called four other subroutines called TEST,

Figure 2.3

Mode of Operation of Program

L1	
≤ 4	Calculated the time of flight spectra only
5	Also calculated the missing mass spectra
>5	Resonance was also allowed to decay
$20 < L1 \leq 26$	Set L3 = 2 and generated three body phase space. Otherwise behaved as L1 = L1 - 20

L3	
0,1	Production of resonance
≥ 2	Generation of phase space

Figure 2.4

Neutron Counter Selection

L2	
0	Inner Ring of 6 neutron counters used
1	Both rings of 12 neutron counters in all used
2	Outer ring of 6 neutron counters used

NICOLA, SCALAR and LOSSES described below.

The purpose of the first subroutine was to calculate the initial mass of the resonance from the properties of the final decay products for a specified number of events as a check on the elaborate structure of the program at this stage. The relation used to do this was :

$$M = \left[\left(\sum_i E_i\right)^2 - \left(\sum_i \left(p_i \ell_i + p_i m_i + p_i n_i\right)\right)^2 \right]^{\frac{1}{2}}$$

where E_i was the energy, p_i the momentum, ℓ_i, m_i and n_i the direction cosines of the ith particle in the laboratory frame.

2.5 The DECAY SUBROUTINE

This subroutine decayed the resonance in its own centre of mass frame. Firstly, it inspected the third particle in the decay level to see if the third mass was zero, and, if so, operated a two body decay. If, however, the third mass was not zero, a three body decay occurred. At this stage, there arose a technical difficulty in that the third particle could not be a gamma. The decay modes built in made it very unlikely that this might have been necessary, but, if it was, the gamma could have been given a mass of 0.1 MeV/c^2 which was sufficient for the program to recognise its presence. This same procedure was adopted for each level of decay by repeated application of the subroutine with different input information supplied by the subroutine TRIXIE.

If the resonance decayed into two particles to start with, the program inspected the value of L5. If the value of this parameter was zero, an isotropic two body decay occurred but if it was greater than zero it followed the angular distribution already indicated in the table in Fig. (2.2). The actual values of the constants in the table were fed into the program by a data statement and so could easily be varied. The possibility of a non-isotropic decay in the centre of mass of the decaying particle only applied

if that particle was, in fact, the resonance and the decay was into two bodies, although further isotropic decays were then possible. The angular decay distribution was then used as a probability function for selecting the direction cosine representing the angle to the beam. The other two direction cosines were then selected at random. The second particle in the decay mode was given the opposite direction cosines of the first in the centre of mass and the total energy in the CMS was calculated.

In a three body decay mode, the program calculated the CMS energy from the mass of the resonance and the decay particle masses, that is,

$$Q = MX - M1 - M2 - M3 \quad .$$

The next step was to calculate the energy of the three particles. If K was the length of the side of an equilateral triangle and H was its height, then :

$$H = K \sin 60^{0} = K\sqrt{3}/2$$

therefore

$$K = 1.154\ H \quad .$$

Consider a Cartesian co-ordinate system with the origin at one vertex, the x-axis along one side of the triangle and negative in that direction and the positive y-axis pointing away from the triangle, as shown in Fig. (2.5). Then, consider any point within this triangle and three vectors drawn from the point to the sides such that they met the sides normally. If these vectors were denoted by a, b, c and the co-ordinates of the point in the triangle were (-X,Y) then :

$$\begin{aligned} a &= Y \\ c &= (X - Y \cot 60^{0}) \sin 60^{0} \\ &= \frac{\sqrt{3}}{2} X - \tfrac{1}{2} Y \\ b &= H - (a + c) \\ &= H - \frac{\sqrt{3}}{2} x - \tfrac{1}{2} Y \quad . \end{aligned}$$

Figure 2.5

CMS Energy Triangle

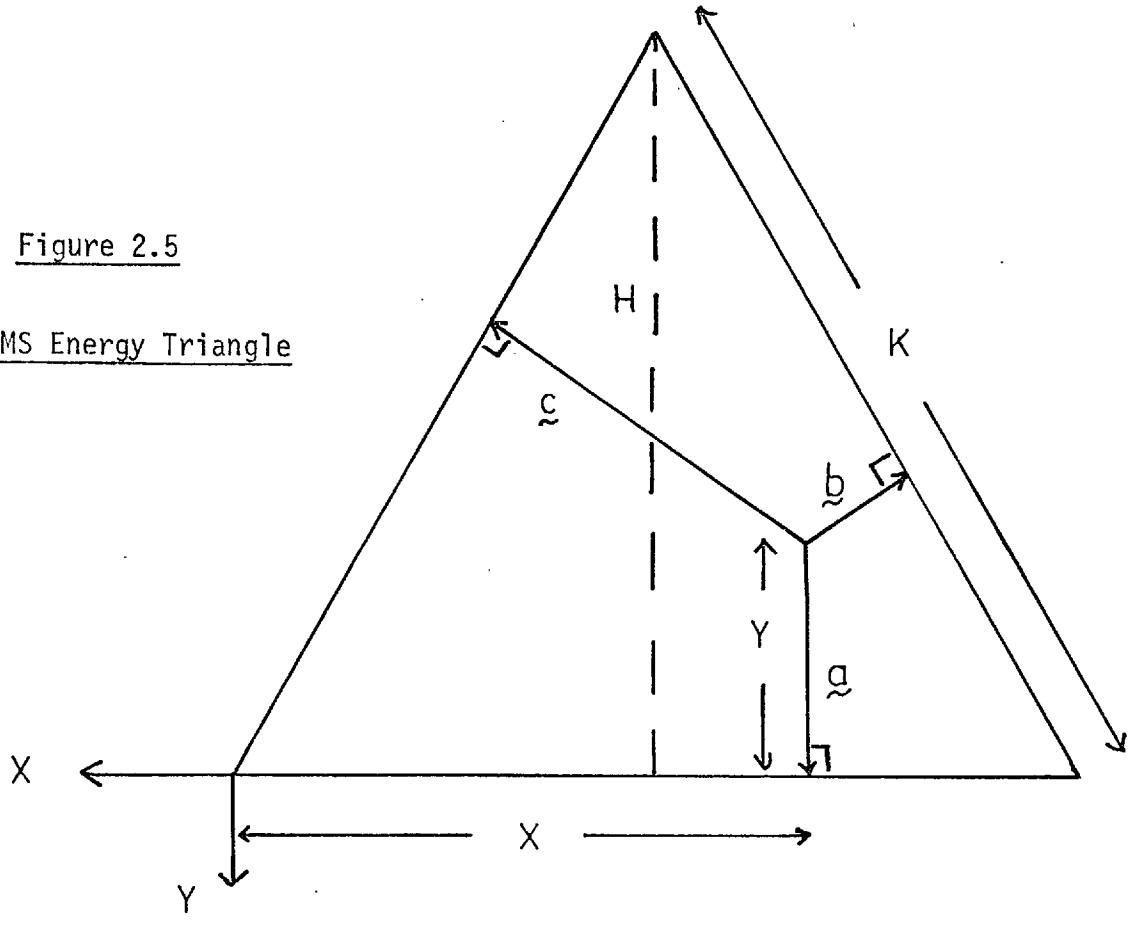

Figure 2.6

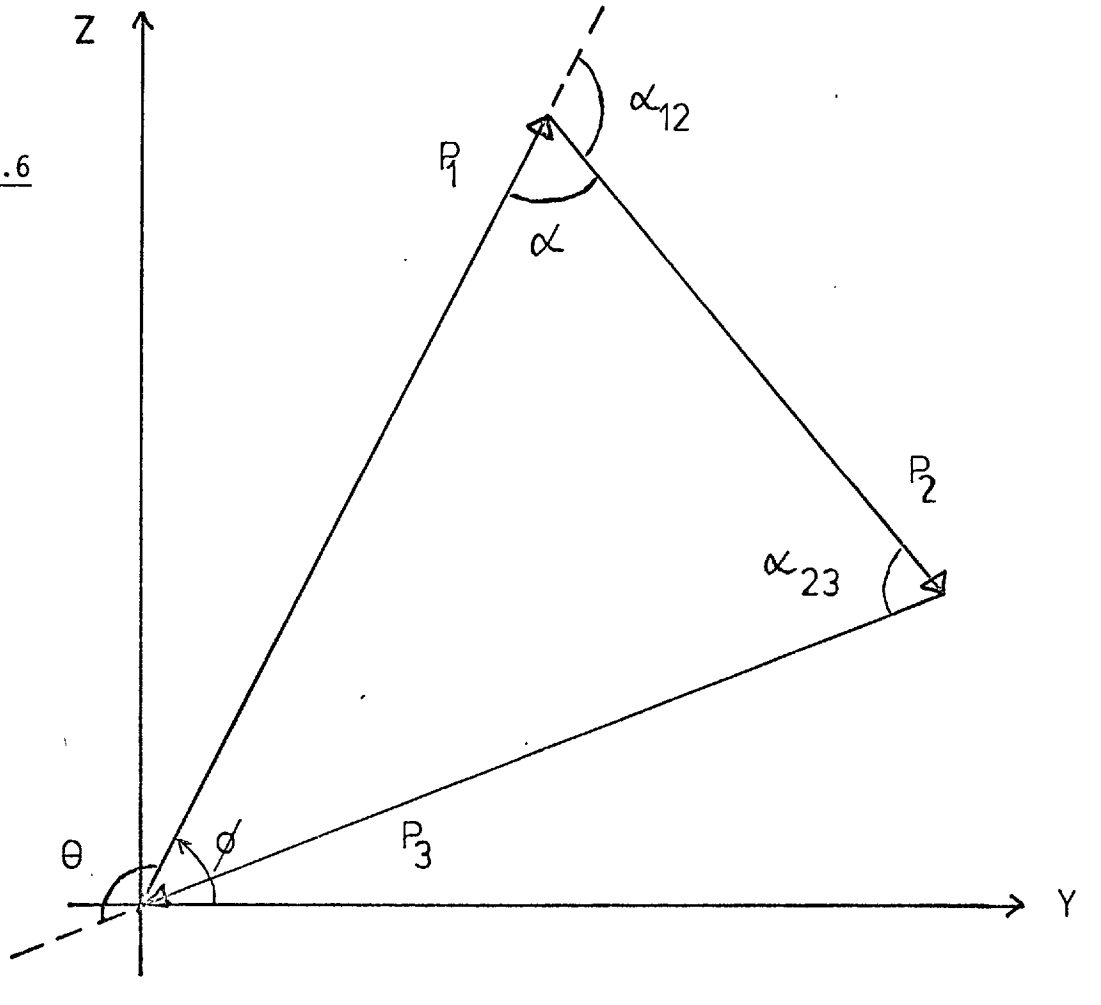

The expression for b followed from the fact that, when lines were drawn from any point inside the triangle to meet the sides normally, they added up to a constant which, in fact, for an equilateral triangle, was the height. Therefore, if a, b and c represented the CMS energies of the three decay products and H represented the total CMS energy, Q, then as :

$$Q = E1 + E2 + E3$$

$$E1 = Q.WY$$

$$E2 = Q[\ 1 - 0.86603\ EX - 0.5\ WY\ ]$$

$$E3 = Q\ [\ 0.86603\ EX - 0.5\ WY]\ ,$$

where EX and WY were chosen randomly and the physical laws were applicable if E1, E2 and E3 were only allowed to be positive. The number WY was chosen to lie between 0 and 1, representing the possible magnitude of the y co-ordinate, that is, not greater than the height of the triangle, whilst EX was chosen to lie between 0 and 1.154 to represent the x co-ordinate, that is, not greater than the side of the triangle.

Defining the angles as shown in Fig. (2.6),

$$\cos \alpha = \frac{p_1^2 + p_2^2 - p_3^2}{2p_1\ p_2}$$

$$\alpha_{12} = \Pi - \alpha$$

$$\cos \alpha_{12} = \frac{p_3^2 - p_1^2 - p_2^2}{2p_1\ p_2}$$

$$\cos \alpha_{23} = \frac{p_2^2 + p_3^2 - p_1^2}{2p_2\ p_3}\ .$$

Consequently, the third angle of the triangle was also defined. A random angle ϕ was introduced to fix the angle of p_1 to the co-ordinate system, Y - Z. Then the direction cosines of the three particles were defined as

$$m_1 = \cos\phi$$

$$n_1 = \sin\phi$$

$$m_2 = \cos[-(\alpha_{12} - \phi)] = \cos(\phi - \alpha_{12})$$

$$n_2 = \sin(\phi - \alpha_{12})$$

$$m_3 = \cos(\theta+\phi) = \cos(\alpha + \alpha_{23} + \phi)$$

$$= \cos(\Pi - \alpha_{12} + \alpha_{23} + \phi)$$

$$n_3 = \sin(\Pi - \alpha_{12} + \alpha_{23} + \phi)$$

Finally, the decay plane itself, Y - Z, was given random direction cosines, ℓ_r, m_r and n_r and the final direction cosines calculated :

$$n_{x1} = n_1,\ n_{x2} = n_2,\ n_{x3} = n_3$$

$$\ell_{x1} = -(m_r \cdot m_1 + \ell_r \cdot n_r \cdot n_1)$$

$$\ell_{x2} = -(m_r \cdot m_2 + \ell_r \cdot n_r \cdot n_2)$$

$$\ell_{x3} = -(m_r \cdot m_3 + \ell_r \cdot n_r \cdot n_3)$$

$$m_{x1} = \ell_r \cdot m_1 - m_r \cdot n_r \cdot n_1$$

$$m_{x2} = \ell_r \cdot m_2 - m_r \cdot n_r \cdot n_2$$

$$m_{x3} = \ell_r \cdot m_3 - m_r \cdot n_r \cdot n_3$$

2.6 The Location and Detection of Decay Particles

The actual location of the decay particles in the detection system was decided by two subroutines called NICOLA and SURFAS.

NICOLA calculated the angle of the particle to the beam axis and then SURFAS decided which of the three cylinder surfaces the particle entered, that is, the cylinder itself, the lid or droop. A label was attached to the particle to indicate which of these were involved and then NICOLA calculated which actual counter in the surface was traversed. In addition, it also labelled the particle according to which side of the counter it was

nearest to, for use in deciding to which side of the counter the shower initiated by the gamma might have spread.

These calculations were carried out for all the final decay products and for a small specified number of events, in order to help in the analysis of the data, the subroutine also printed out three pieces of information for each particle. They were as follows :

(i) The counter entered,

(ii) the angle to the beam,

and (iii) the laboratory momentum.

Another subroutine called SCALAR was used to calculate various geometrical properties of particles and events before actual counter response was taken into account. Firstly, the loss of particles through the various 'holes' in the apparatus was analysed. The program calculated the following :

(i) gammas entering the droop counters

(ii) pions entering the droop hole

(iii) gammas entering the 20th counter hole

(iv) pions entering the 20th counter hole

(v) pions entering the lid hole

(vi) gammas entering the lid hole

(vii) pions entering the ring counter

(viii) number of events in which pions entered the ring counter.

In addition, the following information was calculated for the first two particles in each decay level :

(i) number of particles entering the lid counters

(ii) number of particles entering the droop counters

(iii) number of events with two particles in the lid

(iv) number of events with two particles in droop

(v) number of events with one particle in the lid

(vi) number of events where both particles went in the identical counter

(vii) The spectrum of particle separation in terms of azimuthal counter bins, ignoring the different counter systems.

Two further subroutines were available for use in the analysis of particle behaviour. The subroutine COPLAN was applicable only to two body decay modes in the first decay level. It selected events where the particle separation was greater than a specified number. The second subroutine CORREL took any two specified particles in a decay level and selected events where their separation was within a specified range. Both subroutines only permitted the selected events to enter the final output matrix.

The first subroutine was used to select coplanar events whilst the second was used to select events where particles lay within a particular opening angle in order to facilitate the analysis when and where this approach was useful. For example, a two body decay was very coplanar. The two pion decay mode would have hade 96% of all its events within 1 bin of being coplanar. In a decay such as $R \rightarrow \pi^0 \pi^+ \pi^-$, the two gammas occurred within 3 counter bins of each other in 81% of all events.

2.7 The Subroutine LOSSES

This subroutine was written to take into account all the geometrical inefficiencies of the decay detection system, and in addition, the actual response of the various types of counter. Consequently, the subroutine only dealt with the final decay products in an event and its first purpose was to reject all the particles which were lost in 'holes' in the apparatus. These were as follows :

(i) The axial hole in the inner charged counter array where both pions and gammas were lost.

(ii) The axial hole in the lid gamma counter array where pions were detectable as only inner charged counts and gammas were lost altogether.

(iii) The gap caused by the hydrogen feed pipe passing through the twentieth inner charged and cylinder gamma counters.

(iv) The droop region where gammas were completely lost.

(v) The axial hole in the droop counters where the pions were completely lost, in addition to the gammas.

The subroutine labelled a particle in the following manner. If a particle was detected by an inner charged counter or a droop counter, then, for the ith particle, MIC (I) = 1. If a particle was detected by a gamma counter, then MOC (I) = 1. Otherwise, the parameters were given zero values. Consequently, every final decay particle was labelled with these two parameters depending on how they were detected and not upon their true identity.

In order to evaluate the response of the various counters, extensive tests on the gamma counters were carried out and these are described in Chapter (III). The inner charged counters were assumed to be 100% efficient but particles below 70 MeV were not counted. An energy cut off of 135 MeV was applied to the gamma counters when they were detecting pions, assuming that this was the energy required to reach this type of counter. The gamma counters were also assumed 100% efficient for detecting pions, as were the droop counters.

As a result of the tests carried out on the gamma counters in a beam of gammas, formulae for the detection efficiency of both the cylinder and the lid counters were found empirically. These were used as probability

functions in determining whether a gamma was detected by the gamma counters. In addition, gammas were able to give a signal in two adjacent counters and the probability of this effect in the two types of gamma counter was evaluated from the tests and introduced into the program. To decide on which side the gamma 'doubled' the label given to a particle in subroutine NICOLA was used. This label indicated on which side of the counter the particle entered and this was taken to be the side to which it might spread. The twentieth gamma counter was treated separately by the program as indicated by Section (4.4).

The values of MIC(I) and MOC(I) were reassessed by passage through this part of the subroutine and values of 1 and 0 used to indicate the detection of the particle by the corresponding parts of the apparatus. In the case of a gamma doubling, an extra particle was created with unspecified physical properties but counted as being present in the event.

The re-definition of particles was as follows :

MIC(I)	= 1,	MOC(I)	= 1	pion
MIC(I)	= 0,	MOC(I)	= 1	gamma
MIC(I)	= 1,	MOC(I)	= 0	delta
MIC(I)	= 0,	MOC(I)	= 0	particle lost altogether.

Particles were re-defined if they entered the same counter as another by their effect upon these labels :

$\Pi\Pi$	$\rightarrow$	Π
$\gamma\gamma$	$\rightarrow$	γ
$\Pi\gamma$	$\rightarrow$	Π
$\Pi\delta$	$\rightarrow$	Π
$\delta\gamma$	$\rightarrow$	Π

A study of the data obtained in the preliminary runs with the apparatus

in the experiment introduced other effects than those so far included and in addition to the one which was to be expected, which was the passage of a pion through the region of overlap of the lid and cylinder gamma counters. This last effect made a pion look like two pions and a gamma like two gammas also. The other effects were as follows :

(i) $\pi \rightarrow \pi\gamma$ A pion passing through the system gave rise to a count in an adjacent gamma counter.

(ii) $\pi \rightarrow \pi\delta$ A pion gave rise to a count in an adjacent innercharged counter.

(iii) $\pi \rightarrow \delta$ A pion failed to be detected by a gamma counter because it passed between two of them or failed to be detected by one.

(iv) Extra δ Extra inner charged counts appeared in events and were not next to another particle. There could have been several causes, either a beam pion giving rise to a delta ray or a decay particle giving rise to a delta in passing out of the target and through the air to the detecting counter.

(v) $\pi \rightarrow \pi\pi$ An effect where a pion doubled.

These effects were studied and evaluated empirically, as discussed in Chapter (V). The effects were built into the program and used in the final output matrix. All these effects together with gamma doubles and the inefficiencies of the counters and the system geometry served to smear the appearance of a simple decay mode. A large matrix accumulated events in a manner which described their ultimate appearance and this was printed out at the end of the program. The matrix identified events and listed them in an array showing the numbers of the following in each event :

$$\pi\ (\pi_\gamma)(\pi_\delta)\ \ \delta\ \ (\gamma_2)\ \ \gamma$$

where γ_2 indicated where two gammas were in adjacent counters, the gammas then not being counted separately.

2.8 Conclusions

With the parameters L1, L2, L3, L4, and L5, together with the masses of the decay particles, the program was capable of generating complicated decay modes and subjecting them to a very realistic scrutiny for inefficiences in detection and other effects. The output matrix of the program listed the numbers of events of the various types described that the real decay process looked like and this was directly comparable with the data output from the on-line computer to the experiment.

CHAPTER III

THE EXPERIMENTAL STUDY OF THE BEHAVIOUR OF THE GAMMA DETECTORS

3.1 Introduction

In order to interpret the data which it was hoped that the main experiment would produce, the efficiency response of the two types of gamma counter was needed. The most critical region was for low energies where the efficiency curve rose steeply to the knee of the plateau and, consequently, an experiment was designed to study this crucial region. Several counters of both cylinder and lid types were placed in a beam of gammas obtained at the Rutherford High Energy Laboratory.

The experiment was also designed to measure the effect of gamma doubles. A shower of electrons in a gamma counter, initiated by a gamma ray entering, was capable of spreading to the neighbouring counter in a substantial number of cases. This effect was referred to as the doubles probability and was found to increase fairly rapidly in the energy range of this experiment, without reaching a plateau. Consequently, a further experiment was designed to take place in the partly constructed framework of the main experiment, which was still in its preparatory stages.The purpose of the second experiment was to study the doubles probability at higher energies and as a function of the angle of incidence of the gamma.

The energy range of the 'low energy experiment' was from 30 to 156 MeV, whilst the gammas in the 'high energy experiment' had energies ranging from 560 to 1500 MeV. Both the experiments became known by the Rutherford Laboratory as $\Pi 7\gamma$.

3.2 The Beam Line of the Low Energy Experiment

The conditions of this experiment were far from ideal, in that the beam

line was strictly parasitic. In the first instance, there existed only a hole in the shielding wall around the extracted proton beam from Nimrod, which was used for monitoring background intensities. The hole lay on a line subtending an angle of 120^{o} to the direction of the extracted proton beam. Consequently, beam rates were very small but, nevertheless, a slow yet workable beam of low energy gammas was constructed which remained as a permanent parasitic facility.

The beam line is shown in Fig. (3.1). The extracted proton beam was incident upon a copper target, two of which were being used alternately. The larger measured 100 x 10 x 10 mm whilst the smaller measured 32 x 3 x 3 mm. Negatively charged particles emerging from the hole were selected by the bending magnet, BM1, placed close to the hole. A second bending magnet, BM2, placed some two metres downstream of BM1, produced a horizontal momentum spread of the negatively charged particles passing through it. A narrow momentum band was selected by a counter telescope and precise settings of the magnet currents.

The counter telescope consisted of two counters (1) and (2), defining a narrow beam between the two magnets whilst a halo counter (3) was introduced to veto any beam particles which might have collided with the sides of BM2. This second magnet was used to deflect the beam through 30^{o} and so the second part of the telescope (4), (5) and (7) defined such a beam using three counters to limit accidental coincidences. A very large counter was placed between the hole in the wall and the furthest end of the gamma trigger to limit any background present. The last counter in the telescope, (7), was approximately two metres from BM2.

Immediately following counter (7), was a thin piece of copper, referred to as the radiator, and then a piece of perspex, referred to as the absorber. Following these were two large veto counters (8) and (9) and then a small

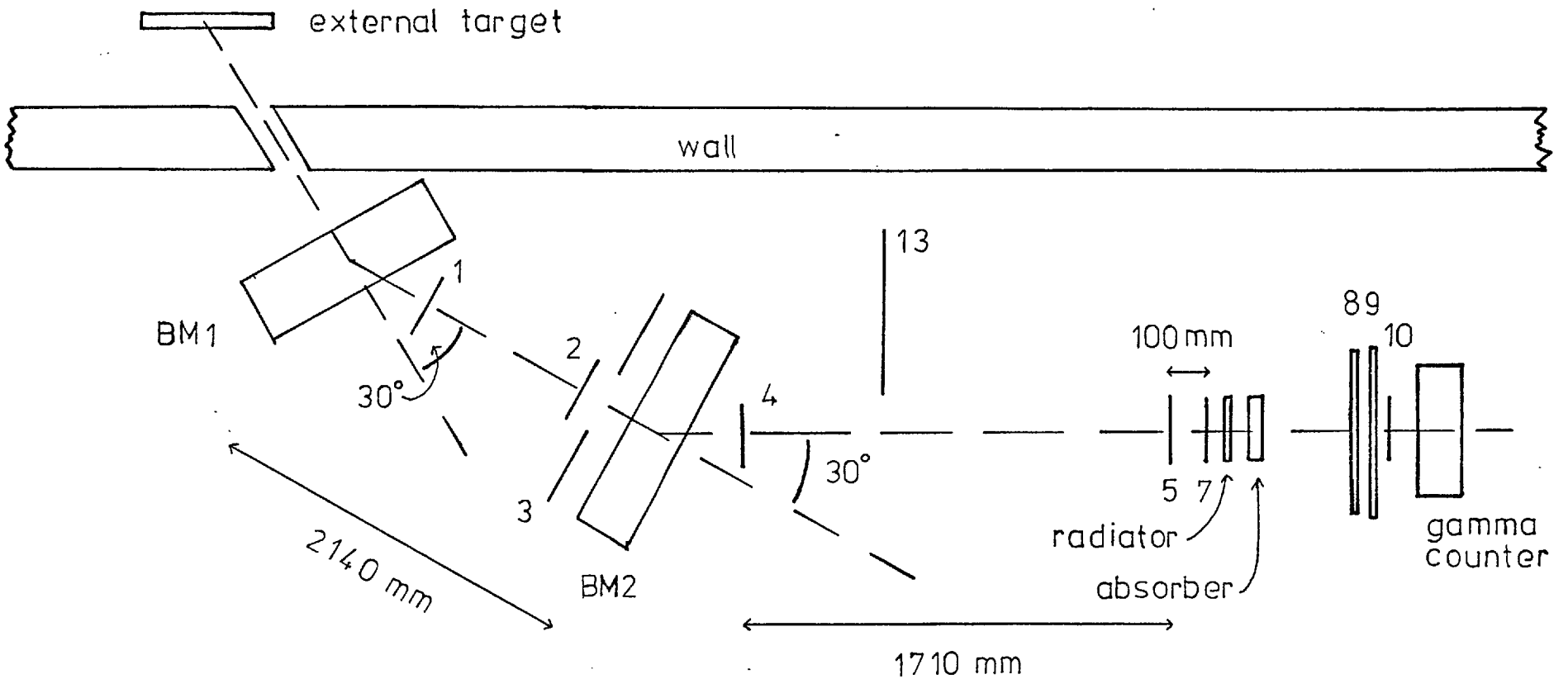

Figure 3.1

$\Pi 7_\gamma$ Low Energy Beam Line

monitor counter (10) whose purpose was to monitor the failure rate of $\overline{(8 + 9)}$ by counting electrons which had not been vetoed.

All the beam counters were made from scintillator 50 mm square and 2.5 mm thick. The halo counter (3), was 300 mm square and 10 mm thick with a central hole 50 mm in diameter. Counters (8) and (9) were 305 mm square and 10 mm thick.

The counter telescope was used to define a beam into and out of BM2 which, therefore, selected a narrow momentum bite of about 10 MeV/c which could be varied by varying the current in BM2. The time of flight technique was used to select the electrons in the beam and so a near monoenergetic beam of electrons entering counter (7) was obtained. The piece of copper following this counter was 1.5 mm thick or $\frac{1}{8}$ radiation length and was the same size as (7). The 25 mm of perspex, equivalent to 0.06 radiation lengths, was also the same size as (7). Their purpose was to cause some electrons to radiate gammas by the Bremsstrahlung process[10], [11]. An electron passing close to a nucleus was slowed down and a gamma ray emitted. This gamma tended to be at a very small angle to the path of the electron, especially when converting most of its energy in this way. The gamma was emitted into a cone of semi-angle of $\frac{mc^2}{mc^2+T}$ [12], where m was the electron mass and T its kinetic energy.

The large nuclei of the radiator were more likely to cause a Bremsstrahlung gamma than the absorber. The purpose of the latter was to provide atoms for ionisation by the escaping electron. If the electron had given up most of its energy to the gamma ray, it could be absorbed. The energy loss by ionisation through such a thickness of perspex was about 5 MeV. An electron which did not radiate most of its energy would have escaped easily as the thickness was small. It was important that the electron should have radiated only once to have the correct energy

assigned to the gamma produced. Electrons could scatter in the radiator and absorber and so affect the cleanness of the gamma beam. A sodium iodide crystal was used to detect the beam of supposed gammas and the efficiency of the crystal in the beam measured. This could then be compared to its known theoretical efficiency to establish that the gamma trigger was working well, (Section 3.3). Several thicknessess of radiator and absorber were tried experimentally and the selection made on the basis of obtaining as many gammas as possible, but with as narrow an energy spread as possible.

The veto counters detected the electrons that either failed to radiate or failed to radiate sufficient energy to be absorbed. The maximum energy of the gamma produced was that of the electron, but the spread below this depended on the most energetic electron which was capable of producing a gamma and just being absorbed by the abosrber. Only a small loss in energy was possible in the transfer, less than 10 MeV, and so, by selecting an electron which stopped in the absorber a nearly monoenergetic beam of gammas was produced in a very forward direction.

The electron beam rate at 80 MeV/c was 5 electrons per burst with the smaller target whilst, with the larger target, there were 10 electrons per burst. The beam diverged from its focus, which, by extrapolation, was found to be somewhere in the hole in the wall, in such a way as to give a vertical full width at half height of 70 mm and not 50 mm, the size of counter (7). A very small angular spread was included in this, due to the production of the gammas.

The background in a gamma counter from non-beam counts was found to be negligible. The failure rate of the $\overline{(8 + 9)}$ veto was measured and found to be 2.2 in every 10^4 electrons. This corresponded to a figure of 5 gammas produced in every thousand electrons and so was an inefficiency of

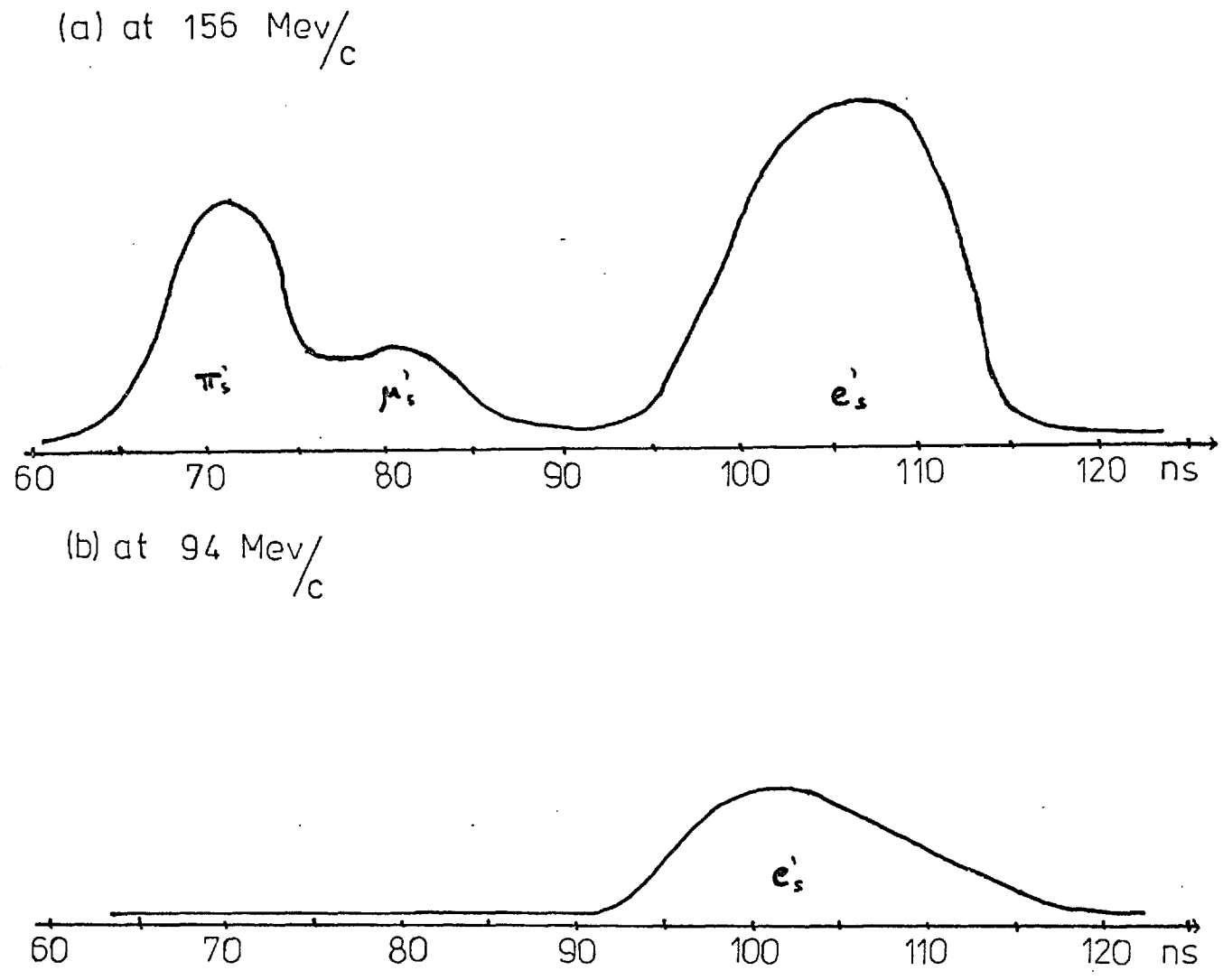

Figure 3.2

Time of Flight Spectra

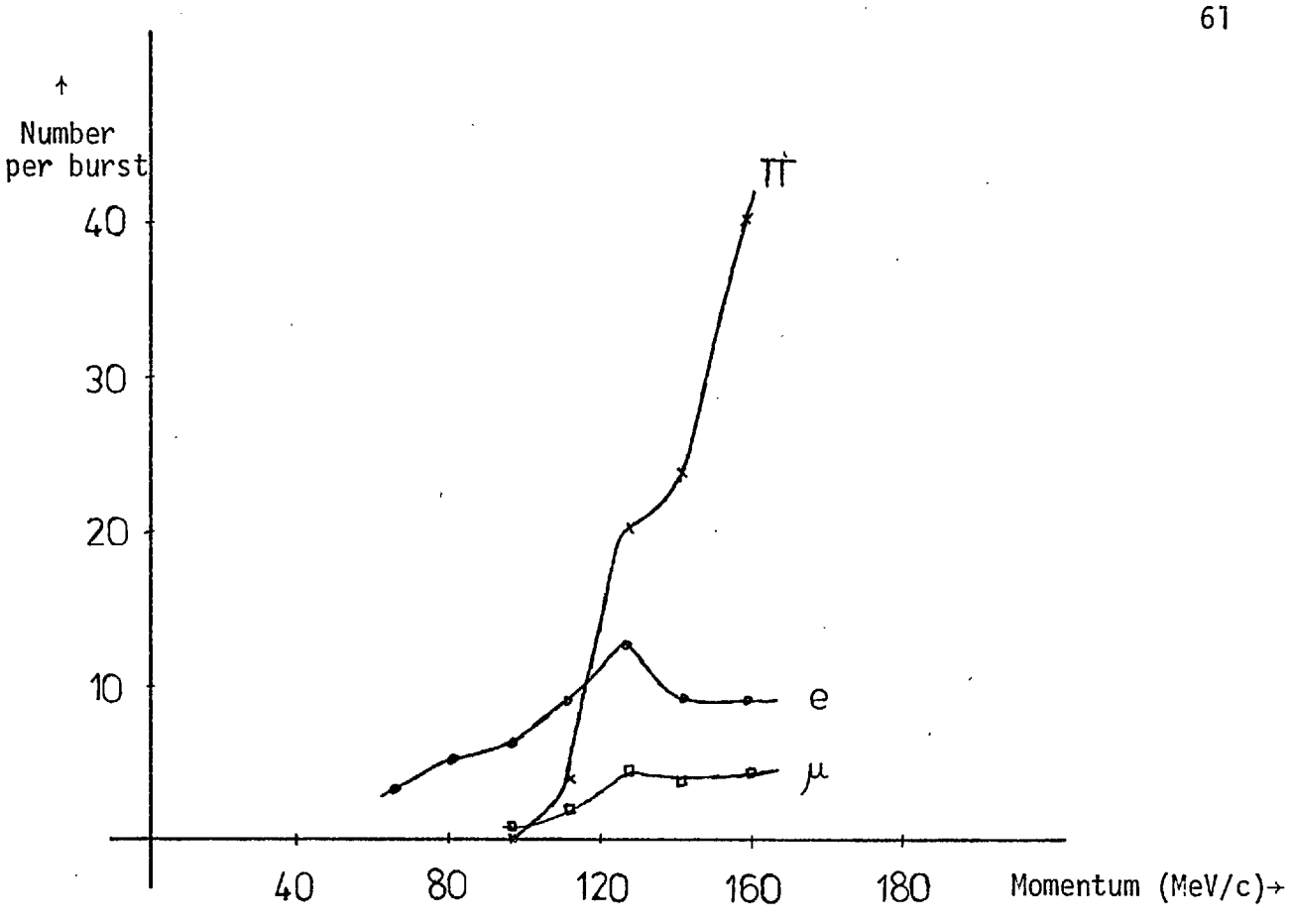

Figure 3.3

about 4%. Consequently, the inefficiency was measured during every run. In the analysis such an electron was considered to be detected with 100% efficiency and so it was subtracted from the gamma counts observed and from the number of beam triggers.

The constituents observed in the negatively charged beam were electrons, muons and pions. As mentioned above, the electrons were selected by positioning a timing gate around the electron peak and selecting only these triggers. Fig. (3.2) shows the time of flight spectra whilst Fig. (3.3) shows the yield of pions, electrons and muons against momentum. The peak yield of electrons was about 125 MeV/c. Below 90 MeV/c, only electrons were observed, whereas, at 125 MeV/c, the beam consisted approximately of

10% muons, 35% electrons and 55% pions.

3.3 The Purity of the Gamma Trigger

The efficiency of a sodium iodide crystal in a beam of gamma rays was known theoretically[14]. By comparing the measured efficiency of such a crystal with theory, confidence in the gamma trigger could be established.

Consequently, a sodium iodide crystal, 150 mm in diameter and 150 mm long, was placed in the beam line and its efficiency for detecting single gamma rays was measured. The measured and calculated efficiencies are shown in Fig. (3.4). The experimental results differed from the predicted efficiency curve only at momenta below 60 MeV/c.

As discussed in the previous section, the energy transfer process and the possible production of more than one Brehmsstrahlung gamma affected the correct assignment of energy to a gamma. This had most effect at the low energy end of the spectrum at or below the knee of the efficiency plateau. In addition, the calculations for the theoretical efficiency were based upon an infinite plane of sodium iodide. The real physical size of the crystal served to reduce the real efficiency compared to the theoretical one.

It was, therefore, reasonable to assume that the real and predicted efficiency curves were compatible and all the gamma triggers were in fact gammas. In order to maintain a check on the purity of the trigger, the performance of the apparatus was periodically monitored with the sodium iodide crystal.

3.4 Floating Wire Measurements

Reference has been made to the momentum of electrons in the counter telescope being set by the current setting of the two bending magnets. These were calibrated by means of floating wire measurements in each of the magnets.

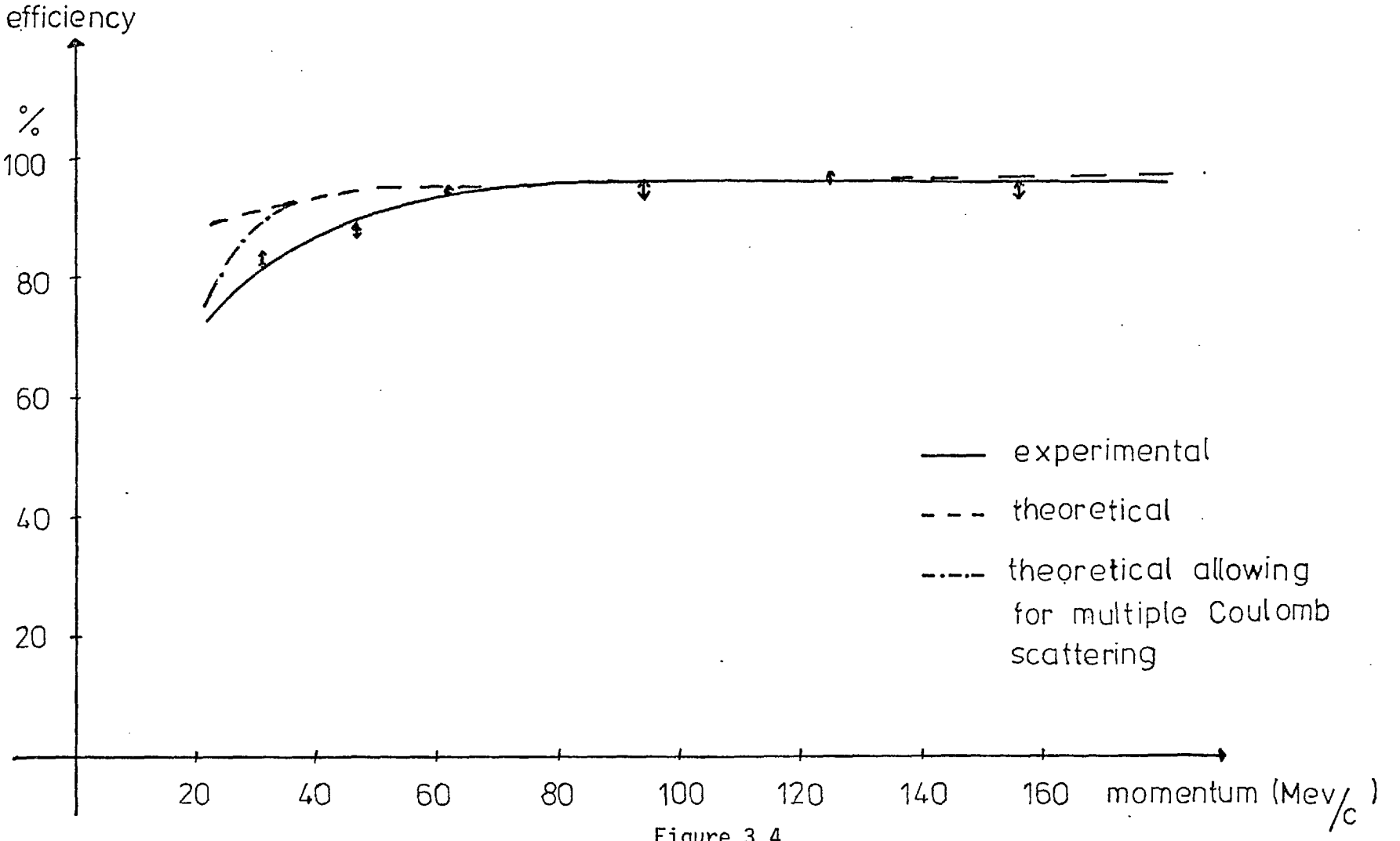

Figure 3.4
Sodium Iodide Curves

To do this for BM1, a wire was attached to a plug in the middle of the hole in the wall and then passed through the magnet past a ruler just outside the magnet edge and then over a pulley. The 'floating wire'[15] could be thought analogous to a particle of known momentum by virtue of the fact that a wire under tension (T gms) and carrying a current (i amps) took up the same trajectory along the beam as a particle of momentum p (MeV/c), such that :

$$P = 2.941 \frac{T}{i} \quad .$$

With a fixed tension of 50 gms, the wire was made to pass along a path from the hole through the positions of the telescope counters around BM1 by means of the fiducial mark on the ruler outside the magnet. Consequently, by varying the current in the wire, a momentum could be selected. The magnet current was then varied until the wire had the required trajectory. It was then this current which was able to produce electrons of that momentum in the telescope.

In order to specify the trajectory of a particle through the counter telescope in BM2, counters (1) and (2) together with a ruler and pulley, were used as fiducials.

Graphs of momentum versus bending magnet current were found in this way, for both magnets and used to select the current settings required to produce electrons of the required momentum.

3.5 The Electronic Logic

The electronic logic is shown in Fig. (3.5). A beam particle entering BM2 was recognised electronically by the coincidence (1) (2) $(\overline{3})$, whilst a particle leaving BM2 through the counter trigger was defined by (4) (5) (7) $(\overline{13})$. As a result, a coincidence that occurred within a selected

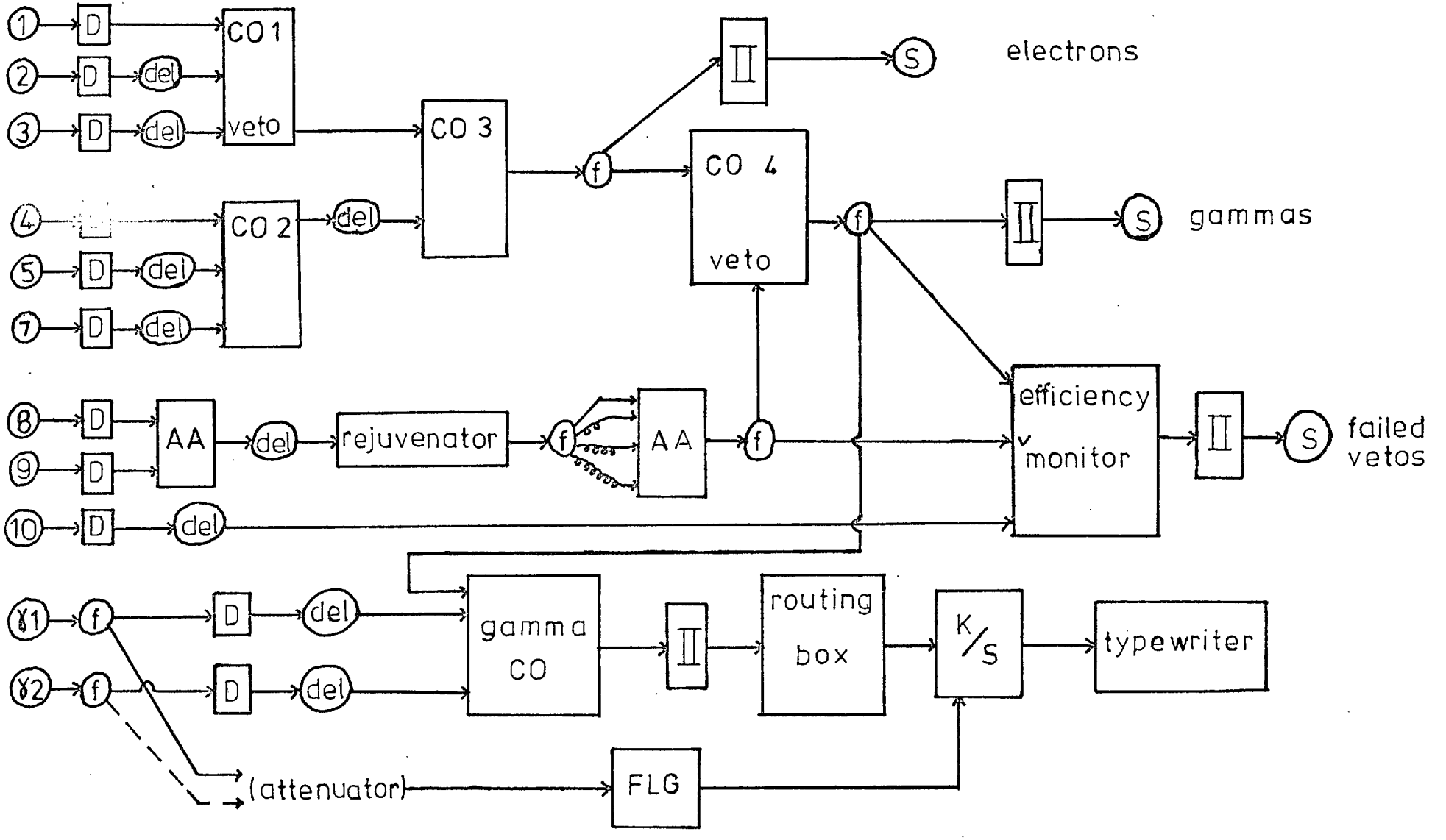

Figure 3.5

Electronic Logic for the $\pi 7\gamma$ Low Energy Experiment

time of flight gate was defined as an electron by :

$$(1).(2).(\overline{3}).(4).(5).(7).(\overline{13})_{TOF} \quad .$$

Consequently, a gamma was defined by this time of flight coincidence together with vetos in (8) and (9), that is, as :

$$(1).(2).(\overline{3}).(4).(5).(7).(\overline{13})_{TOF} \; (\overline{8}).(\overline{9}) \equiv M/Co \quad ,$$

whereas failed vetos were defined by :

$$(1).(2).(\overline{3}).(4).(5).(7).(\overline{13})_{TOF} \; (\overline{8}).(\overline{9}).(10) \quad ,$$

or $\quad M/Co \; . \; (10) \quad .$

If the beam then entered a gamma counter (γ_i) which was adjacent to a second gamma counter (γ_j), then the efficiency of γ_i at the point of entry of the beam was given by :

$$\eta = \frac{M/Co \; . \; (\gamma_i)}{M/Co} \quad ,$$

and the doubles probability was given by :

$$\frac{M/Co \; . \; (\gamma_i) . \; (\gamma_j)}{M/Co} \quad .$$

The logic thus measured the ratio of gamma rays detected to those entering the counter as the singles efficiency. The kicksorter built up a histogram of these events by sorting the pulse heights of the signal detected. If, however, a double gamma was detected, that is, a gamma was detected by two neighbouring counters, the kicksorter re-routed the signal to another histogram where it was sorted according to the pulse height in the first counter. Consequently, the singles efficiency was given by totalling detected events of both types, whereas the doubles probability was found only from the latter block. Events which failed to be detected altogether still entered the first histogram but were sorted into a zero pulse height, called the pedestal. The number of events detected by M/Co was equivalent

to the pedestal plus the events in both the other blocks. Failed vetoes were taken to be electrons which failed to be detected by (8) and (9). Consequently, they had to be subtracted from the gamma trigger (M/Co) and from the non-pedestal events, presuming that they would have succeeded in being detected by the gamma counter, as they did not require conversion.

There was no pedestal in the doubles histogram as the routing was done by a signal being present in the second gamma counter large enough to trigger its discriminator[13], [16], and this, therefore, presumed a signal present in the first counter to give rise to the signal in the second.

3.6 Efficiency and Doubles Probability Measurements

The first tests were on the cylinder gamma counters with a normally incident beam. Two counters were placed side by side and the beam was then directed centrally into one, then at the junction between the two counters and finally, into the centre of the second counter. This was repeated with the beam incident at an angle of 54^{o} and then repeated at different energies. Both angles of incidence were used to make the same measurements for other pairs. The procedure was repeated for several pairs of lid gamma counters, where the angles of incidence used were 0^{o} and 41^{o}. The maximum angles of incidence into cylinder and lid gamma counters were approximately 63^{o} and 45^{o} respectively and hence the choice of these particular angles.

The measurements made with the beam centrally placed through a counter gave a measurement of singles detection efficiency and doubles probability for gammas entering a 50 mm square region at the centre of the counter. At the junction, the same measurements were obtained, but due to the magnitude of the doubles effect, this was done in two separate ways. Firstly, the raw pulse of one of the pair of counters was examined, whilst the discriminator

of the other was used to route the information according to whether a double was registered. Then, the signal cables were changed over so that the raw pulse of the second counter was examined, whilst the discriminator of the first was used for routing purposes. This gave two measurements of both the efficiency and the doubles probablity in this crucial position.

In order to estimate the effect of the core of duralumin upon the efficiency of the gamma counters, a piece of duralumin the same thickness was placed in front of the gamma counters being tested. An increase in efficiency of less than one standard deviation was observed. As an increase of less than 1% was expected, the core was assumed to have a negligible effect upon counter response. At 500 MeV, the probability of pair production was 60% per radiation length, and only 5% at 40 MeV, whilst the aluminium present was only approximately a tenth of a radiation length.

3.7 The High Energy Experiment Beam Line

The beam line, shown in Fig. (3.6) was the same as that used for the main experiment, upstream and inclusive of the momentum telescope and this portion is discussed in Section (1.3). Effectively, a beam of negative particles consisting of 80 - 90% of negative pions, less than 1% of negative kaons and about 10% of electrons, with some muons, was transported to a Cerenkov counter, C_1, which was 3.05 metres long, 200 metres in diameter and filled with carbon dioxide at two atmospheres pressure. After C_1, there was a momentum telescope consisting of a series of magnets, a collimator and two hodoscopes.

From then on, the beam line was intrinsic to this particular experiment. The beam so far was designed to select negative pions and it was found not to select electrons efficiently enough to produce a sufficiently clean

Figure 3.6

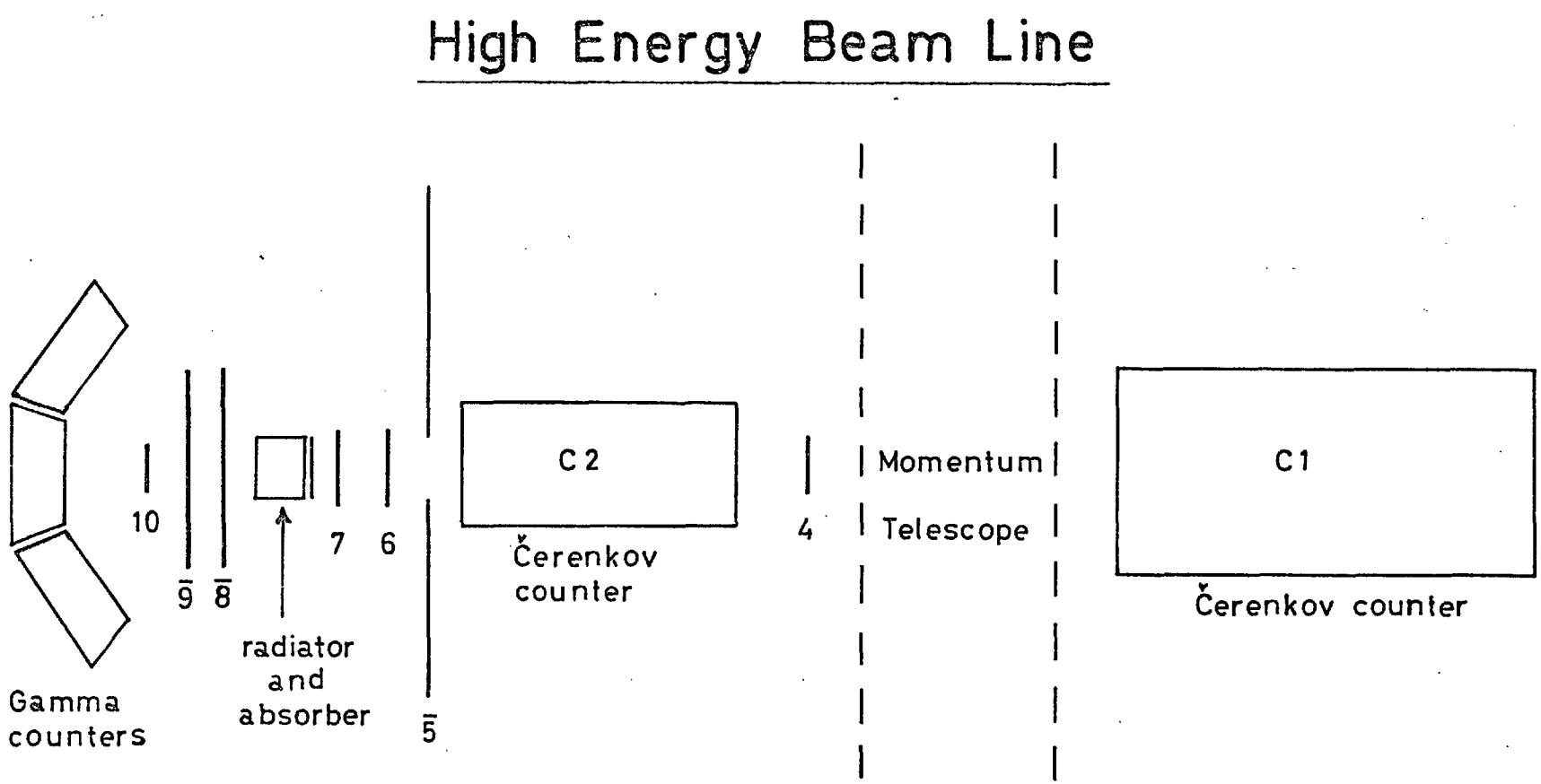
High Energy Beam Line
10
9̄
8̄
7
6
5̄
C 2
Čerenkov counter
4
Momentum Telescope
C 1
Čerenkov counter
Gamma counters
radiator and absorber

gamma trigger. Consequently, the beam line was extended through a beam defining counter (4) to another smaller Cerenkov counter C_2, 90 mm in diameter and 1 metre long, containing air at four atmospheres pressure. This counter was then used for identifying further electrons.

A halo counter (5) was used in conjunction with a second beam defining counter (7) to define the entry of an electron into the radiator and absorber immediately following counter (7). The radiator was a piece of copper 50 mm square and 1.5 mm thick whilst the absorber was a block of perspex immediately following the radiator and was 57 mm thick. Their cross sectional area was the same as counter (7). There were 0.12 radiation lengths of copper and 0.13 radiation lengths of perspex making 0.25 radiation lengths in all.

Next were the veto counters, (8) and (9), used in the low energy experiment, as well as the monitor counter (10). Counters (4), (7) and (10) were 50 mm square and 2.5 mm thick whilst the veto counter (5), used to eliminate beam associated background, was 300 mm square, 10 mm thick and had a circular hole 50 mm in diameter in the middle.

Just upstream of counter (7) was placed another counter (6), which was 2.5 mm thick, 50mm in vertical height but only 6 mm in horizontal width. This counter was used in conjunction with counter (7) to define a specially narrow beam when required for detailed counter response over the counter width.

The gamma counters were mounted on a specially constructed rig which allowed easy translational movement across the beam of three heavy gamma counters placed side by side. The rig also allowed the three counters to be set at various angles to the beam.

The $\overline{(8 + 9)}$ veto was found to be efficient to one part in 10^5 or to have a failure rate equivalent to less than 1% of the gamma triggers. The inefficiency of counter (5) was found to be less than one part in 10^3. The

beam was defined in size by the 50 mm diameter hole in counter (5), together with the 50 mm square counter (7). When the horizontal beam size was measured, it was found to be 45 mm full width at half height.

3.8 The High Energy Logic

The electronic logic is shown in Fig. (3.7). The gamma trigger was defined by M/Co where :

$$M/Co = (4).(7).(\overline{5}).(C_1).(C_2).(\overline{8}).(\overline{9}) \quad ,$$

whilst the narrow beam was defined by M/Co . (6).

As before, the kicksorter examined the raw pulse of one counter whilst using the discriminator of a second to re-route the pulse to a second block of data in the case of a double signal. In addition, the discriminator of the third counter was used to re-route the pulse into a third block if this was triggered as well. There were two types of trebles and both were capable of detection by the kicksorter. The first type was where a gamma initiated electron shower spread from the counter of entry in both directions, thus giving a signal on either side. The second type was where the electron shower spread from the initial counter through its neighbour into yet another counter.

The kicksorter, consequently, produced three histograms. The first contained the pedestal and singles count in the initial counter where no second or third counters also fired. The second contained the doubles counts where there was no third counter with a signal, whilst the third contained trebles only.

Singles efficiency was, therefore, given by :

$$M/Co \cdot \frac{[\gamma_1 + \gamma_1.\gamma_2 + \gamma_1 \cdot \gamma_2 \cdot \gamma_3]}{M/Co} \quad ,$$

whereas doubles were counted as :

$$M/Co \cdot \frac{[\gamma_1 \cdot \gamma_2 + \gamma_1 \cdot \gamma_2 \cdot \gamma_3]}{M/Co} \quad ,$$

Figure 3.7

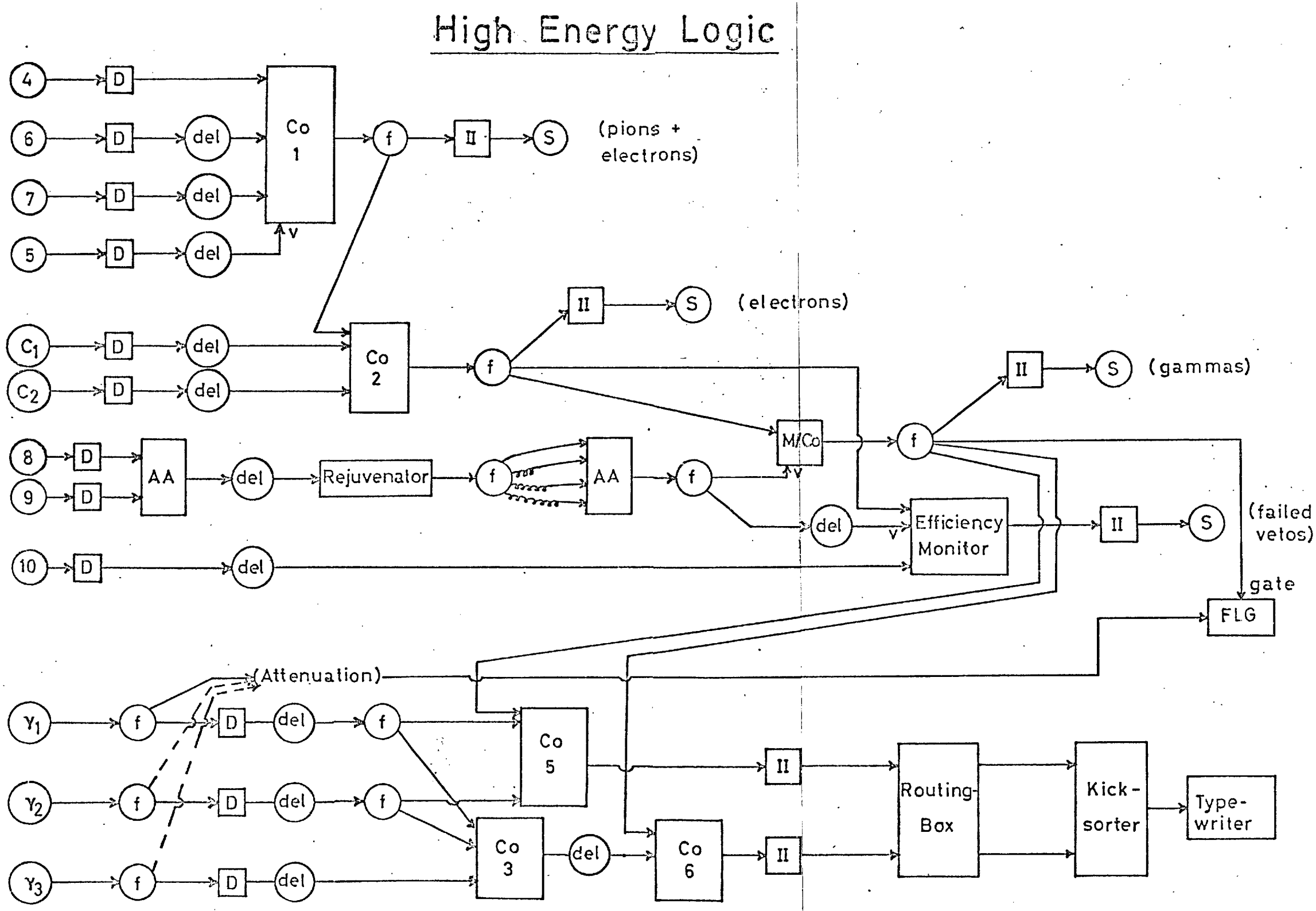
High Energy Logic
4
6
7
5
D
del
Co 1
v
f
II
S
(pions + electrons)
C1
C2
Co 2
(electrons)
8
9
AA
Rejuvenator
10
M/Co
Efficiency Monitor
(failed vetos)
gate
FLG
(Attenuation)
γ1
γ2
γ3
Co 5
Co 3
Co 6
Routing-Box
Kick-sorter
Type-writer
(gammas)

and trebles counted as :

$$\frac{M/Co \cdot \gamma_1 \cdot \gamma_2 \cdot \gamma_3}{M/Co} .$$

Care was taken in defining the pedestal as there were pulses of all sizes, including very small ones, as well as zero pulses. The method of defining the pedestal used is described in Section (3.10).

3.9 Measurements made at High Energies

The high energy experiment was not merely an extension of the low energy experiment but involved more detailed examination of the counters in the higher intensity beam. The energies used for measurements were 560, 900 and 1500 MeV. The basic measurements made were for singles efficiency and doubles probability at these three energies for normal incidence and one other angle. The cylinder gamma counter measurements were at 54^{o} and the lid gamma counter measurements were at 41^{o} to correspond to the low energy data.

The positioning of the beam gammas at the junction of two counters was critical to the doubles measurements and a criterion was adopted for the selection of good data. Some gammas were lost between the counters, but at high energies, this was a small effect. Consequently, the zeros (or pedestal) when one counter was examined corresponded to gammas that had entered the other and were then counted as singles in it. Therefore, the ratio of zeros to singles $(\frac{z}{s})$ in one counter should have been approximately unity if the beam were centrally positioned on the junction. Hence, the criterion adopted was that :

$$\frac{z_1}{s_1} \sim \frac{z_2}{s_2} < 2 .$$

Otherwise, the basic measurements made were similar to the ones made

in the low energy experiment. With three counters of one type positioned side by side, three centre measurements were made, one in each counter. This was followed by two sets of junction measurements, each set consisting of a measurement made by one of the adjoining counters and then by the other.

In addition to these measurements at the energies and angles already specified, narrow beam scans were also made, using the same angles and energies to study the counter response along its width in more detail. Such scans were made at both ends of the counters to examine any differences and both singles efficiency and doubles probability were measured each time.

The most critical region for the occurrence of trebles was at the narrowest counter width; that is, at the tip of the lid counters where the scintillator was only 30 mm wide. Even here, the trebles probability was found to be $< \frac{1}{2}\%$ and so this effect was not pursued after this fact had been established.

Another important series of measurements were made and this was to study the doubles probability as a function of angle in the two types of counter, in detail.

Initially, the data obtained for the doubles probability were statistically inconsistent, this being the most critical measurement at these energies. The selection criterion for junction measurements mentioned above improved the statistical fluctuations but not sufficiently. As the EHT had been set by inspecting the efficiency versus voltage curve of the counters and choosing a value such that the counter was set in the plateau region, and readily sensitive to a single electron passing through a single layer, this left quite a possible variation in EHT on this plateau. The doubles probability curve was not found to reach a plateau in the energy range studied and so the precise EHT setting could have affected the doubles probability measurements made. Consequently, a more rigorous criterion for setting EHT was chosen

and this is described in Section (3.10). As a result, the differences in the doubles probability measured by different counters of the same type became insignificant. However, there was still a measureable difference between the doubles probability measured by the two different types of gamma counter.

3.10 The EHT Settings

The usual procedure for setting the EHT of a counter was to set to a position on the plateau of the efficiency versus EHT curve for a particular counter. As the noise in a photomultiplier tube increased with increasing EHT, the position chosen was just a little above the knee of the plateau. The doubles probability verses EHT, was a steadily rising curve which did not reach a plateau within the operational range of the photomultiplier used. In the normal range of use, the doubles probability was found to increase by approximately 2½% per 100 volts at the junction. This was quite a large change for such a small change in voltage, and so a voltage setting criterion was essential.

The problem was that there existed two contradictory requirements on the counters. The first was that the singles efficiency should have been as high as possible and well over the knee of the plateau so that small voltage fluctuations would not affect the stability of the efficiency. The second was that the presence of a large doubles probability would have impeded the definitive analysis of data in the main experiment. Consequently, this required the EHT to be as low as possible in order to reduce the doubles effect as much as possible.

In the low energy experiment, a criterion had been chosen such that the counter was able to detect the passage of a single electron passing normally through a single layer of scintillator. In order to set the EHT to this criterion of efficiency, holes had been cut in selected layers of

lead in the counters, as described in Chapter (I). These holes were made to allow the insertion in each counter of a small source of electrons. The electrons passed freely into a layer of scintillator and were detected by a counter placed directly above the source.

The raw signal from the gamma counter was fed into the kicksorter and accepted only if it coincided with an electron reaching the detecting counter above the gamma counter. The signal from the gamma counter was also passed through a discriminator to a coincidence unit with a similar signal from the detecting counter. This coincidence was then used to route the kicksorter so that one histogram compiled pulses failing to fire the discriminator, called the pedestal, which were undetected by the electronic logic, whilst a second histogram compiled pulses that actually triggered the gamma counter discriminator. If the two pairs were superimposed on each other, the point where the two curves crossed, called the 50% point, was where the pulse height in the gamma counter was such that it stood a 50% chance of triggering or failing to trigger the discriminator. From the curves, (shown in Fig. (3.8)), the zero pulse height position was measured (z) and then the distance of the cross over point (D) from it. A study of pulse heights without the routing being introduced, was used to estimate the distance of the most common pulse height from the pedestal (M).

The ratio $^{M}/_{D}$ was then found and if this ratio was equal to one this meant that the mean pulse height had a 50%chance of being detected. A value greater than one meant that the counter was more sensitive than this. In the low energy experiment, values greater than unity had been used and so this meant that an electron passing normally through a single layer of scintillator had better than a 50% chance of being detected. For subsequent measurements in the high energy experiment, a compromise was necessary so that a little low energy singles efficiency was lost for the sake of reducing the doubles probability. Values of $^{M}/_{D}$ were chosen for the lid and cylinder gamma counters, on this basis. The value chosen was different for the two

Figure 3.8

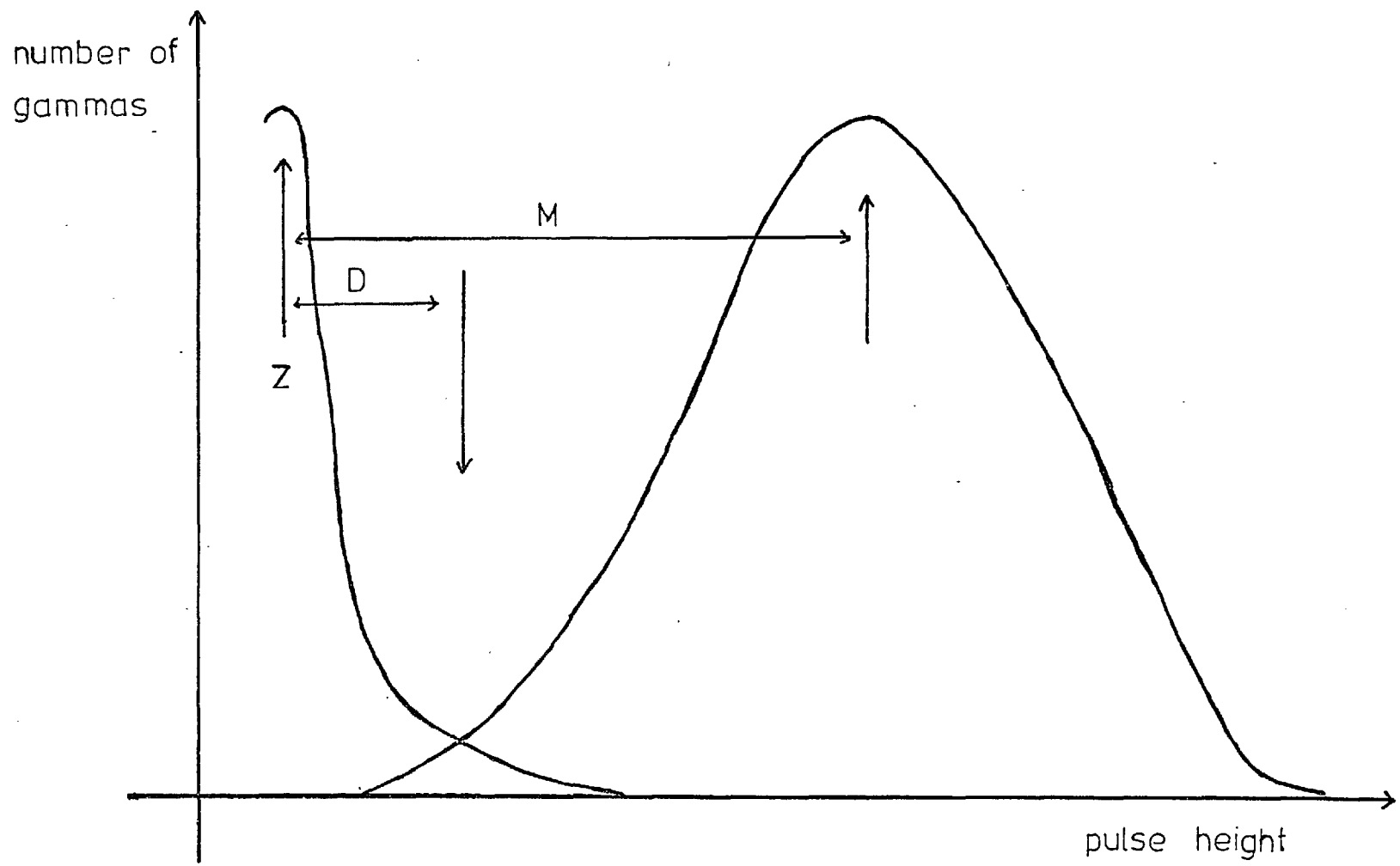

types, namely 2.0 and 0.9 respectively for reasons discussed below. With the counters set to these values, the apparent differences between counters of the same type disappeared. The particular values for $^{M}/_{D}$ were arbitrarily selected by examining the low energy singles efficiency in both counters and weighing againstthis the different doubles probability curves observed in the two types of counter. The $^{M}/_{D}$ value could have been changed considerably without making very much difference to the singles efficiency whereas the doubles probability was greatly affected. Consequently, the cylinder value of $^{M}/_{D}$ was quite large to reduce the considerably larger doubles probability in this type of counter.

The data obtained in the low energy experiment and during the earlier part of the high energy experiment were still of great value because, knowing the value of $^{M}/_{D}$ for those measurements it was possible to compensate for the different values by changing the effective discrimination point in the histograms obtained. As the purpose of the study of the $^{M}/_{D}$ value had been to reduce the number of double gammas observed, the earlier data had more doubles than the new setting would have produced. The effect of changing the discrimination point was to cut out some of the smaller doubles pulses in the doubles histogram and so this could be done satisfactorily. The data before and after introducing the $^{M}/_{D}$ criterionwere perfectly consistent after these corrections, thus validifying the method used.

The difference between the two types of counter constituted a problem. It could not be explained in terms of the 18^{o} angle between the cylinder counters compared with the planar array of the lid counters. This would have made less than a 5^{o} difference taken from the $^{1}/_{\cos\theta}$ probability curves, as against the real difference of nearly 20%.

A clue to the difference between the two types of counter came from a study of the attenuation of the signal caused by a beam of monoenergetic pions passing normally through the counters at different positions along

their length. Measurements were made with a number of counters of both types and a mean attenuation of the signal for both types found from the variation of $^{\Pi}/D$ against the length. The ratio $^{\Pi}/D$ had the same meaning as $^{M}/D$ but was measured by detecting the signal initiated by pions instead of electrons passing through the counter. This ratio was far more accurate as it corresponded to the passage of a pion normally through six layers, not one, as for an electron, and thus averaged out any differences between individual layers as well as being six times more sensitive. Due to the construction of the counters, the top layer used in the $^{M}/D$ measurements was likely to be less sensitive than a middle layer. The differences between the senstivity of $^{\Pi}/D$ measurements against $^{M}/D$ measurements was also likely to be more pronounced where measurements were made more than 800 mm from the photomultiplier tube and thus less sensitive. In fact, the average equivalent values for $^{\Pi}/D$ where $^{M}/D$ had been set to the values indicated, was 12.8 for lids and 8.9 for cylinder gamma counters.

The results of the attenuation measurements is shown in Fig. (3.9). The values given are of $^{M}/D$ variation with length, calculated from the $^{\Pi}/D$ data. The shape of the curve for the cylinder gamma counters was the expected shape but, for the lid gamma counters, the signal detected by the counter was greater the further the point of entry of the beam from the photomultiplier. It was thought that this effect was the result of some focusing property of the counter caused by its geometry.

The variation in $^{M}/D$ for the lids was between 1 and 2.0, whilst for the cylinders, the variation was from 0.9 to about 1.3. The equivalent change in EHT was about 120 volts for the lid counters and 65 volts for the cylinder counters. The variation in the doubles probability at the junction of the counters at normal incidence, equivalent to a change of 1.0 to 2.0 in $^{M}/D$, and averaged over the two types of counter, was about 3% irrespective of

Variation of M/D with length in cylinder gamma counter

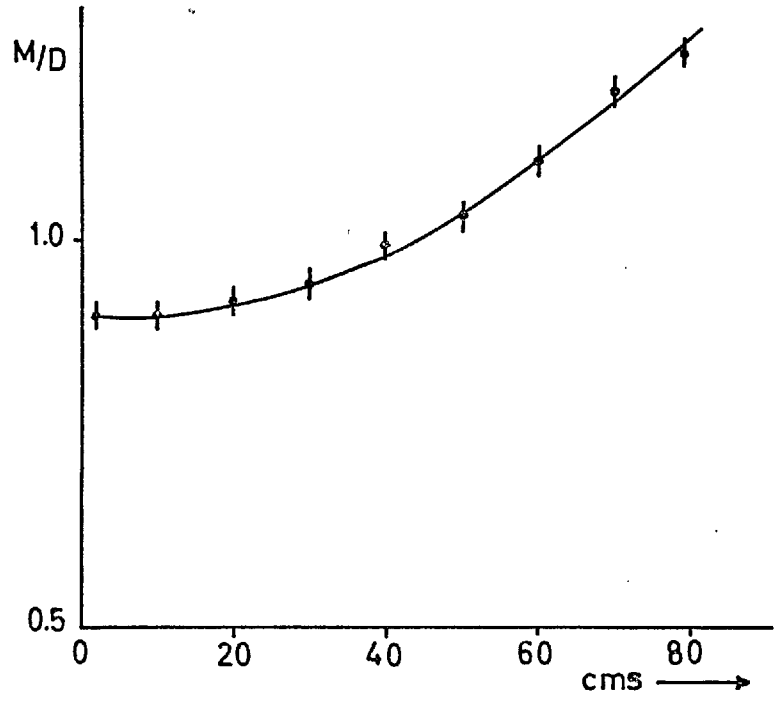

Variation of M/D with length in lid gamma counter

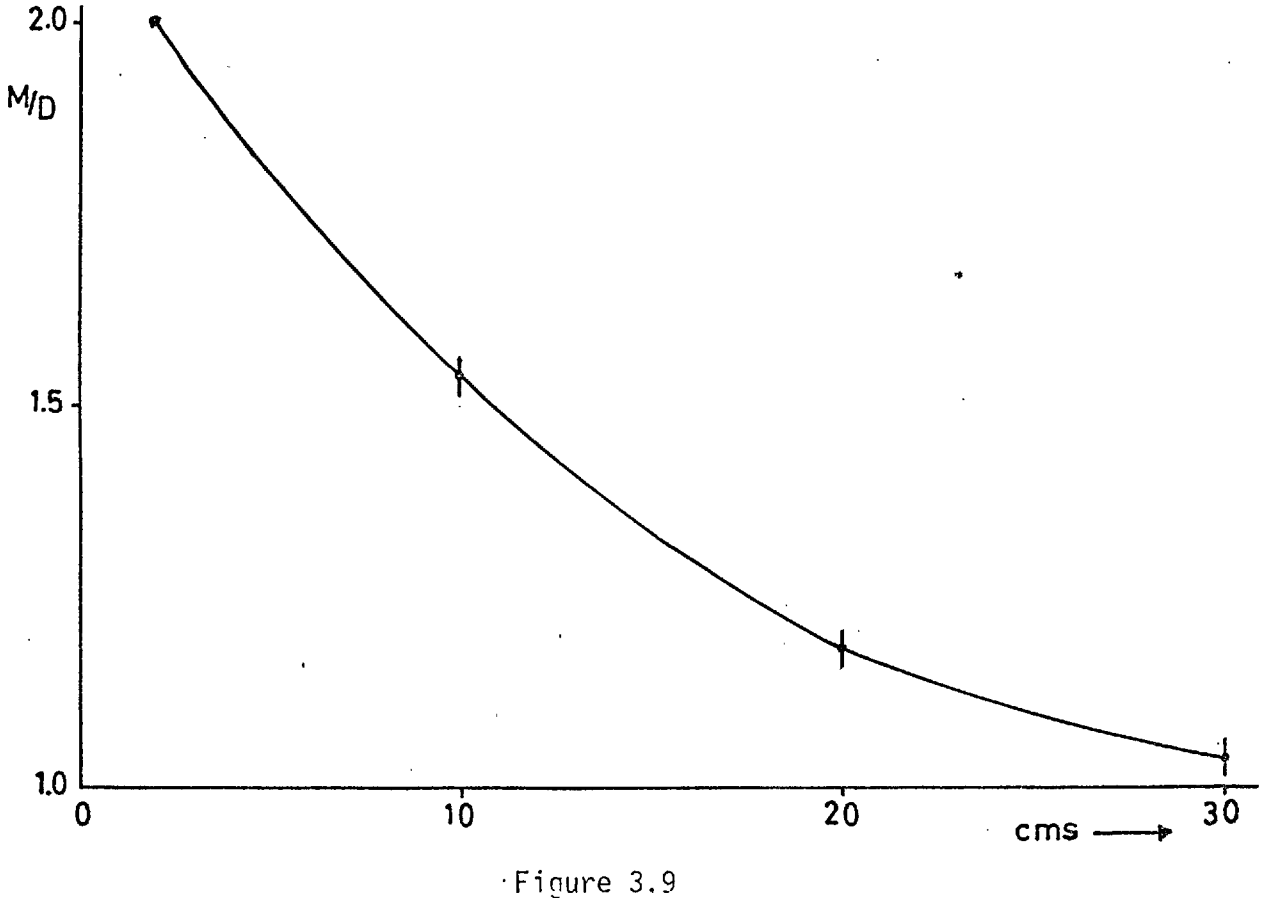

Figure 3.9

momentum. At the centre of the counters, the change was negligible. The junction measurement was, therefore, consistent with the direct measurement of the change of doubles with EHT made in the high energy experiment only.

The difference in the $^{M}/_{D}$ settings between the two counter types would only have caused about 1% difference in the doubles probability and was thus not the cause of the two different doubles measurements. The only explanation was, therefore, that of a geometrical focusing effect. The main requirement of the $\pi 7\gamma$ measurements was to obtain data on the response of the counters so that they were self consistent and reliable. Although this one difference not given an analytical study was a fairly large effect, it was fully investigated quantitatively.

3.11 The EHT Settings for the Main Experiment

The procedure adopted for the setting of the gamma counter EHT's before installation in the array of the main experiment was as follows.

Each counter was taken in turn and its EHT set according to the $^{M}/_{D}$ criterion. Then it was placed in a monoenergetic pion beam and $^{\pi}/_{D}$ measured. From these measurements a mean $^{\pi}/_{D}$ value was found, as discussed in Section (3.10). Any significant variations from the mean were investigated and the relevant counter stripped down for examination. A broken or somewhat crazed layer was identifiable by the change in $^{\pi}/_{D}$ caused and was then replaced. With a value for $^{\pi}/_{D}$ equivalent to the $^{M}/_{D}$ criterion, all the counters were again taken in turn and their EHT reset.

A measure of stability was that a change of 100 volts would have caused a change of about 1% in the doubles probability averaged over the detection area of a counter. This was a small figure compared to the size of the doubles effect.

CHAPTER IV

THE ANALYSIS OF THE $\pi 7\gamma$ EXPERIMENT AND ITS IMPLEMENTATION INTO THE DECAY SIMULATION PROGRAM

4.1 Introduction

The response of the counters to singles and doubles was calculated in detail for both types of counter. Both efficiency and doubles probability were found as functions of energy, angle and position in the counters. Empirical formulae were then developed and written into the Decay Simulation Program to simulate counter response.

4.2 The Singles Efficiency of the Cylinder Gamma Counters

Measurements of the singles efficiency were made at the centre of the counters at the end furthest from the photomultiplier at angles of incidence of 0^{o} and 53.8^{o}. The results of these measurements are shown in Fig. (4.1) as a function of the energy of the incident gamma. Along the plateau, there was a difference of 3% between the two curves.

The singles efficiency at the centre of a counter was measured as the ratio of the number of gammas seen by the counter to the number of real gamma triggers. At the junction of two counters, the singles efficiency was measured by the ratio of the number of real gammas seen in either or both counters to the number of real gamma triggers. With this latter definition, the singles efficiency was found at the junction of two counters as a function of energy at the same two angles. These measurements were also made at the end of the counter furthest from the photomultiplier (see Fig. 4.2).

As both of these measurements were over a 50 mm width of counter and as the actual counter width was approximately 100 mm, the mean of the centre

and junction efficiency measurements gave a figure for the overall efficiency of the counter across its width. Curves showing the difference between the two angle measurements for the full width values of efficiency are shown in Fig. (4.3). Along the plateau, there was a difference of about 4% between the two curves.

The difference between measurements made at either end of the counter's length was negligible as is shown in Fig. (4.4).

Consequently, the efficiency of all the tested gamma counters was averaged over length, width and angle to give a curve which was a function of energy only. Figs. (4.5) and (4.6) show these curves over the whole energy spectrum considered and then in the crucial region of the knee of the plateau. The efficiency curve was found to plateau after about 200 MeV and have an energy cut off at about 20 MeV. Empirical formulae were developed to fit the data over the entire energy spectrum for use in the decay simulation program. They were as follows :

$$0 \leqslant E \leqslant 20 \qquad p = 0.0$$

$$20 < E \leqslant 100 \qquad p = 0.9\ [1 - e^{-(E-20)/20}]$$

$$100 < E \qquad p = 0.975\ [1 - e^{-(E-32)/30}]$$

where E was the energy of the gamma and p its probability of detection.

4.3 The Singles Efficiency of the Lid Gamma Counters

The spread of angles of incidence of gammas entering the lid counters in the main experiment was less than those entering the cylinder counters. The maximum angle of incidence in each case was about 45^{0} and 63^{0} respectively. Exactly the same measurements were carried out for the lid gamma counters except the angles chosen were 0^{0} and 41^{0}.

The efficiency of the lid counters for single gammas is shown in Fig. (4.7) where the gammas were incident upon the centre of the counters

at the two specified angles. The difference between the two curves was about 1% along the plateau. Also shown in the figure is a Monte Carlo prediction of the counter efficiency from a program written by Dr. D.M. Binnie. The program assumed normal incidence of gammas on an infinite plane of lead and scintillator sheets. It also assumed simple formulae for pair production and Brehmsstrahlung cross sections and ignored Compton scattering. In addition, the program scattered all electrons through the mean scattering angle and both electrons and gammas were given energy cut offs of 10 MeV. The statistical error on the curve obtained from the program was about 3% and the agreement between this curve and the data obtained was very good.

The final efficiency curve, showing the energy dependence of the efficiency averaged over counter width and length as well as angle, is shown in Figs. (4.8) and (4.9). The curve has an energy cut off at 20 MeV and levels out at about 150 MeV to 200 MeV. The difference between the efficiency of the cylinder and lid gamma counters was about 1% along the plateau. At 800 MeV for example, the efficiency of the cylinder counters was 97% as against 96% for the lid counters. The difference was within the statistical errors of the data. The cylinder curve would possibly have had a greater plateau value owing to the fact that the angular spread for the incident gammas was larger and the efficiency increased with angle of incidence.

The curves used to fit the data into the program were as follows :

$$0 \leqslant E < 20 \qquad p = 0.0$$

$$20 \leqslant E < 200 \qquad p = 0.94[\,1 - e^{-(E-20)/20}\,]$$

$$200 \leqslant E \qquad p = 1.92 \times 10^{-5} E + 0.9412 \quad .$$

4.4 The Singles Efficiency of the 20th Cylinder Gamma Counter

The response of this counter was not too critical as it was the only

one of its type and used to fill a hole in the detection array. As the Monte Carlo program used to predict the efficiency of the gamma counters gave rise to a curve which compared favourably with the singles efficiency data in the lid counters, this same program was used to predict the efficiency of this counter. The thickness of the lead sheets used and their number were different in this counter and so its efficiency curve was quite different. The curve obtained is shown in Fig. (4.10).

The empirical formulae used in the decay simulation were as follows :

Low Energies : $p_1 = 0.00625\ E - 0.042$

High Energies : $p_2 = 0.00011\ E + 0.845$.

The program calculated both p_1 and p_2 and chose the value of p_2 unless this was less than the value of p_1, when it took that value or zero, whichever was the greater.

4.5 Doubles Probability in the Cylinder Gamma Counters

The doubles probability was measured at the centre and junction of the counters at the same angles as the efficiency was measured, that is, at 0^o and 53.8^o. These measurements were averaged over the length of the counters and the results shown in Figs. (4.11) and (4.12) for the centre and junction respectively. The difference between the curves obtained was considerable. At 800 MeV, for example, the doubles probability at the centre was 6% and 16% at 0^o and 53.8^o incidence respectively. At the junction, the corresponding values were about 38% and 68%.

Fig . (4.13) shows the doubles probability averaged over the length and width of the counters at angles of incidence of 0^o, 45^o and 54^o. These curves did not reach a plateau within the energy range of these tests. The actual angular dependence of the doubles probability was measured in detail (at 900 MeV). As the path length through the counter

was dependent on $^{1}/\cos\theta$, the doubles probability was plotted as a function of $^{1}/\cos\theta$. The resulting data are shown in Fig. (4.14). Less detailed measurements were made at other energies and averaged over the length and width of the counters. The resulting curves are shown in Fig. (4.15). From these two curves, it appeared reasonable to assume that these curves could be represented by two linear portions, one below 45^{o} and one above 45^{o}.

As the data were averaged over length and width, the curves applied to a gamma entering a cylinder gamma counter anywhere. The 'characteristics' of Fig. (4.15) were readily calculated from the doubles probability at 0^{o}, 45^{o} and 54^{o}, approximating the curves to two straight lines. Consequently, if the computer was given the empirical curves for the doubles probability at these three angles only, it could work out the characteristic for any energy required and from this, extract a value for the probability at the requisite angle of incidence.

Angles not less than 45^{o}

Let $p_1(\theta)$ be the probability of doubles in this region, and $\sigma(45)$ and $\sigma(54)$ be the doubles probability at an angle of incidence of 45^{o} and 54^{o} respectively. Then, at some particular energy, the equation of the characteristic is :

$$p_1(\theta) = m\,(^{1}/\cos\theta) + c$$

and $$\sigma(45) = m\,(1.4142) + c$$

thus $$c = \sigma(45) - 1.4142\,m$$

and $$m = \frac{\sigma(54) - \sigma(45)}{0.73}$$

Therefore, $$p_1(\theta) = m\,(^{1}/\cos\theta) + \sigma(45) - 1.4142\,m$$

$$= m\,(^{1}/\cos\theta - 1.4142) + \sigma(45)$$

$$p_1(\theta) = \left[\frac{\sigma(54) - \sigma(45)}{0.73}\right](^{1}/\cos\theta - 1.4142) + \sigma(45) \quad \text{(Eq. 4.1)}.$$

Angles not greater than 45^{o}

Let $p_2(\theta)$ be the probability of doubles in this region and $\sigma(0)$ and $\sigma(45)$ represent the doubles probability at angles of incidence of 0^{o} and 45^{o} respectively. Then at some particular energy, the equation of the characteristic is :

$$p_2(\theta) = m\,(1/\cos\theta) + c$$

and $$\sigma(0) = m + c$$

thus $$c = \sigma(0) - m$$

and $$m = \frac{\sigma(45) - \sigma(0)}{0.4142}$$

Therefore, $$p_2(\theta) = m\,(1/\cos\theta) + \sigma(0) - m$$

$$= m\,(1/\cos\theta - 1) + \sigma(0)$$

$$p_2(\theta) = \left[\frac{\sigma(45) - \sigma(0)}{0.4142}\right](1/\cos\theta - 1) + \sigma(0) \quad \text{. (Eq. 4.2)}$$

Then, if $p_2 > p_1$, the doubles probability was equal to p_1 and if $p_2 \leq p_1$, the doubles probability was equal to p_2. The computer used Equations (4.1) and (4.2) to calculate the doubles probability for any angle and energy after first calculating the values of $\sigma(0)$, $\sigma(45)$ and $\sigma(54)$ from the empirical formulae below.

$\sigma(0)$

0	$\leq$	E	$\leq$	20	p	= 0.0
20	<	E	<	62	p	= 0.00107 E - 0.0214
62	$\leq$	E			p	= $0.46[\,1 - e^{-(E+90)/1400}\,]$

$\sigma(45)$

0	$\leq$	E	$\leq$	20	p	= 0.0
20	<	E	<	150	p	= $0.23[\,1 - e^{-(E-20)/100}\,]$
150	$\leq$	E			p	= $0.48[\,1 - e^{-(E+80)/500}\,]$

σ (54)

$$0 \leqslant E \leqslant 20 \qquad p = 0.0$$

$$20 < E < 125 \qquad p = 0.23\left[1 - e^{-(E-20)/100}\right]$$

$$125 \leqslant E \qquad p = 0.53\left[1 - e^{-(E+50)/500}\right]$$

4.6 Doubles Probability in the Lid Gamma Counters

The calculation of the doubles probability in the lid counters was more complex. In addition to the energy and angle dependence of the probability, there was also a length factor involved. Previously, the attenuation in signal due to length was the only length factor necessary but, as the width of the lid counter varied with length, the contribution of the centre and junction probabilities to the overall effect varied with length as well. To introduce this width factor, the actual position of the counter in an array was considered and so the width was taken to be 0.317 times the distance of the point of entry of the gamma from the centre of the lid disc.

The doubles probability averaged over length attenuation is shown in Figs. (4.16) and (4.17) for the centre and junction respectively, at angles of 0^0, 30^0 and 41^0. The difference between centre and junction measurements after taking an average between 0^0 and 30^0 is shown in Fig. (4.18).

The same $1/\cos\theta$ dependence was assumed for the doubles effect in the lid counters and the $1/\cos\theta$ characteristics were drawn for the centre and junction separately, as shown in Figs. (4.19) and (4.20). As angles of incidence less than 45^0 were possible only, the characteristics were represented by just a single straight line passing through the measured values at 0^0 and 30^0 incidence. Although most of the lid doubles data were obtained at these angles, the data at 41^0 was found to be

compatible with the straight lines obtained. As before, these curves yielded the doubles probability as a function of angle and energy, averaged over the length of the counter but, this time, without taking account of the width factor.

During the course of the experiment, a narrow beam scan across two counters was carried out at normal incidence for energies of 560 and 900 MeV, and also at 30^{o} incidence for 560 MeV. The measurements at normal incidence were taken at 60 mm and 240 mm from the tip of the counters whilst the third measurement was carried out at 230 mm from the tip only. From a knowledge of the dependence of $^{M}/_{D}$ on length, it was possible to predict the data that would have been obtained at the opposite ends of the counters, from the histograms obtained, giving two separate sets of data for each measurement. Close agreement was found between directly measured and predicted data.

By studying the $^{z}/_{s}$ ratio, and observing the peak of the doubles curve and the cross over point of the singles efficiency curves in the two counters, the actual position of the junction could be found. Examples of the curves obtained are shown in Fig. (4.21). The doubles obtained were measured first in one counter and then in the other and so the average of these two measurements was found. By pin pointing the junction, the doubles curve was folded about the middle and the two halves averaged. This was done for both ends of the counter and then the two sets of data were themselves averaged. As a check on the results obtained, a value for the wide beam measurement was predicted and close agreement found. The predicted and actual wide beam measurements differed by less than 1%, thus validifying the procedure for junction positioning.

Energy	Angle	Narrow Beam Measurement	Wide Beam Measurement
900	0^{o}	$20.2 \pm 2\%$	$21.0 \pm 3\%$
560	0^{o}	$18.0 \pm 2\%$	$18.3 \pm 2\frac{1}{2}\%$
560	30^{o}	$18.6 \pm 2\%$	$19.2 \pm 2\frac{1}{2}\%$

The data obtained at opposite ends were compared in the same way and the differences obtained were well within the errors of measurement. A difference of about 3% was expected as described in Section (3.10).

Energy	Angle	240 mm	60 mm	Difference
900	0^{o}	$20.2 \pm 2\%$	$21.7 \pm 2\%$	$1.5 \pm 4\%$
560	0^{o}	$18.0 \pm 2\%$	$19.3 \pm 2\%$	$1.3 \pm 4\%$
560	30^{o}	$21.0 \pm 2\%$	$21.0 \pm 2\%$	$2.4 \pm 4\%$

Wide Beam Measurements

The folded curves for doubles probability averaged over counter length were extrapolated over the width of the counters. As the predicted and measured wide beam values were in such close agreement, the wide beam central measurement was used in the extrapolation. From this curve, the probability of a double gamma on one side of the counter only, could be calculated as a function of radius (as shown in Fig. (4.22)). This was done by imposing a cut off on the curve measured from the junction and equal to the width of the counter at the radius concerned. In order to be able to do this for any energy and angle of incidence, the shape of the folded doubles curve had to be given in terms of the probabilities at the angles used in the energy dependence measurements.

Initially, the process was the same as before. The computer was given the doubles probability curves at 0^{o}, 15^{o} and 30^{o} incidence, averaged over length attenuation at both the centre and junction. The 15^{o} data was found from averaging the 0^{o} and 30^{o} data. The computer calculated the probability at these angles for the specific energy required

and then it calculated the centre and junction $^{1}/\cos\theta$ characteristics from these values. The same equation was applicable for either the centre or the junction. Let $p(\theta)$ be the doubles probability at either the centre or junction. Let $\sigma(0)$, $\sigma(15)$ and $\sigma(30)$ be the doubles probabilities at the specific energy of the incident gamma at angles of incidence of 0^{o}, 15^{o} and 30^{o} respectively.

Then,

$$p(\theta) = m\,(^{1}/\cos\theta) + c$$

$$\sigma(15) = m\,(^{1}/\cos 15^{o}) + c$$

therefore $$c = \sigma(15) - 1.035\,m$$

and $$m = \frac{\sigma(30) - \sigma(0)}{0.153}$$

Therefore, $p(\theta) = m\,(^{1}/\cos\theta) + \sigma(15) - 1.035\,m$

$$= m\,(^{1}/\cos\theta - 1.035) + \sigma(15)$$

therefore, $$p(\theta) = \left[\frac{\sigma(30) - \sigma(0)}{0.153}\right](^{1}/\cos\theta - 1.035) + \sigma(15) \quad \text{(Eq. 4.3)}$$

The doubles probabilities at the centre were as follows :

$\underline{\sigma_c(0)}$

$0 \leqslant E \leqslant 20$ $\quad p = 0.0$

$20 < E$ $\quad p = 0.0615\,[1 - e^{-(E-20)/400}]$

$\underline{\sigma_c(30)}$

$0 \leqslant E \leqslant 20$ $\quad p = 0.0$

$20 < E < 200$ $\quad p = 0.05\,[1 - e^{-(E-20)/100}]$

$200 \leqslant E$ $\quad p = 0.078\,[1 - e^{-(E+200)/500}]$

$\underline{\sigma_c(15)}$

$0 \leqslant E \leqslant 20$ $\quad p = 0.0$

$20 < E < 400$ $\quad p = 0.074\,[1 - e^{-(E-20)/500}]$

$400 \leqslant E$ $\quad p = 0.07\,[1 - e^{-(E-20)/400}]$

The doubles probabilities at the junction were as follows :

$\underline{\sigma_j\ (0)}$

$$0 \leqslant E \leqslant 20 \qquad p = 0.0$$

$$20 < E < 200 \qquad p = 0.142[1 - e^{-(E-20)/100}]$$

$$200 \leqslant E \qquad p = 0.135[1 - e^{-(E+300)/1000}]$$

$\underline{\sigma_j\ (30)}$

$$0 \leqslant E \leqslant 20 \qquad p = 0.0$$

$$20 < E \leqslant 200 \qquad p = 0.182[1 - e^{-(E-20)/100}]$$

$$200 < E \qquad p = 0.388[1 - e^{-(E+300)/1000}]$$

$\underline{\sigma_j\ (15)}$

$$0 \leqslant E \leqslant 20 \qquad p = 0.0$$

$$20 < E \leqslant 320 \qquad p = 0.16[1 - e^{(E-20)/100}]$$

$$320 < E \qquad p = 0.372[1 - e^{-(E+200)/1000}]$$

The subscripts c and j were used to distinguish between centre and junction measurements. Equation (4.3) was used to determine the $^1/\cos\theta$ characteristic at any required energy. Consequently, the centre and junction doubles probabilities, σ_c and σ_j, were found as a function of energy and angle. No radial dependence had been introduced at this stage. To do this, the following empirical equation was introduced to fit the data similar to that shown in Fig. (4.22).

$$p = (A + Be^{-r/R}) \qquad \text{(Eq. 4.4)}$$

The doubles probability was, in fact, twice this value as account had to be taken of a gamma spreading to both sides of the counter.

Let p_3 be the asymptotic value of the doubles probability at large

radii. Let p_1 and p_2 be the values of the probability at r_1 and r_2 where $r_2 = 2r_1 = 158$ mm.

As $r \to \infty$, $p \to A$ and, therefore, $A = p_3$.

At (p_1, r_1), $$\frac{p_1 - A}{B} = e^{-r_1/R} ,$$

At (p_2, r_2), $$\frac{p_2 - A}{B} = e^{-r_2/R} = (e^{-r_1/R})^2 .$$

Therefore $$\frac{p_2 - A}{B} = \left[\frac{p_1 - A}{B}\right]^2 ,$$

and $$B = \frac{(p_1 - A)^2}{p_2 - A} . \quad \text{(Eq. 4.5)}$$

Also $$\frac{p_1 - A}{p_2 - A} = \frac{e^{-r_1/R}}{(e^{-r_1/R})^2} = e^{r_1/R} .$$

Therefore $$\frac{r_1}{R} = \log_e \left[\frac{p_1 - A}{p_2 - A}\right] ,$$

and $$R = \frac{r_1}{\log_e \left[\frac{p_1 - A}{p_2 - A}\right]} . \quad \text{(Eq. 4.6)}$$

The values of p_1 and p_2 were calculated from a study of the counter widths at these radii, whilst the value of p_3 was found empirically to fit the curves to the data. The values used were as follows :

$$p_1 = \sigma_j$$
$$p_2 = \tfrac{1}{2} (\sigma_j + \sigma_c)$$
$$p_3 = \tfrac{3}{16} (\sigma_j + \sigma_c) .$$

These values could be calculated directly from the Equation (4.3) for σ_j, and σ_c, and so the doubles probability at any specific radius could be found

as a function of energy and angle, averaged over attenuation along the length of the counter.

A measurement of σ_j corresponded to 100 gammas entering a 50 mm wide box centred on the junction. Therefore, of the 50 gammas that entered the 25 mm strip on one side of the box, $\frac{1}{2}\sigma_j$ would have doubled to one side only. The percentage of doubles to one side would then be σ_j. Consequently, $p_1 = \sigma_j$ as the width of the counter at 79 mm radius was 25 mm.

At a radius of 158 mm, the counter width was 50 mm. If 100 gammas were incident on this width, 50 would have fallen within 25 mm of the junction and again have given $\frac{1}{2}\sigma_j$ doubles to one side. A measurement of σ_c corresponded to 100 gammas entering a central region 50 mm wide and was the number doubling to one side only. Therefore, for 50 gammas, the number of doubles would have been $\frac{1}{2}\sigma_c$ and this would be the number from the 25 mm strip furthest from the junction. The total number of doubles to one side would then have been $\frac{1}{2}(\sigma_j + \sigma_c)$ for 100 gammas. Hence $p_2 = \frac{1}{2}(\sigma_j + \sigma_c)$.

With these values for the computer to calculate A and B, the doubles probability for the lid gamma counters was then :

$$p = 2 (A + B_e^{-r/R}) .$$

Figure 4.1

Efficiency of cylinder gamma counters at the centre

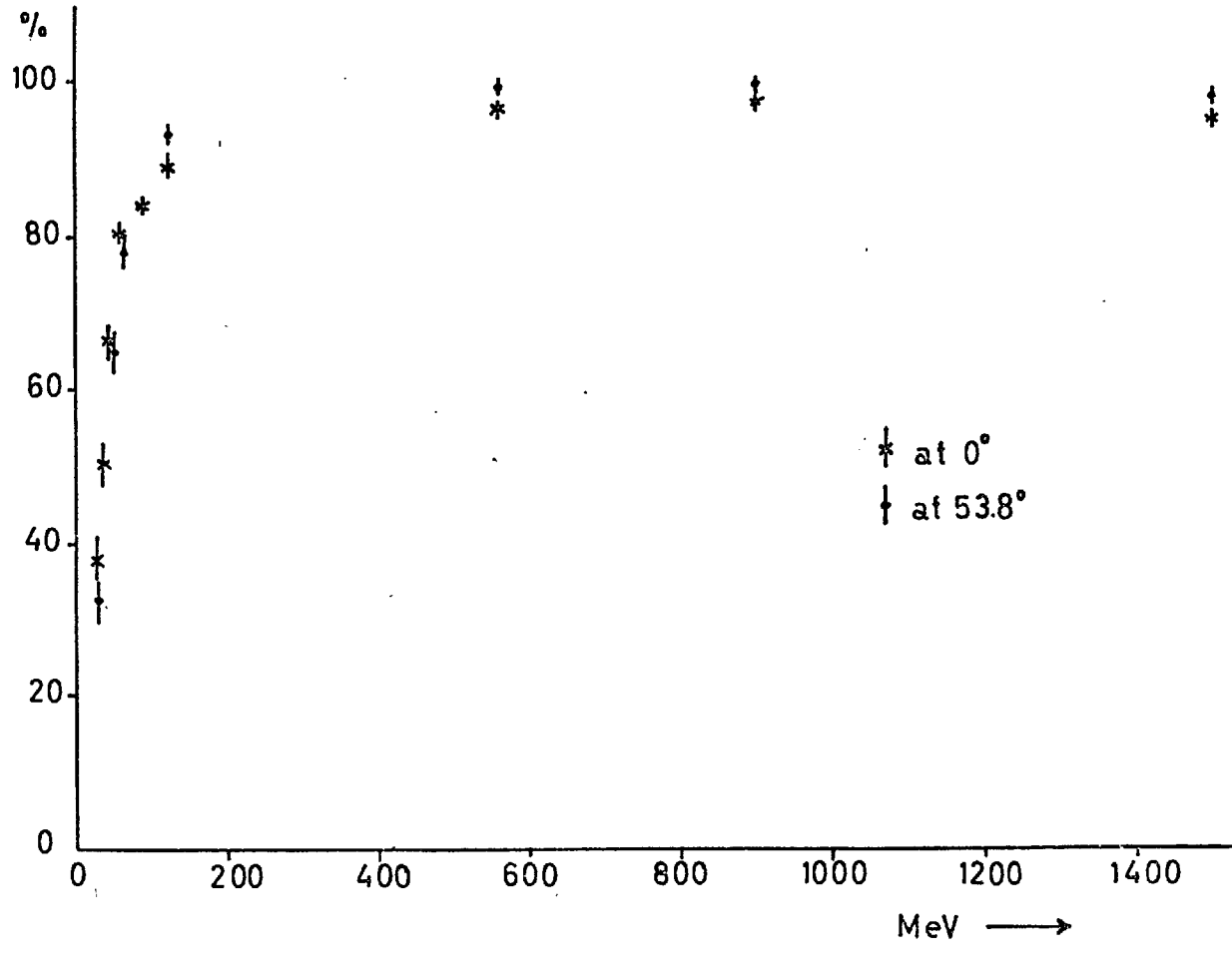

Figure 4.2

Efficiency for single gammas at the junction between two cylinder gamma counters, measured at the opposite end to the photomultiplier.

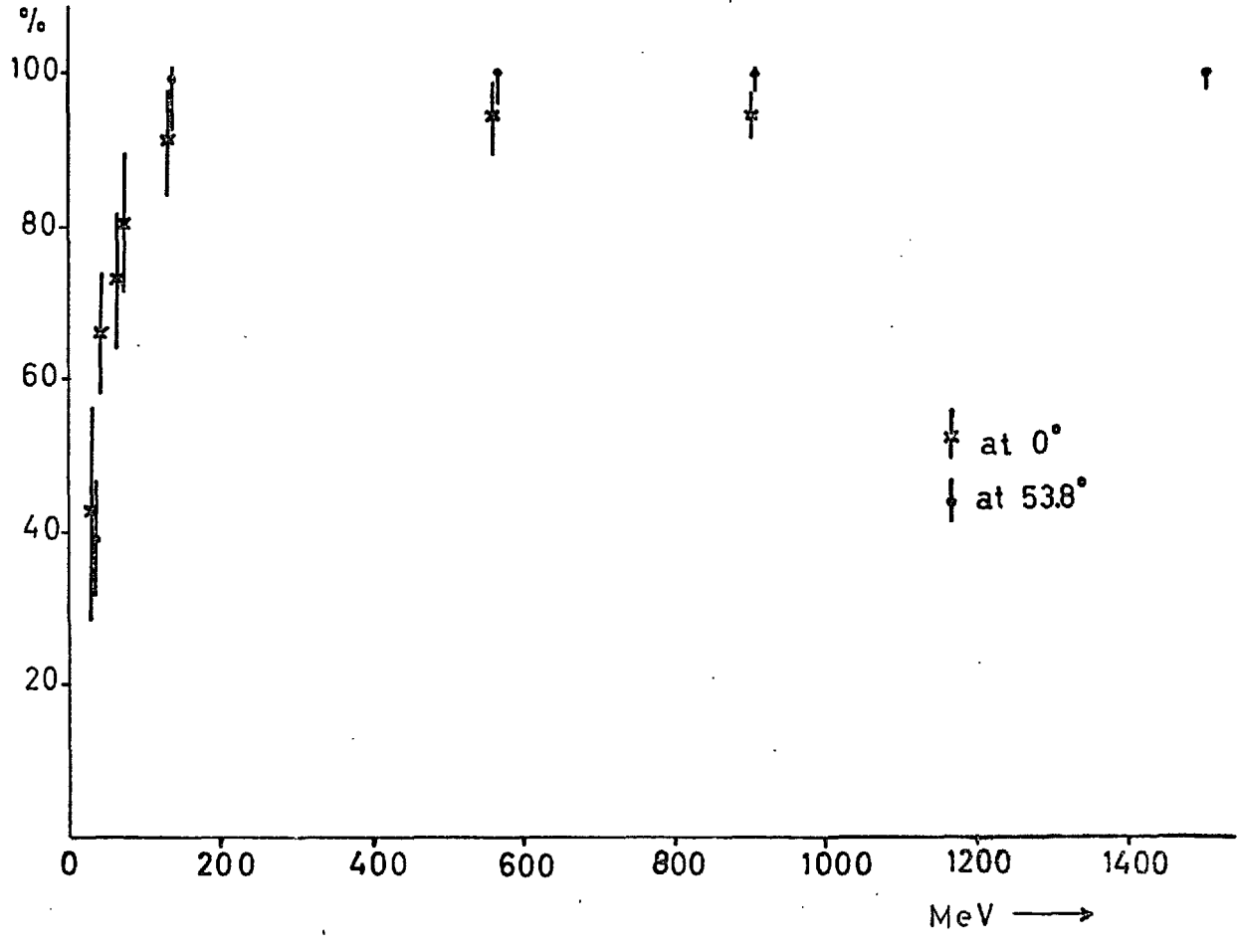

Figure 4.3

Efficiency of cylinder gamma counters at any position across width

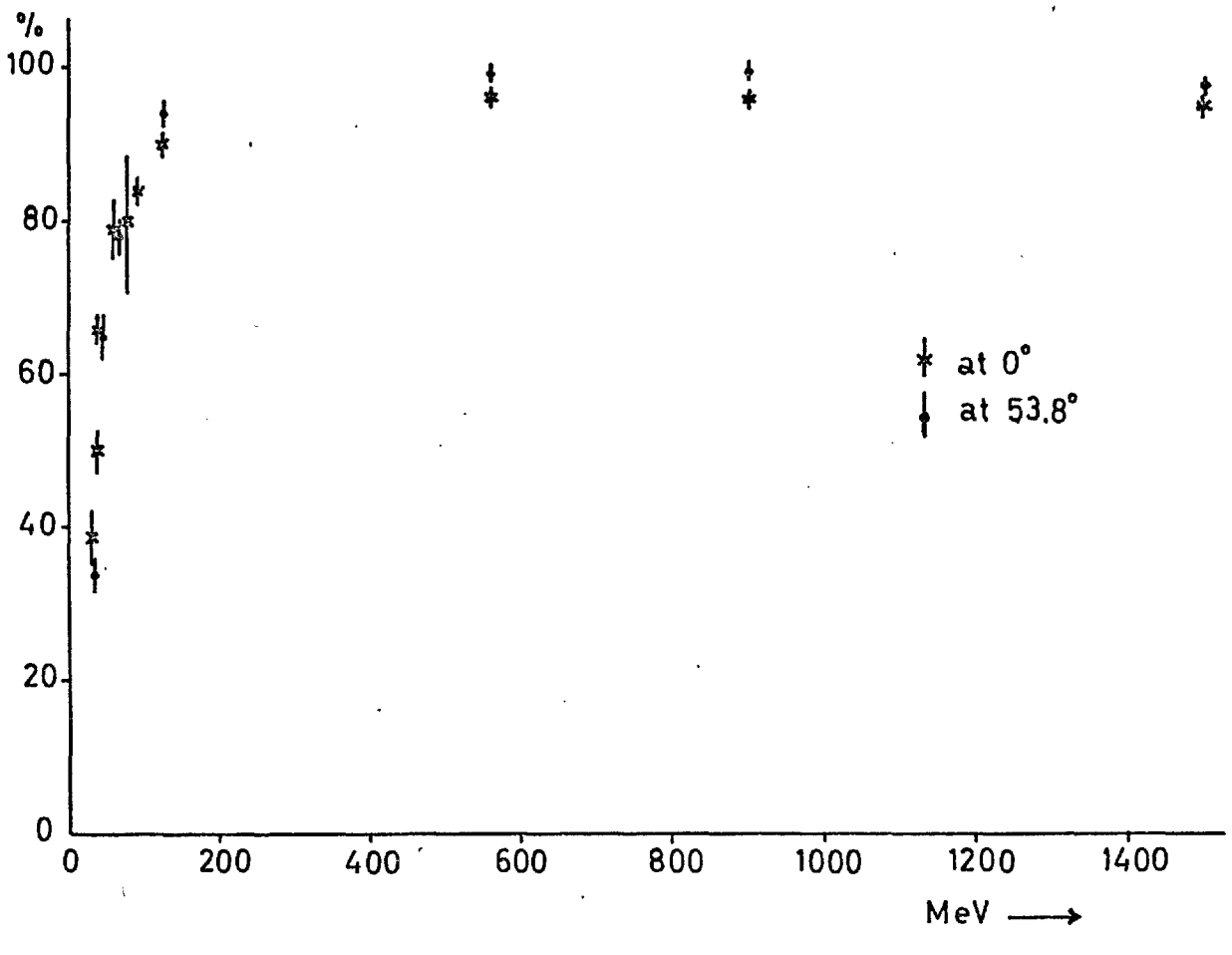

Efficiency of cylinder gamma counters for single gammas incident at any angle, any position across width

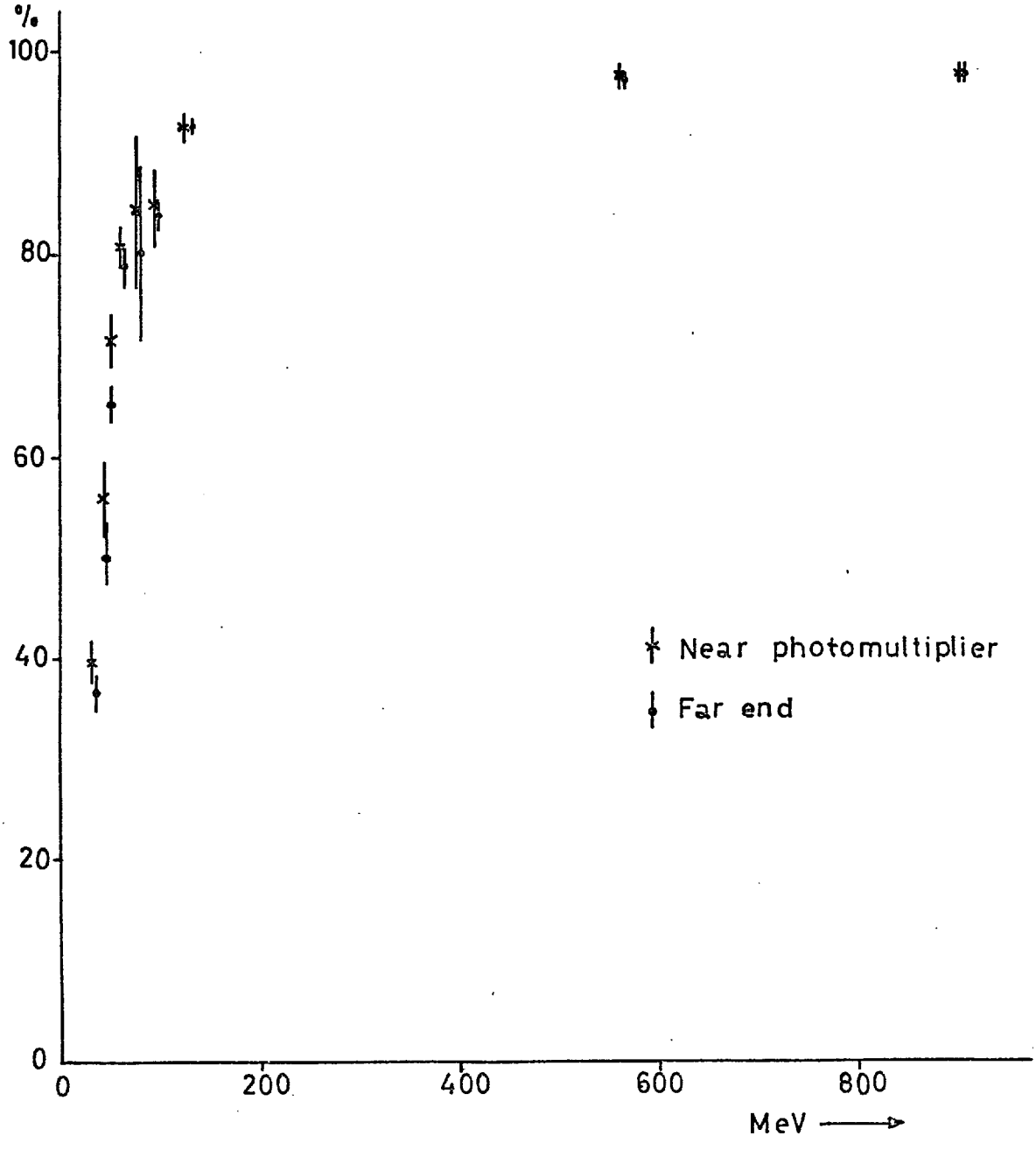

Figure 4.4

Efficiency of cylinder gamma counters for single gammas

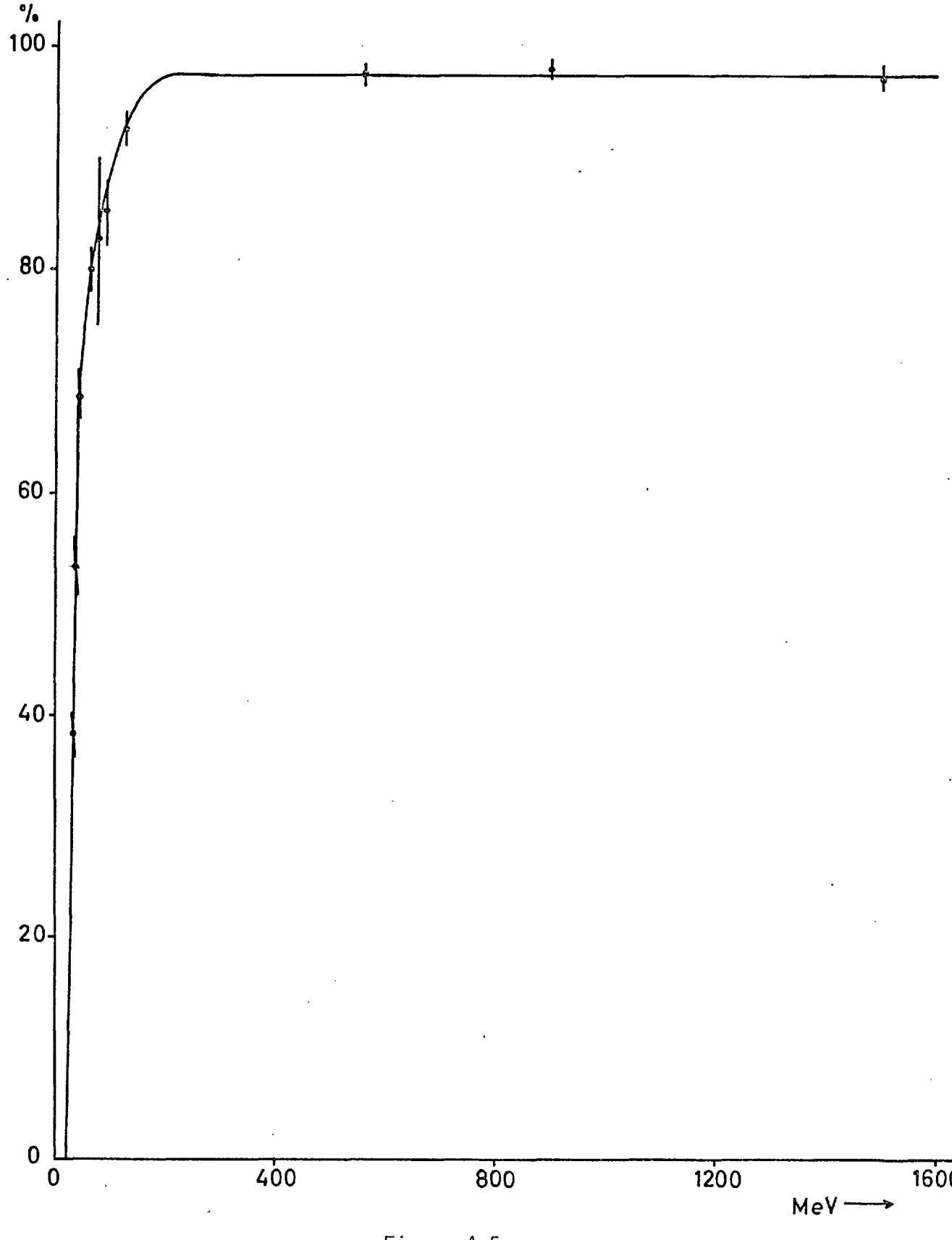

Figure 4.5

Efficiency of cylinder gamma counters for single gammas at low energy

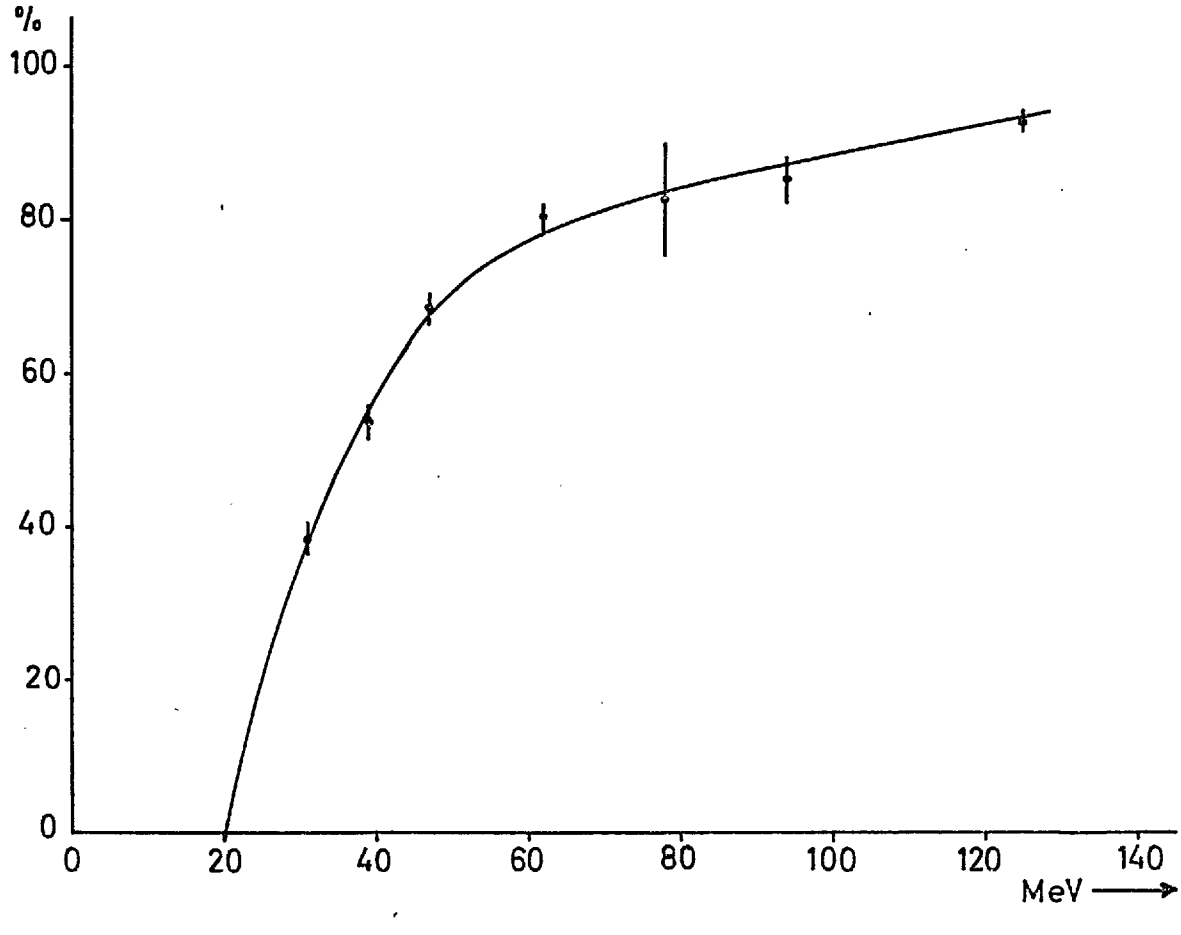

Figure 4.6

The efficiency at the centre of the lid gamma counters for single gammas

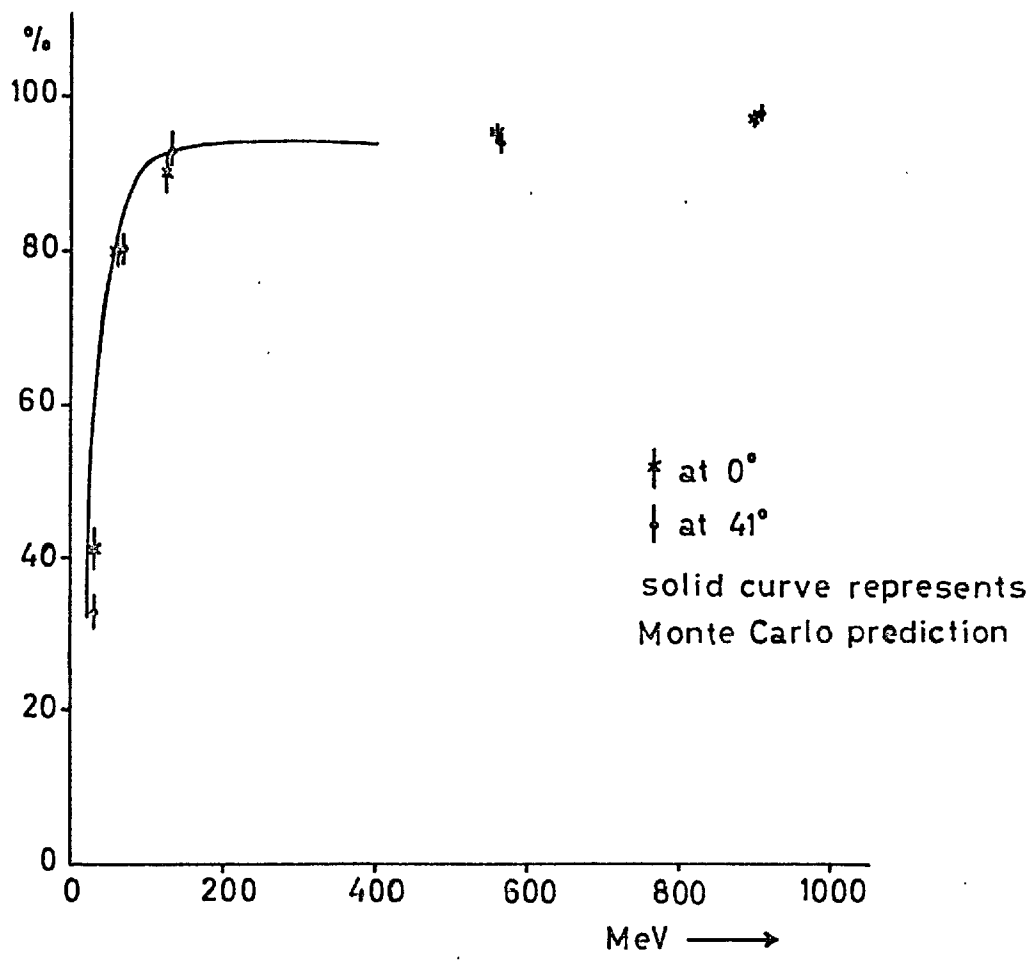

Figure 4.7

Efficiency of lid gamma counters for single gammas

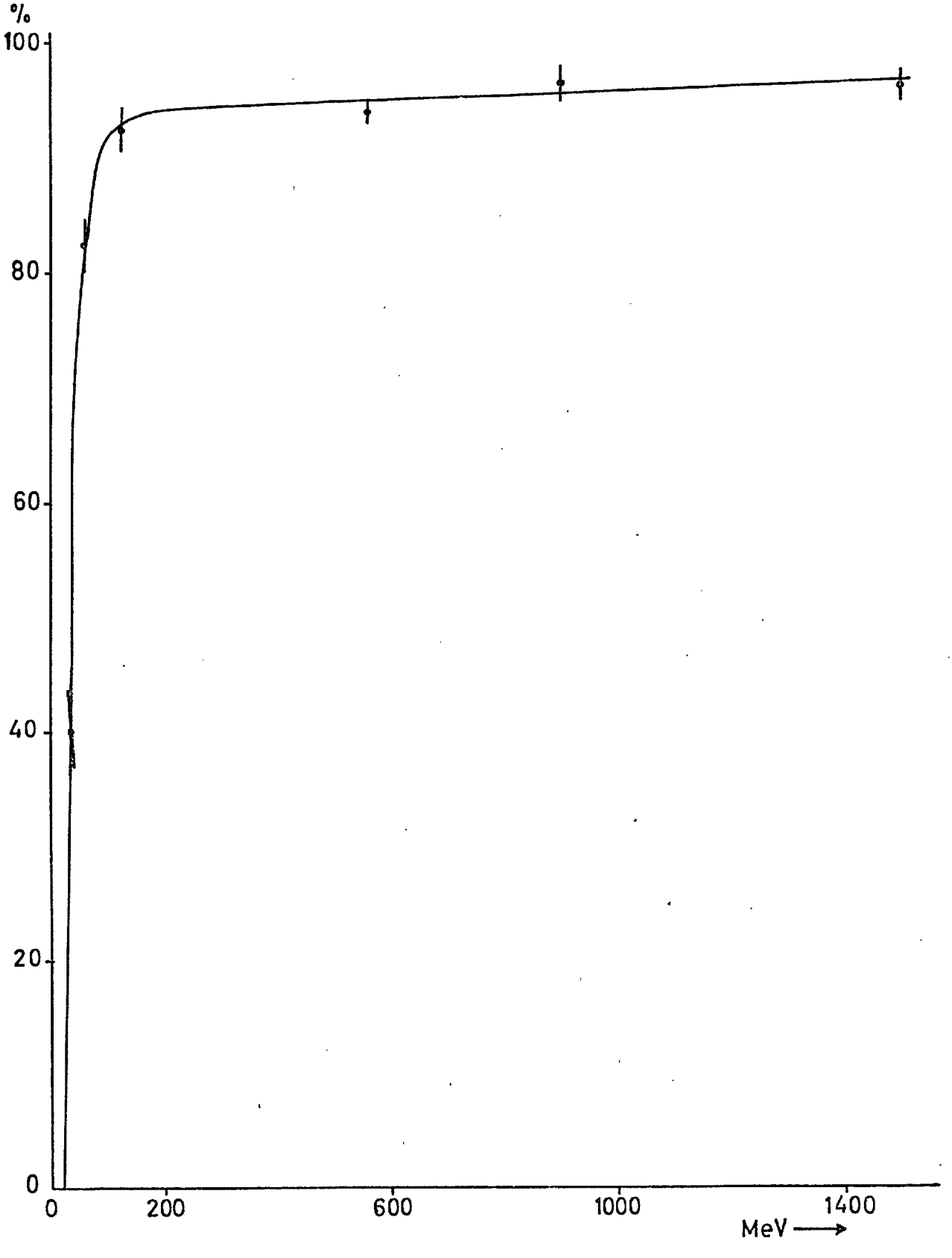

Figure 4.8

Efficiency of lid gamma counters for single gammas at low energy

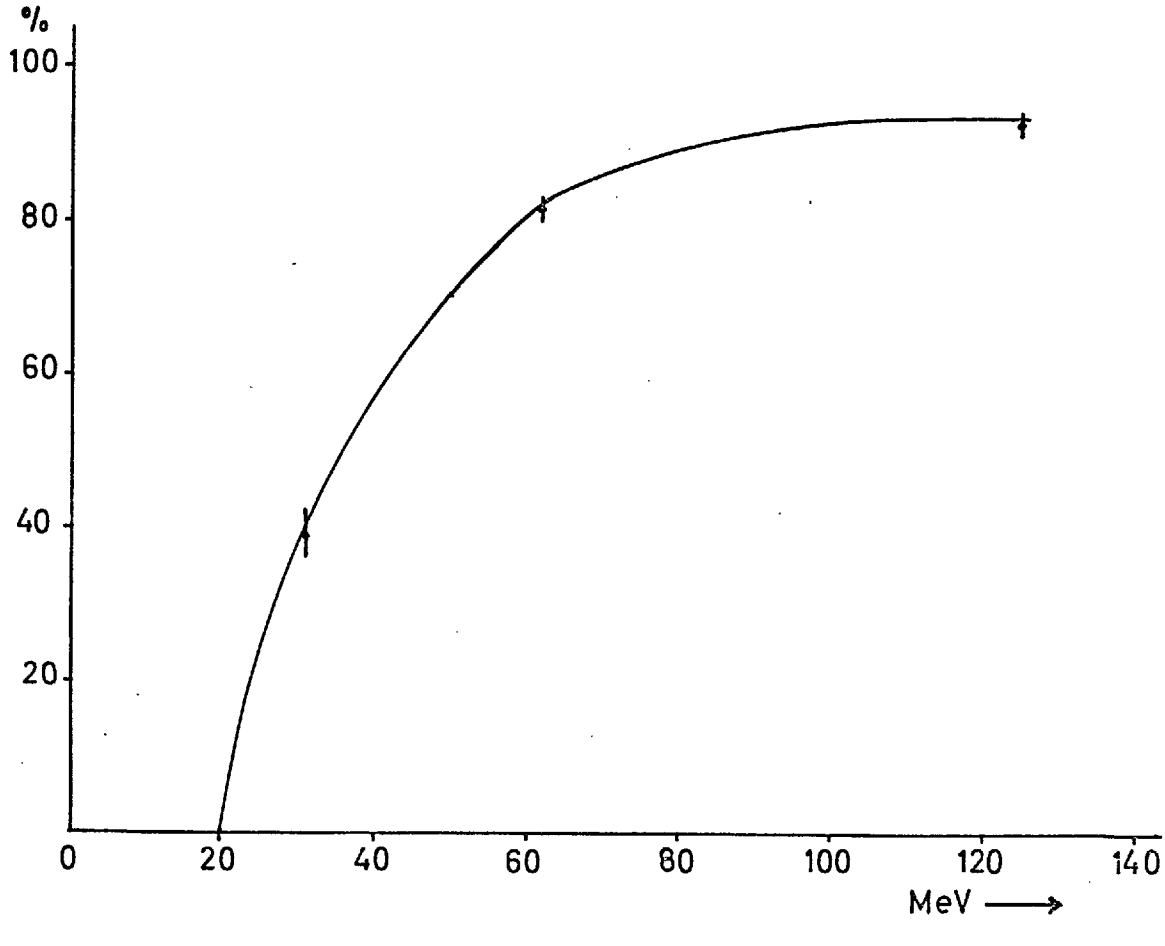

Figure 4.9

Efficiency of 20th cylinder gamma counter calculated by Monte Carlo program

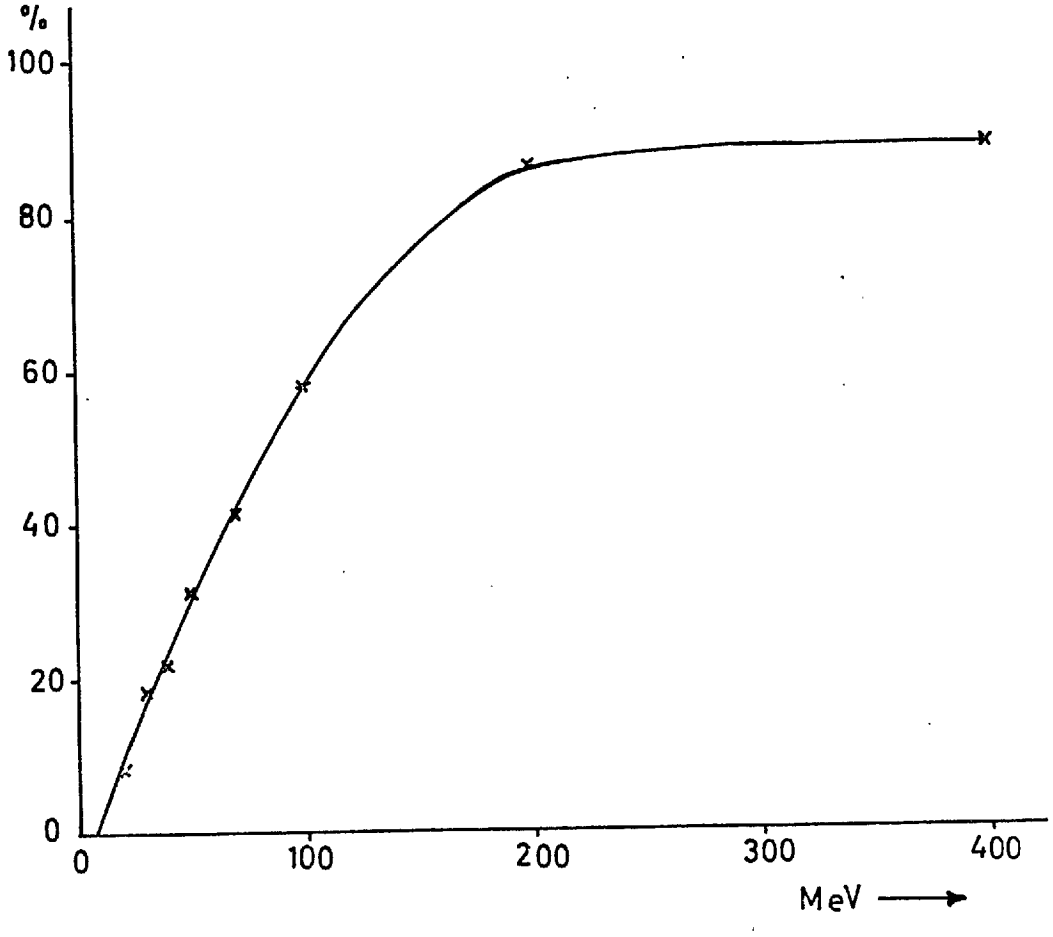

Figure 4.10

Doubles probability at the centre of a cylinder gamma counter, at any position along the length.

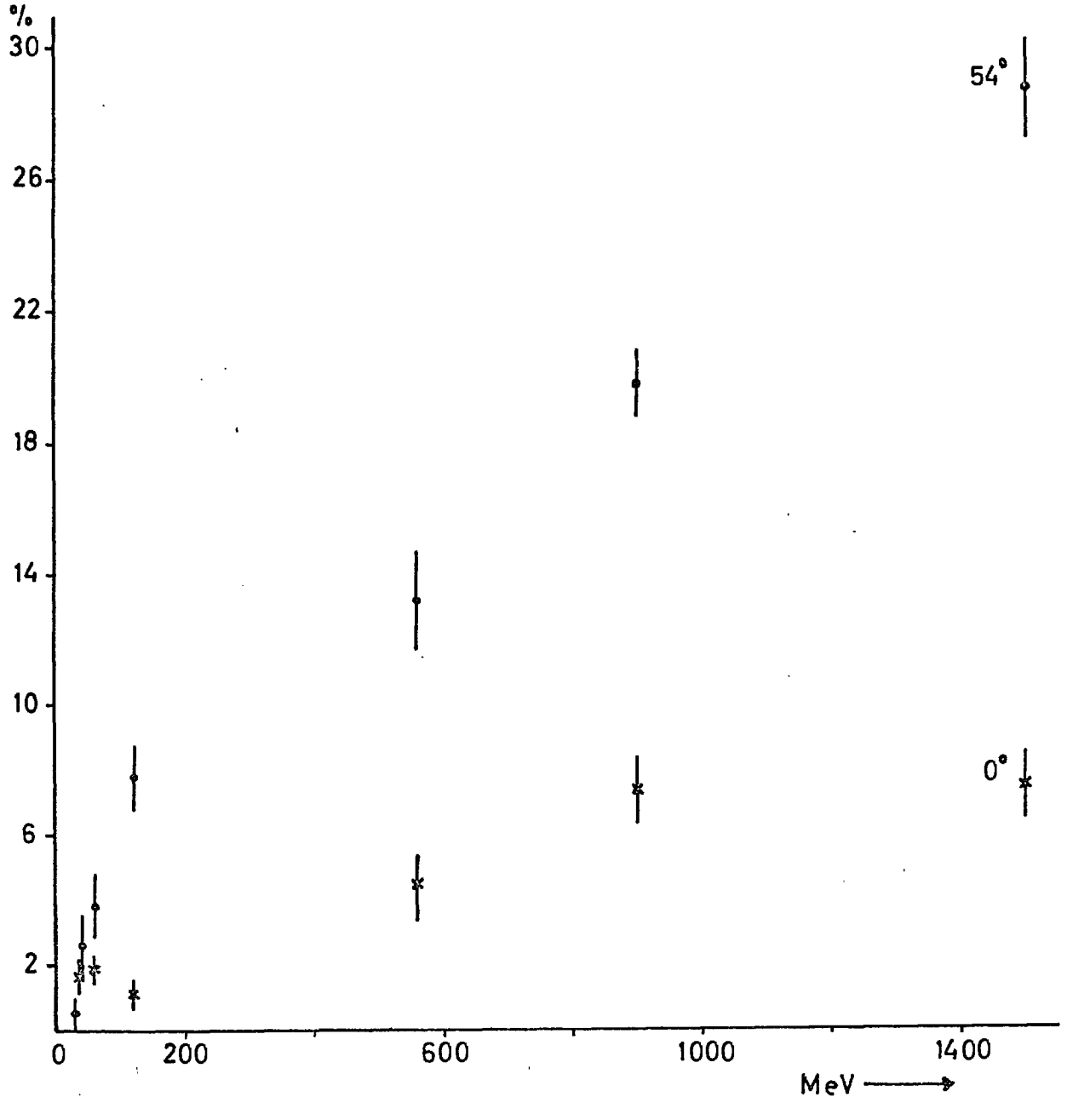

Figure 4.11

Doubles probability at the junction between two cylinder gamma counters, at any position along the length.

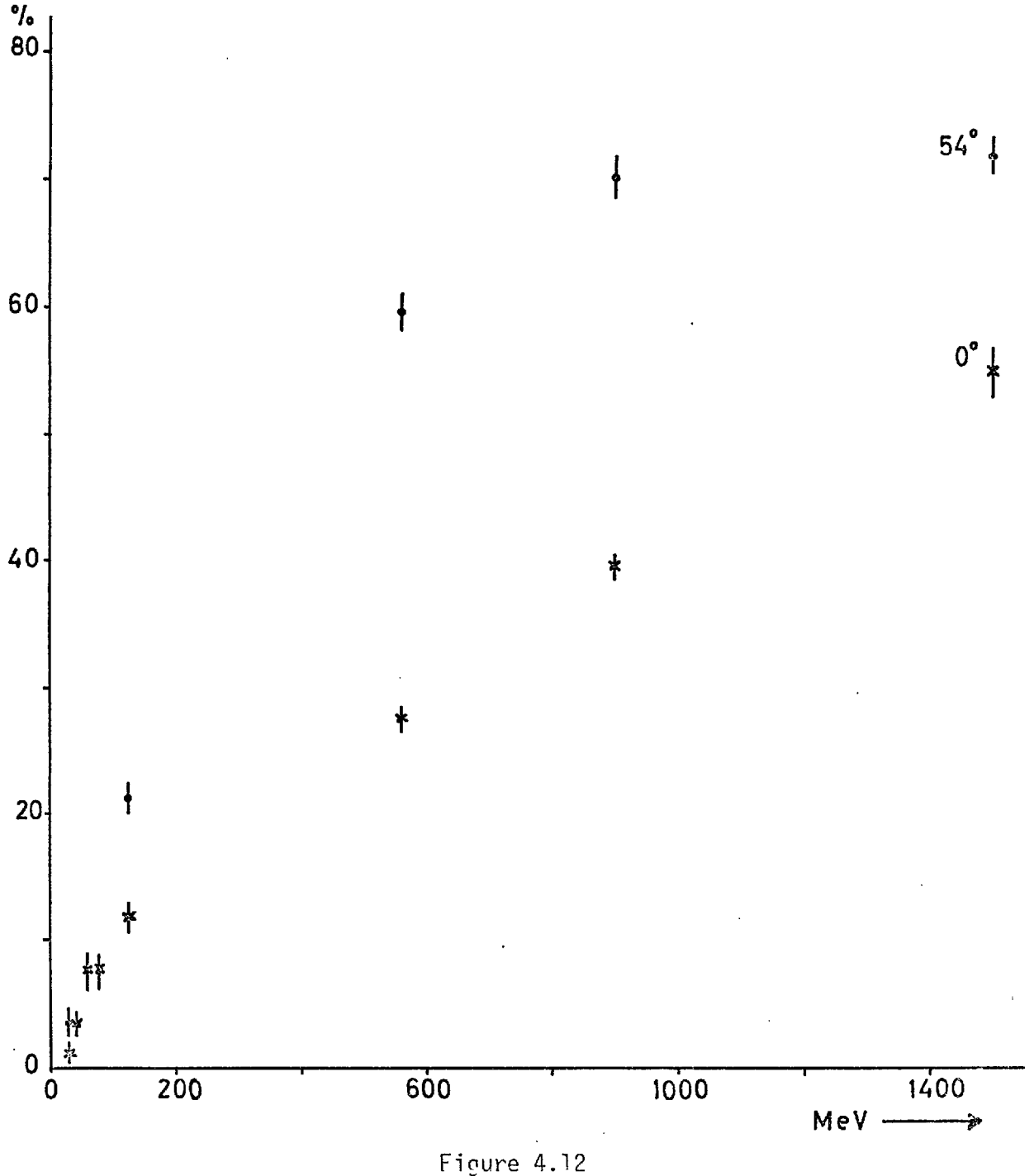

Figure 4.12

Cross over doubles in cylinder gamma counters, averaged over length and width

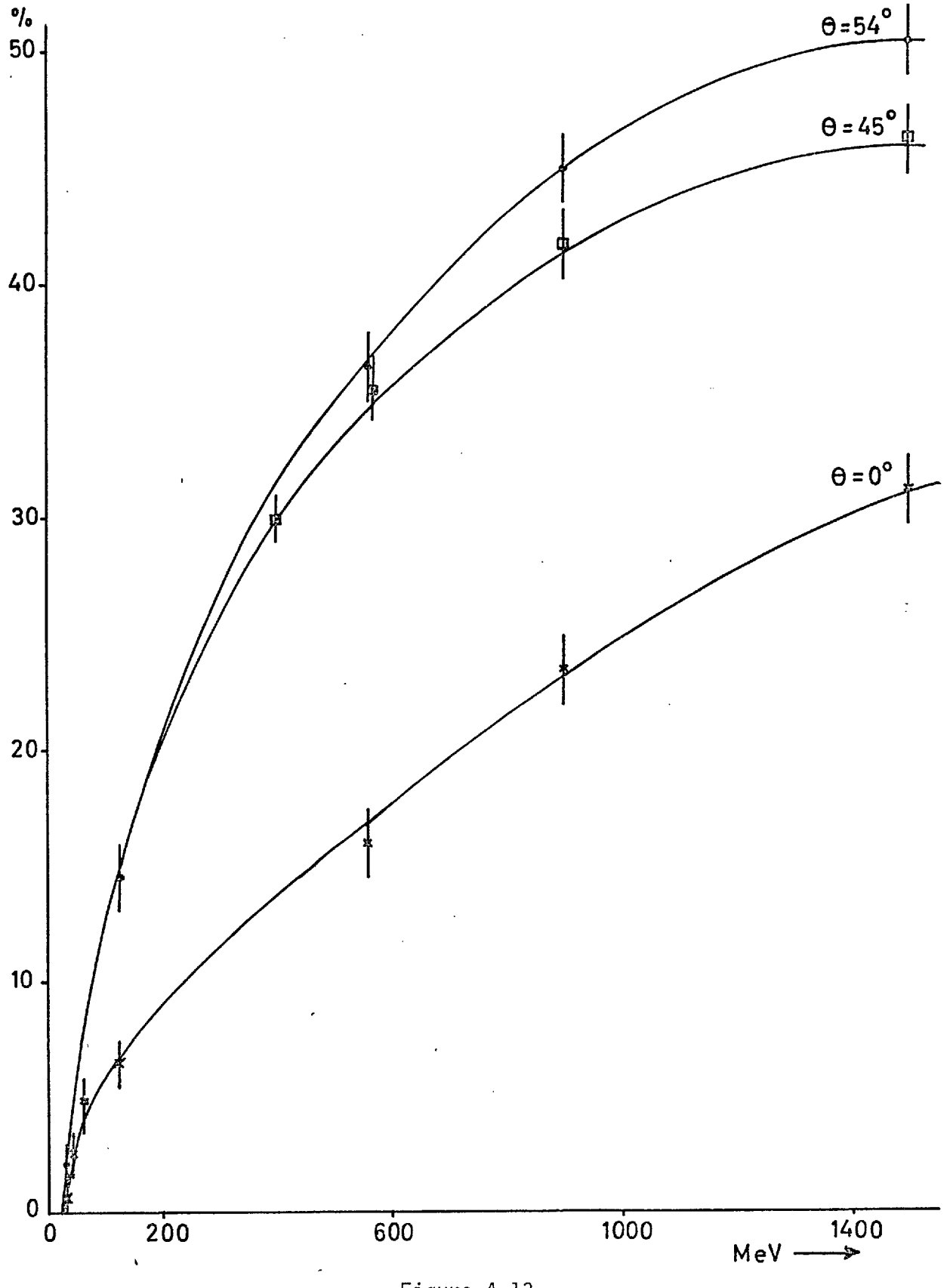

Figure 4.13

Cross over doubles at the junction between two cylinder gamma counters, as a function of $1/\cos\theta$ at 900 MeV/c

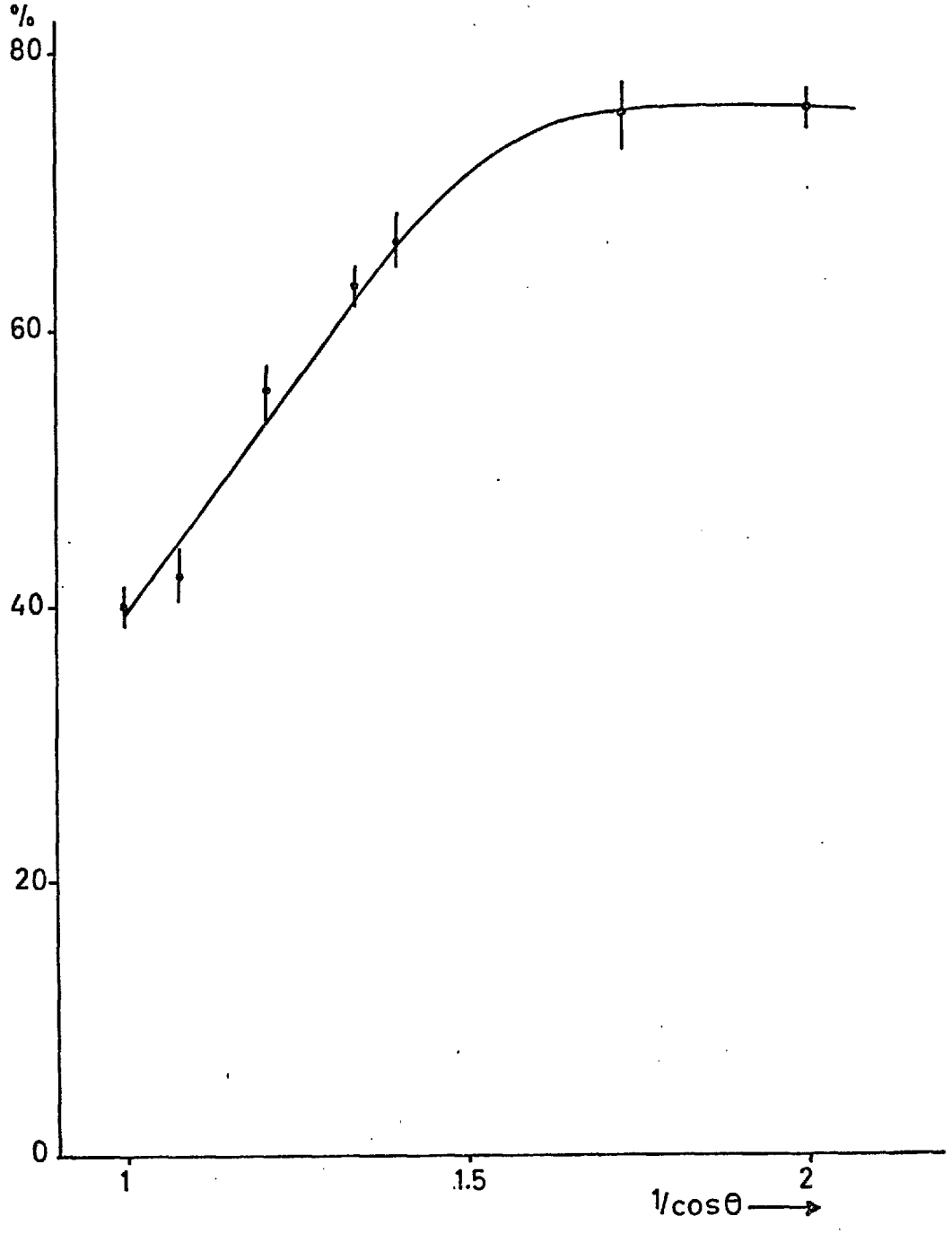

Figure 4.14

Cross over doubles averaged over length and width, as a function of $1/\cos\theta$, in the cylinder gamma counters

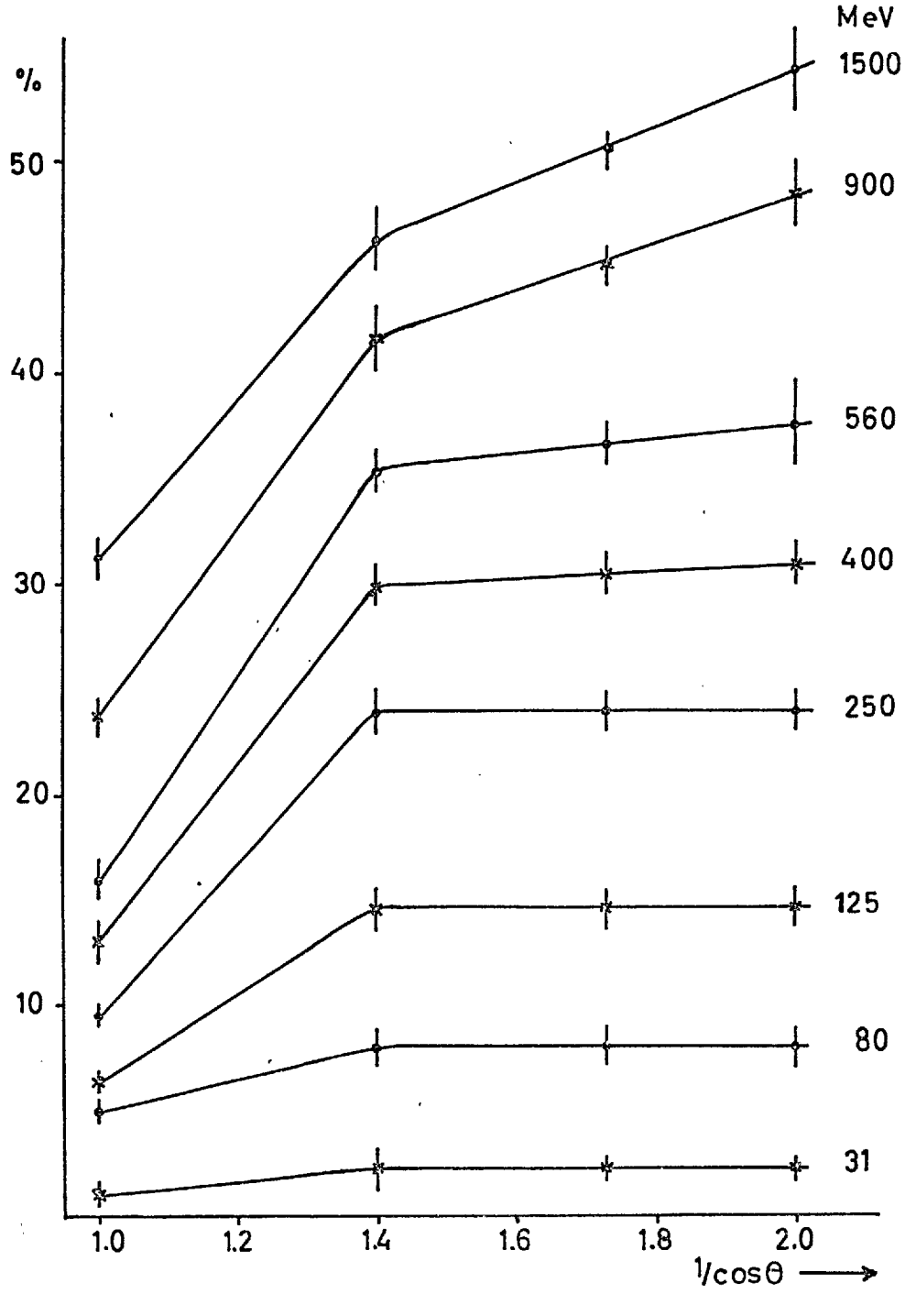

Figure 4.15

Cross over doubles at the centre of two lid gamma counters, averaged over length.

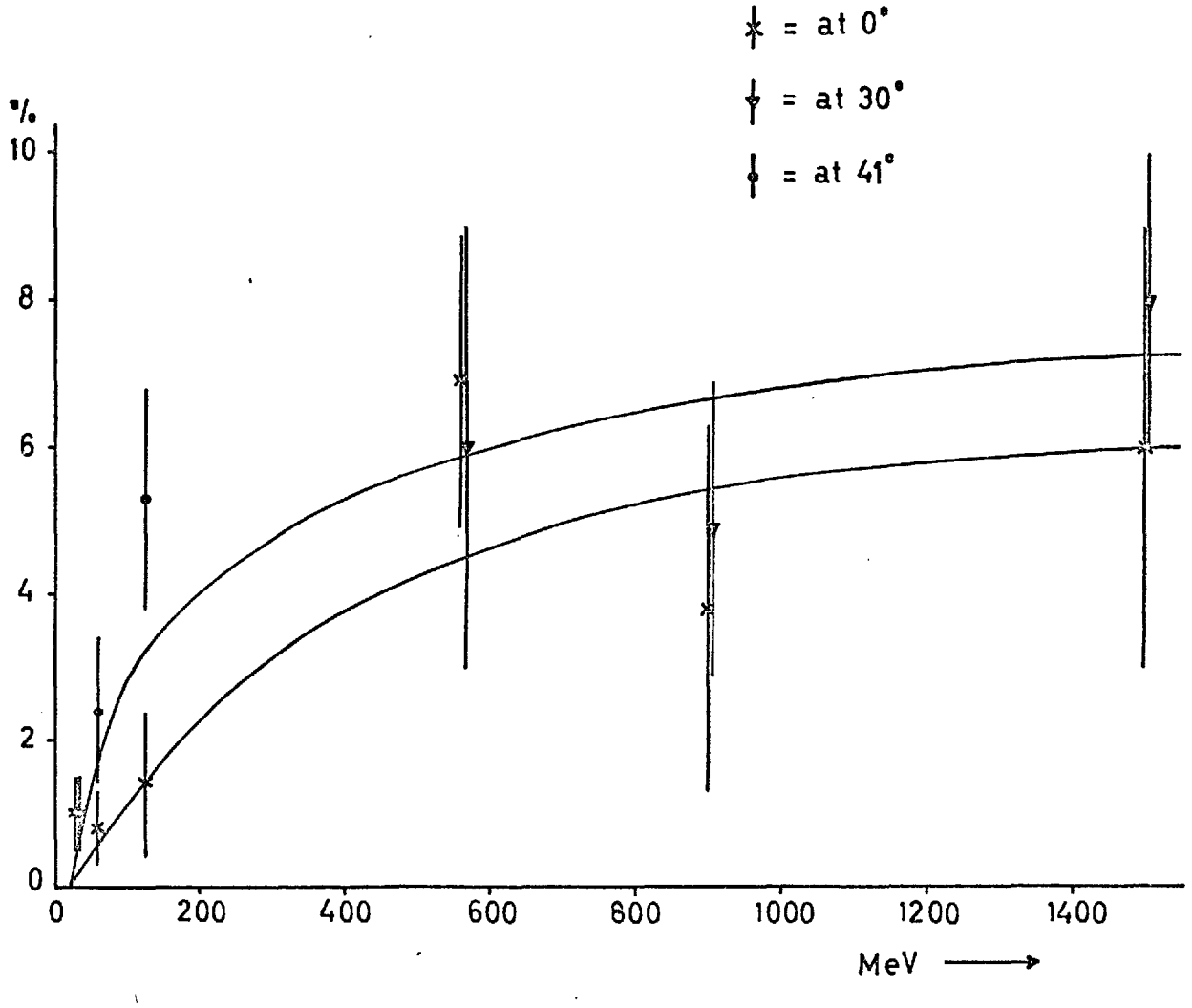

Figure 4.16

Cross over doubles at the junction between two lid gamma counters, averaged over length.

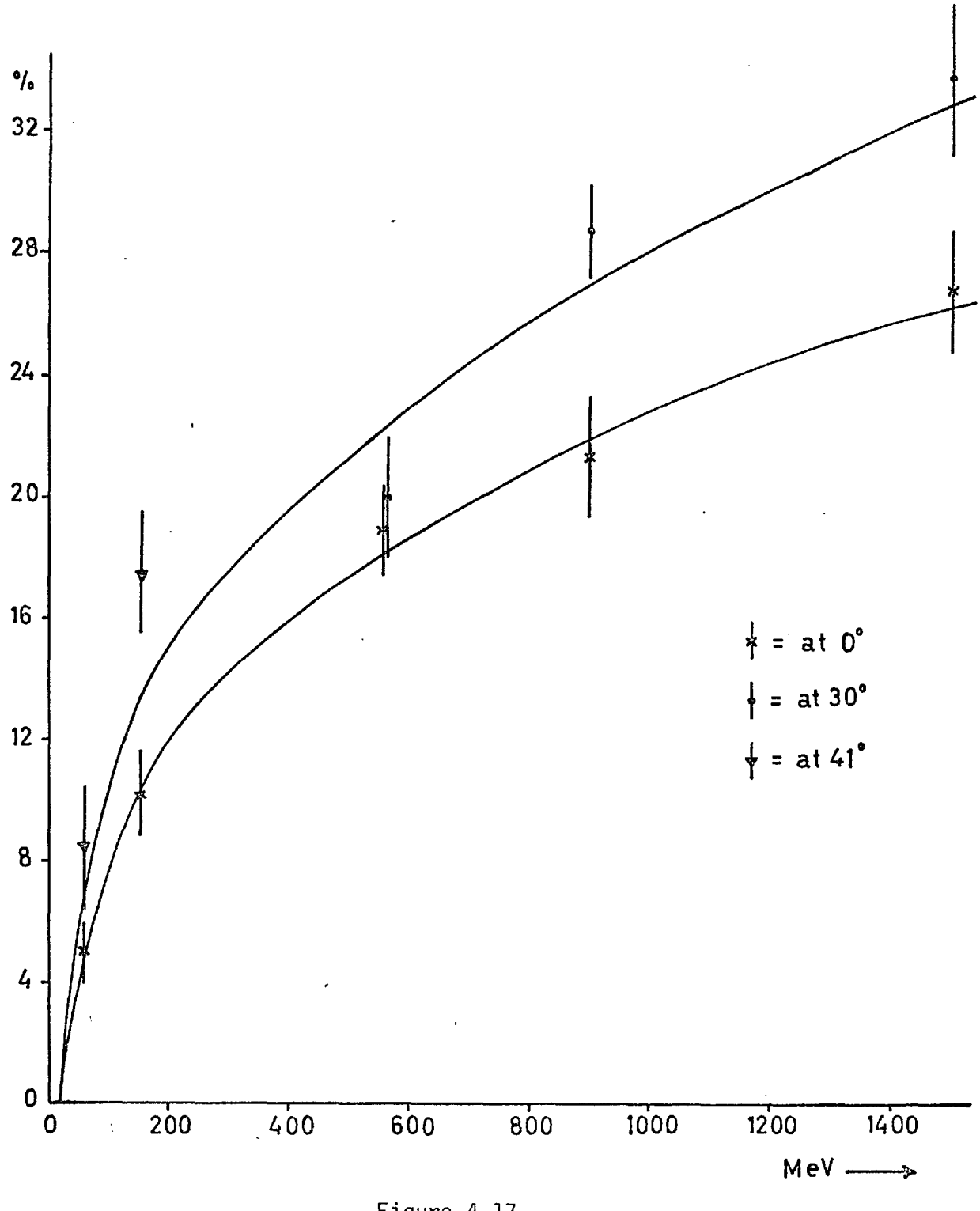

Figure 4.17

Cross over doubles at the junction and at the centre of two lid gamma counters, averaged over the length and between 0° and 30°.

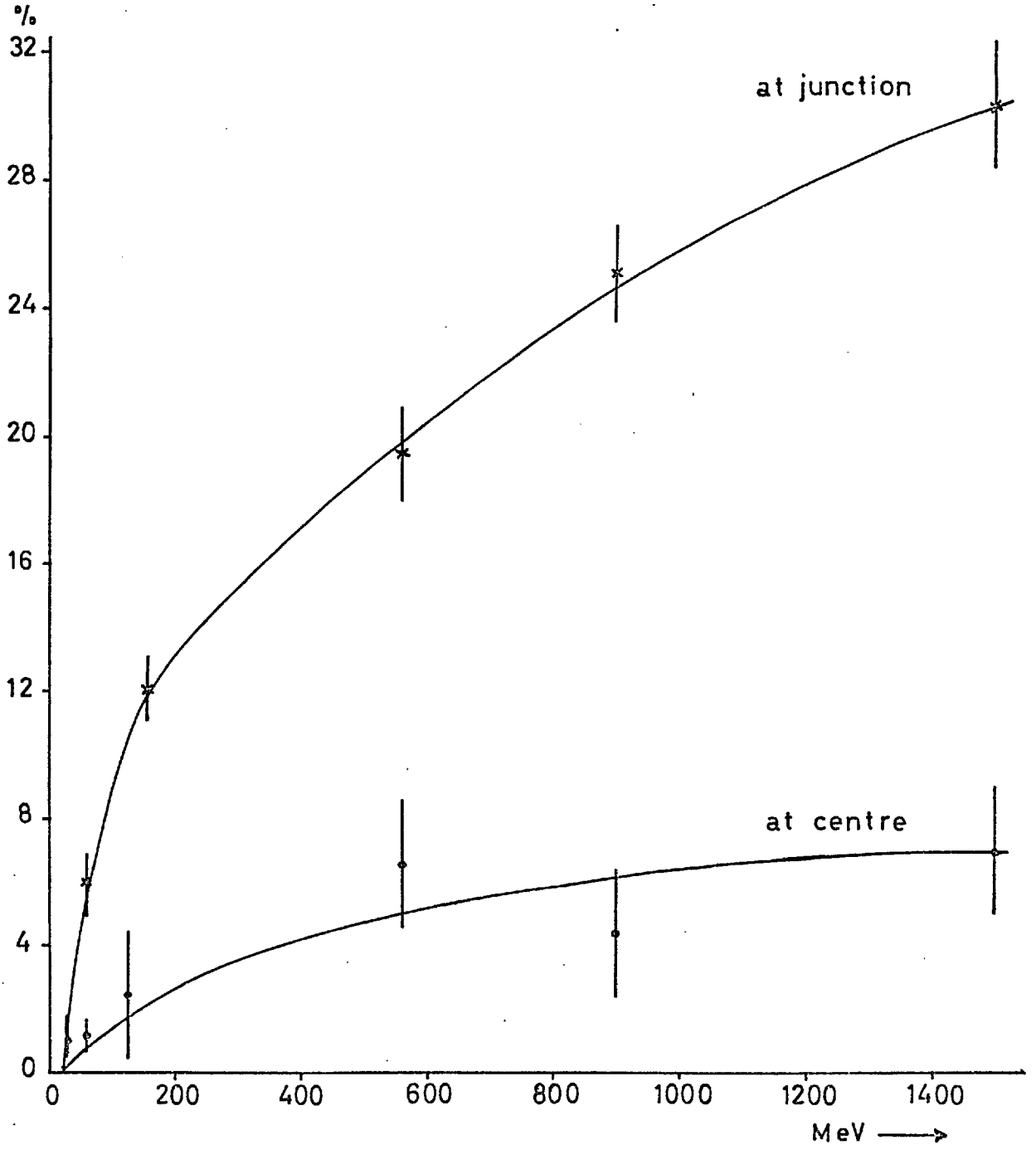

Figure 4.18

Cross over doubles at centre of lid gamma counters as a function of $1/\cos\theta$ averaged over length.

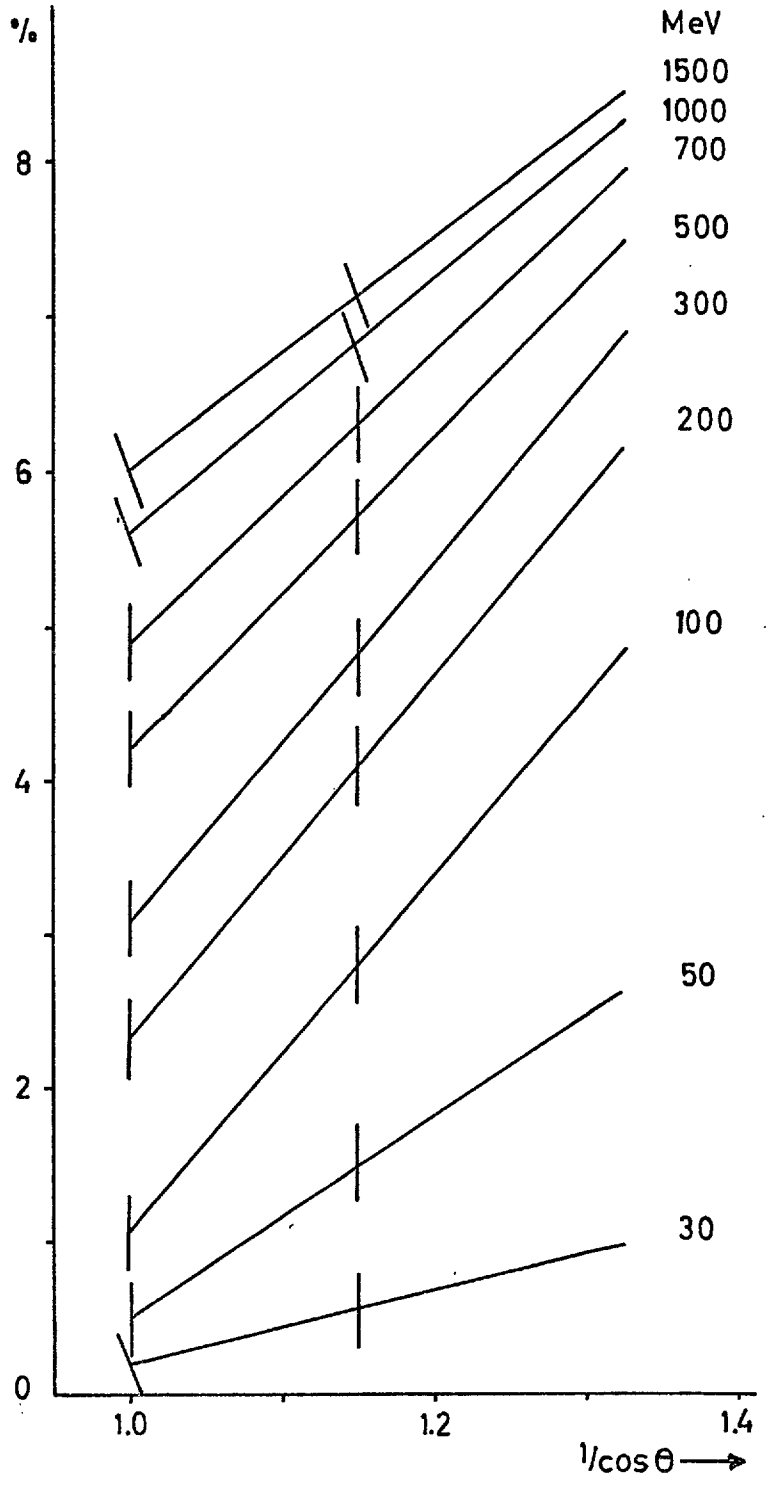

Figure 4.19

Cross over doubles at the junction between two lid gamma counters, as a function of $1/\cos\theta$, averaged over length.

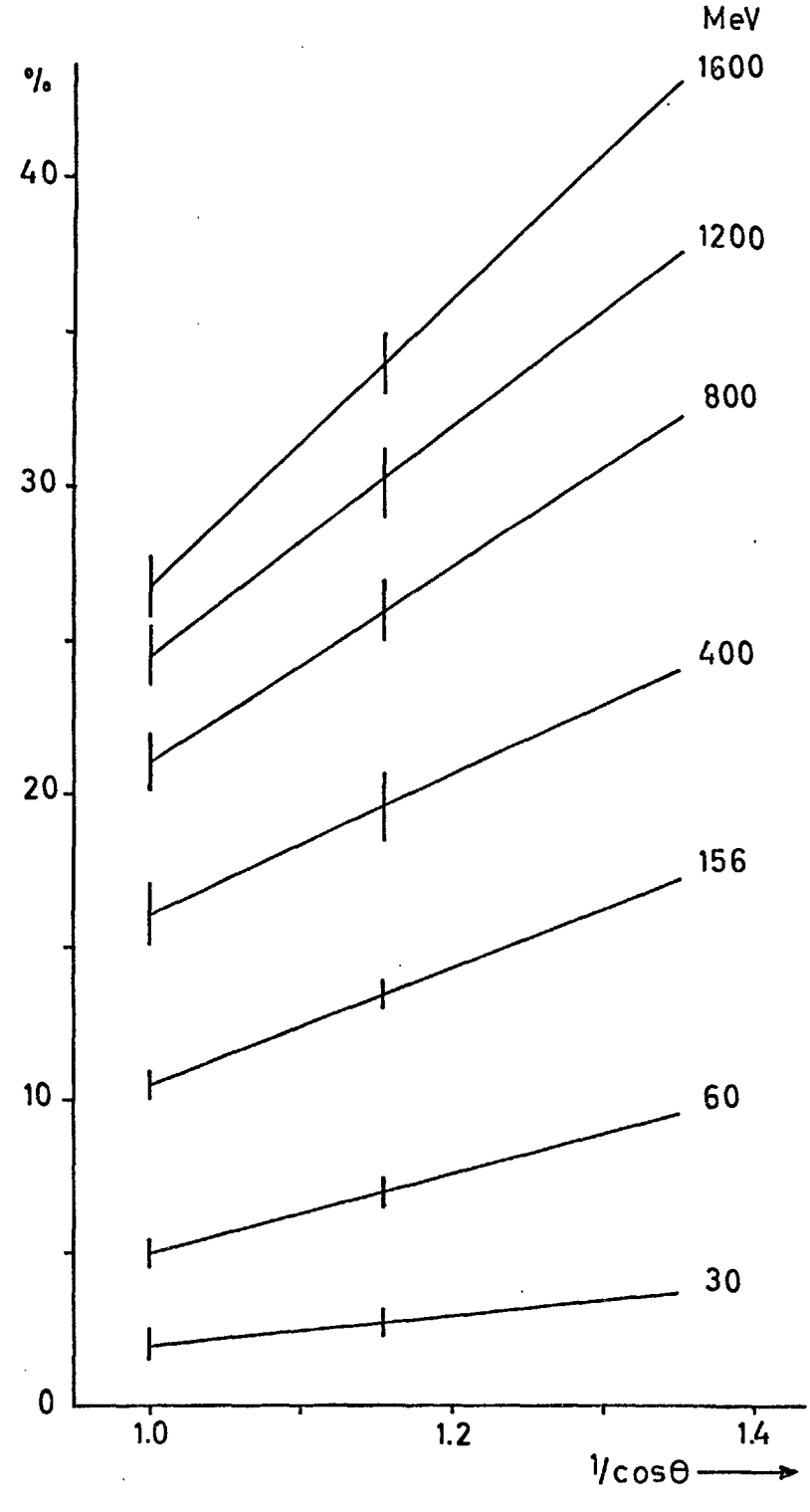

Figure 4.20

Figure 4.21

Narrow beam scan in lid gamma counters at 560 MeV and normal incidence, measured near to the photomultiplier.
a) Singles efficiency b) Doubles probability

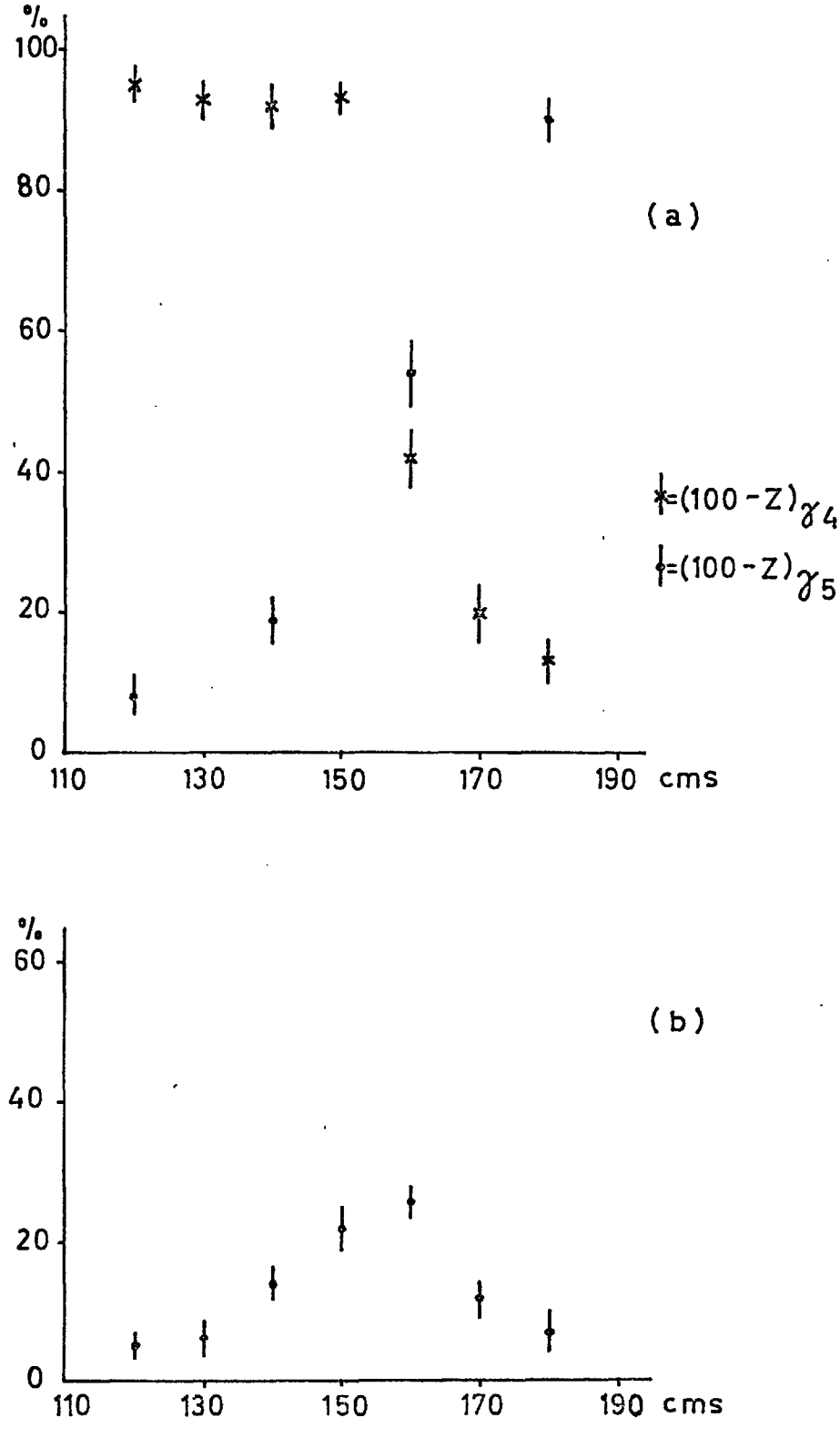

Doubles in lid gamma counters as a function of radius averaged over width.

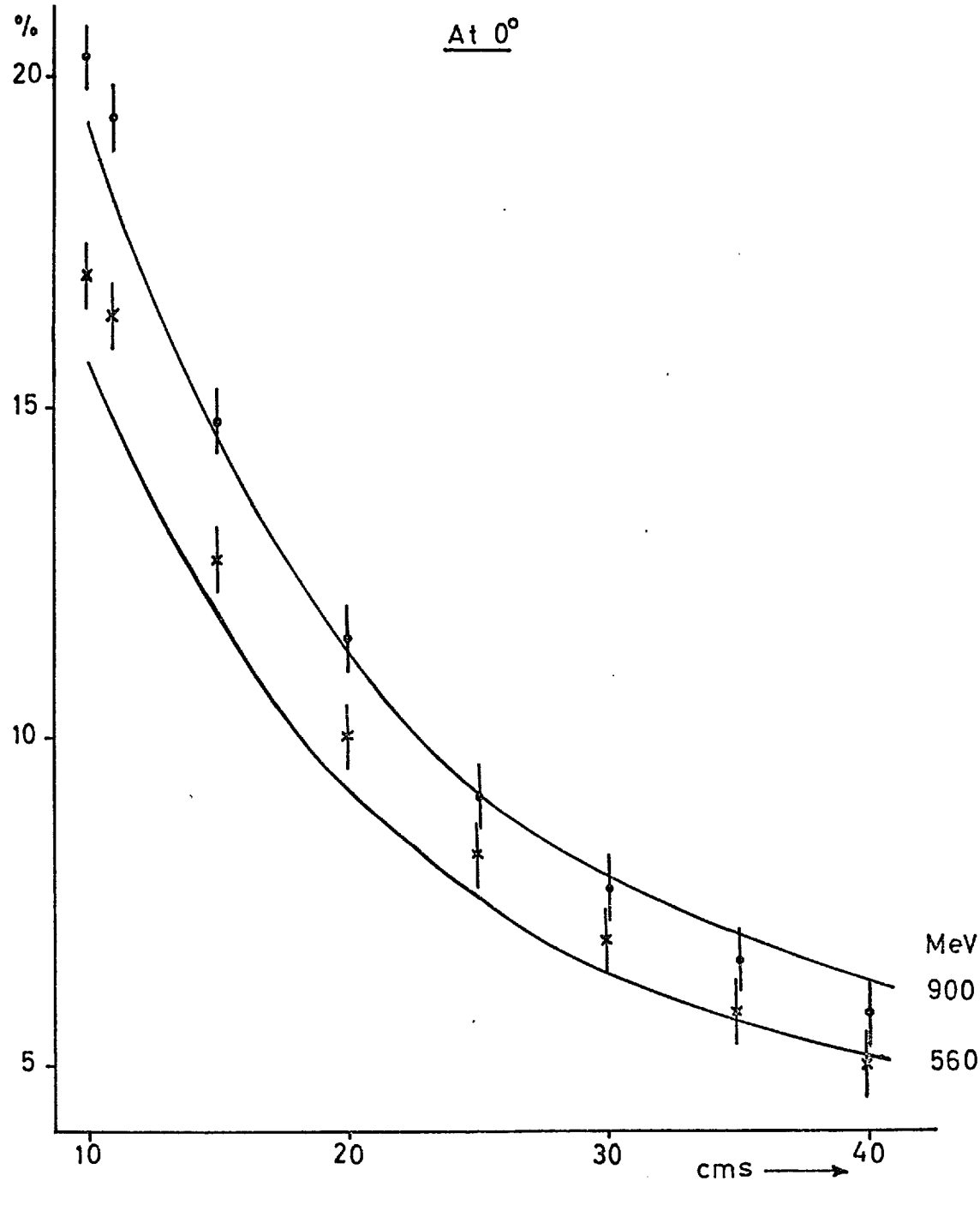

Figure 4.22

CHAPTER V

THE STUDY OF THE DECAY COUNTER SYSTEM IN OPERATION

5.1 Introduction

After a thorough study of the decay counters placed in a beam of gammas by themselves or with one or two adjacent counters of the same type, the performance of the entire array surrounding the hydrogen target in its proper place in the experiment was of great interest.

The gamma detection efficiency and doubles probability were measured by studying the gammas produced in the decay of the omega meson. The relative abundance and narrowness of the omega made it an interesting resonance to study, especially because of its two major decay modes, $\pi^0 \gamma$ and $\pi^+\pi^-\pi^0$.

As soon as datawere obtained from the omega, it was evident that many other effects were smearing the signature of the omega decay channels more than expected. In order to pursue these effects, a data collection run was made on the eta meson, which decayed partly into two gammas. Again, the abundance and narrowness of this meson together with the especially useful 2γ decay mode made it an ideal choice. The decay system was particularly useful in the application of coplanarity to a two body decay mode, giving an extremely clear selection mechanism. Unfortunately, there was no similar two charged pion decay mode to use for the study of pion effects. Consequently, the $2\pi n$ background was used for this purpose.

The principle effects observed were caused by delta rays from the beam or secondary pions and were seen mainly as random inner charged counts or adjacent inner charged counts. These effects and others were studied and the larger ones were measured at various energies. The background mode of $\pi^-\pi^0$ p was used to study the effects where possible as a

comparison to $2\pi n$ events. An account of this work follows. In order to categorise the effects, a nomenclature is described in Fig. (5.1).

5.2 A Measure of Gamma Efficiency and Gamma Doubles Probability at the Omega Momentum

The first step in verifying the analysis and performance of the apparatus was to measure the straight forward gamma efficiency. The omega meson is a narrow, well defined resonance and so this was chosen for the study, especially as it has two main decay modes only. The primary mode is the $\pi^+\pi^-\pi^0$ decay which occurs in approximately 90% of all decays whilst the second is the $\pi^0\gamma$ mode which occurs approximately 10% of the time. The momentum chosen for the investigation of omega was 1153 MeV/c which gave a high yield with a sharp forward peak of events in the time of flight spectrum. In order to subtract background events from the omega data, runs were made at 1018 and 1044 MeV/c which were below the omega threshold. In doing this, the assumption was made that other background in the region would not have varied much, and this was checked by Monte Carlo runs on known backgrounds.

The modes investigated were $2\pi_s 2\gamma_s$, $2\pi_s\gamma_s$, $2\pi_s\gamma_2$ and $2\pi_s\gamma_s\gamma_2$. Clearly $2\pi_s\gamma_s$ gave a measure of the gamma inefficiency if allowance was made for the two gammas to go in the same counter or neighbouring counters. This also involved checking what fraction of $2\pi_s\gamma_2$ was due to two gammas in neighbouring counters and what was due to an undetected gamma whilst the second doubled. The efficiency was found to be $86 \pm 2\%$ compared with about $81 \pm 3\%$ as expected from $\pi 7\gamma$.

Almost the whole of the $2\pi_s\gamma_2$ signal appeared to have come from two gammas adjacent to each other, the number of double gammas was found from the $2\pi_s\gamma_s\gamma_2$ mode and estimated as $6 \pm 1\%$ compared with a value of $5 \pm 1.5\%$ from $\pi 7\gamma$.

Figure 5.1

Table of Decay Detection Effects

γ_s	A simple gamma count consisting of a count in a gamma counter with no neighbouring counts
γ_2	A count in two adjacent gamma counters due to either a spread of one shower to a second counter or two gammas close to each other
Π_s	A simple pion count consisting of a count in the corresponding inner charged counter and gamma counter
Π_γ	A pion count with an extra count in an adjacent gamma counter
Π_δ	A pion count with an extra count in an adjacent inner charged counter
δ	A count in an inner charged counter only

5.3 Other Gamma Associated Effects Observed

The expected response of the decay system was that a gamma would be detected or not, depending on the counter efficiency, giving a γ_s signal. Otherwise, the gamma could initiate a shower in two adjacent counters and be classed as γ_2. This class also included those cases where two gammas were produced in an event but entered adjacent counters. With a multiplicity of gammas, more than one gamma could enter a single counter and the system would then have only recognised the presence of a single gamma.

From the data runs, it became immediately evident that other effects were also present. Amongst the events were apparent decays of omega with one less gamma and one more pion than expected. This was important as charge conservation demanded only an even number of pions in the neutron time of flight spectrum and the system was very efficient in detecting pions. It, therefore, appeared that a gamma was able to simulate a pion by triggering an inner charged counter as well. There were also events with extra inner charged counts present. Data runs with no pion beam were used to test if the inner charged counters were sufficiently noisy to cause spurious signals and this was found to be negative. A further study of the data indicated that the spurious inner charged signal was, in fact, often adjacent to a gamma signal. There appeared to be a random 'δ' signal but there was a peak in the channel for the adjacent counter when the spectrum of counter separation was examined. Finally, a number of events were observed where an otherwise standard event had a random gamma present, unassociated with any other particles in the event.

In order to understand the situation, runs were made at the eta momentum to look for the abundant $\eta \rightarrow \gamma\gamma$ mode where the strong coplanarity selection would be used to clearly identify the decay mode. The momenta used were 709 and 753 MeV/c.

Firstly, a comparison was made between $\eta \rightarrow \gamma_s\gamma_s$ and $\eta \rightarrow \gamma_s\Pi_s$ after a coplanarity selection. The ratio of Π_s/γ_s in the cylinders was measured as $12 \pm 1\%$. The effect could not be explained in terms of pair production by the photon which in its path length through the air, hydrogen, aluminium and part of the plastic of the inner charged counter, would have amounted to less than 4% in either case, with less than 1% difference between the two types of counter. These figures were estimated from the maximum likely path length through those media, including the passage of the gamma through three quarters of the inner charged counter scintillator before production of electrons still capable of detection. Approximately 60% of 200 MeV gammas produced a pair of electrons in a radiation length[4]. The slight difference between the two types of counter was introduced by the longer path length possible in hydrogen for a gamma passing through to a lid counter. The material through which the gamma passed was about 0.06 and 0.07 radiation lengths for cylinder and lid counters respectively

The probability of a delta ray associated with the beam entering the same counter as a gamma was less than $\frac{1}{2}\%$, based on the figures discussed in Section (5.5). A subsequent explanation was proposed which was that low energy isotropic gammas[13][17][18] of about 1 MeV were created which produced electrons in the inner charged scintillator by the Compton process[5][10][12][19]

A second effect not previously accounted for was that of a gamma passing through the region of the counter array where the cylinder and lid gamma counters met. As there were numerous effects spreading the signal from the original decay description, this effect was now also important. In this region, it was possible for a gamma to initiate a signal in two corresponding gamma counters, one in the lid array and one in the cylinder array. Again, the cleanest method of measuring this effect was to look at apparent $\eta \rightarrow 3\gamma_s$ events with a selection criterion of those events where two gammas were coplanar. The number of events with a third gamma in the

same angular counting bin, but in the lid and not the cylinder gave a direct measure of the effect. This was found to be $2.5 \pm 0.5\%$ as against an estimated figure of about 1% per gamma per cm of cross over region. Allowing for counter inefficiency, about a 4% effect was expected.

From a study of apparent $\eta \to 3\gamma_s$ with a coplanarity selection on two of the gammas it was quite clear that an otherwise perfect two gamma decay mode had a third gamma present randomly distributed about the array. This was not at all understood but a figure of 5% per event was obtained for the effect.

The last two effects were observed together in the omega data in the $2\pi_s$ $3\gamma_s$ channel and a figure of $10.8 \pm 2.6\%$ was obtained, compared with 5% plus twice $2\frac{1}{2}\%$ from the eta data. The information obtained for the two resonances appeared to be consistent, therefore.

One more gamma effect was observed in the omega data and this was where a gamma was detected as an inner charged signal with an adjacent gamma count. This was thought be be due to the low energy isotropic gammas causing $\gamma_s \to \pi_s$. The pair production effect described in that context gave a 4% effect. As the electrons were produced in a very forward direction, this would be a negligible source of the $\gamma_s \to \gamma_s + \delta$ effect now under consideration. If the cause was the isotropic gammas, the typical solid angle subtended by the inner charged counters was about 115^0 for the $\gamma_s \to \pi_s$ effect and 28^0 for the $\gamma_s \to \gamma_s + \delta$ process. If allowance were made for the pair production in the figures for $\gamma_s \to \pi_s$, the expected effect from isotropic gammas would then have been about 3.7% for the $\gamma\delta$ process, allowing for angular acceptance. The observed figure was between 3% and 4% consistent with this origin. There was still no measureable contribution from beam associated deltas, as discussed in Section (5.5).

5.4 The Pion Associated Effects Observed

With a neutron time of flight, only even numbers of pions were possible in a decay mode due to the zero charge of the parent resonance. If the system was 100% efficient for pion detection, the only problem in event classification was counting the number of gammas. In the $\pi 7\gamma$ experiment, the counters were not measured with a view to estimating the efficiency for pion detection. The gamma sandwich counters were assumed to be highly efficient for pions, if they were capable of detecting a single electron in one layer. The EHT of the inner charged counters was set to be very definitely on the plateau of the efficiency curve and were measured to be highly efficient to the passage of a single electron through the counter.

Three basic inefficiencies were expected. Firstly, there were various holes in the apparatus and it was also possible for a pion to pass between the counters. In the decay simulation program , these were treated separately, the former being taken into account in a geometric examination of each particle. The second expected inefficiency was where the pions did not have sufficient energy to reach either the inner charged counters or the gamma counters. The third was the overlap region of the two types of gamma counter doubling a pion as it did a gamma.

From the omega data, there were clearly other effects diffusing the signal and smearing it over numerous decay identification channels. These effects were pursued and are discussed below. In order to examine the effects observed in the omega data, special data runs were made over a large range of energy to examine the pion effects in $\pi^+\pi^-n$ and $\pi^-\pi^0$ p. These two completely different processes with different timing particles would, therefore, prove fairly conclusively what the pion effects were, if consistent.

The $2\pi n$ data were extremely useful in that a coplanarity condition could

be applied to cleanly select these events. Typically, about 80% of all $2\pi n$ events were coplanar within one counter bin. The $\pi^-\pi^0$ data were more difficult to select clean events. The method introduced was for the two gammas from the π^0 to be selected and the angular bisector between them found. A two dimensional spectrum was then plotted of the separation between this bisector and the charged pion against the separation of the two gammas themselves. This then allowed a coplanarity selection between the π^- and π^0, as well as an opening angle selection on the gammas from the π^0, which was expected to be small. Fig. (5.2) shows such a spectrum obtained from a Monte Carlo simulation written by Dr. W.G. Jones. In the analysis of the data, the background present was assessed from the regions where $\pi^-\pi^0$ p events did not occur. Within one counter bin of coplanarity between the π^0 bisector and the charged pion and with less than four bins gamma separation, there were approximately 70% of all Monte Carlo generated events. Consequently, this too was quite a clean selection technique as was indicated in Fig. (5.2) by the lack of events over large regions of the spectrum.

Apart from the three inefficiencies already mentioned, one possible effect was that caused by the elastic scattering of pions leaving the target and thus giving both a pion and a proton in the decay counter array. With a cross section of 30 mb in hydrogen[24], this was less than a $\frac{1}{4}$% effect in a two pion decay mode .

For the expected inefficiencies, the probability of an overlap pion was measured in $2\pi n$ and $\pi^-\pi^0$ p as $2.0 \pm 0.3\%$, whereas the measured effect in the omega data was $0.6 \pm 0.1\%$. Again, a<4% effect was expected. The probability of a pion being lost altogether other than through non-counter regions, was contributed to by two separate effects. Firstly, a pion was able to pass between two counters and the estimated upper limit of this

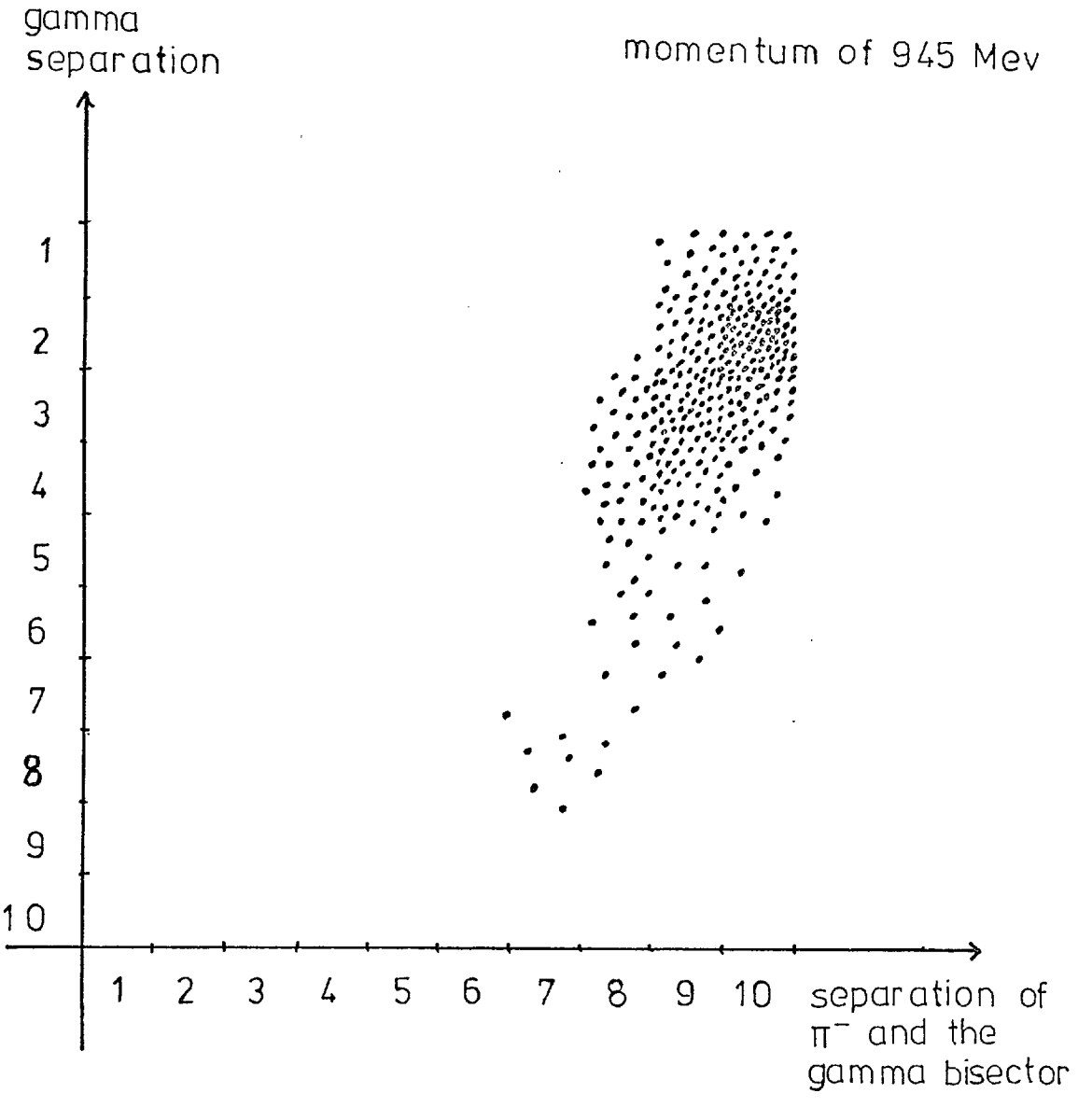

Figure 5.2

$\pi^-\pi^0 p$ Monte Carlo Events

effect was about 4%. Secondly, it was possible that the energy of the pion was insufficient for it to reach the inner charged counter. About 70 MeV/c was required for this purpose, whilst 135 MeV/c[20] was required for the pion to reach the gamma counters after passage through the core and the tin of the counter holder. The probability of the former happening was estimated from the decay program to be about 4% also. A measurement was made of the two effects together and a figure of $4 \pm 3\%$ obtained.

The first unexpected effect was the large number of events with an inner charged count ('δ') present on its own. Apart from being found in an adjacent bin to a gamma as discussed in Section (5.3), δ's were found next to pion counts instead of pions, and also randomly distributed as extra particles in an event. The first of these considered was where a pion appeared only as a δ due to insufficient energy to reach the gamma counters. An order of magnitude calculation was made by estimating the equivalent length of hydrogen of all the material present through which the pion would have to pass to be detected, firstly, by the charged counters and then by the gamma counters. Range-momentum curves for pions in hydrogen then indicated the momenta required to be detected. The estimates were only approximate as the angle of incidence chosen affected the figures but, more importantly, so did the amount of penetration into the counters required for detection. With these momentum values, the decay simulation program gave a figure of about 12% in the omega region for $\pi \rightarrow \delta$. By looking for $\pi\delta n$ and $\delta\pi^0 p$ in $2\pi n$ and $\pi^-\pi^0 p$, the effect could be investigated through a large range of momentum, from 1 GeV/c to 2.7 GeV/c and an empirical formula obtained to fit the data :

$$p\,(\pi \rightarrow \delta) \;=\; 0.067 \;+\; 0.011\; p_\pi \quad ,$$

where p_π was the pion momentum. It was surprising to observe that this

effect increased with momentum. The reason for this was not understood. An estimate of $9.5 \pm 0.9\%$ was made from the omega data compared with 7% from the formula.

The second of the delta processes considered was where the δ was adjacent to a pion, after eliminating the random effect. The process was labelled $\pi\delta$ and believed to be due to delta rays produced by a pion on its way to the decay counters. A further discussion of this is given in the next section. The process was measured in $2\pi n$ and $\pi^-\pi^0 p$ by looking for an extra inner charged count next to the charged pion and eliminating the random delta background. A momentum dependent formula was found empirically :

$$p\ (\pi \rightarrow \pi\delta) \quad = \quad 0.019 + 0.009\ p\pi \quad ,$$

giving a figure of about 2% in the omega region. From the omega data, a measurement of $2.4 \pm 0.4\%$ was obtained.

The random delta effect was assumed to be from two sources, the beam pion passing through the target and also the secondary pion produced in an event passing out towards the decay counters. There was necessarily some bias towards the counter of entry but the earlier a delta was produced in flight by the second process, the more likely it was to be random in its counter of detection. Both $2\pi\delta n$ and $\pi^-\delta\pi^0 p$ data were studied but the latter was complicated by the presence of the proton, which passed through the remaining hydrogen and thus had a considerable effect. The process was therefore measured in $2\pi n$ and the following formula obtained :

$$p\ (\text{random delta from secondary pion}) \quad = \quad 0.0146 + 0.029\ p\pi \ .$$

The effect of delta rays from the beam was measured by removing hydrogen from the target and the probability obtained was as follows :

$$p\ (\text{random delta from beam pion}) \quad = \quad 0.025 + 0.015 \times p_{beam} \ .$$

This whole subject is treated in more detail in the next section.

Another important process observed was where a pion and a gamma occurred adjacent to each other in a manner which indicated the gamma was extraneous to the event as in $2\pi n$. This effect was labelled π_γ and was caused by the same process as gamma doubles. Measurements were made in $\pi_\gamma \pi_s n$ and $\pi_\gamma \pi^o p$ and a formula derived to fit the data;

$$p\ (\pi \rightarrow \pi_\gamma) \quad = \quad 0.045 \quad + \quad 0.01\ P\pi \quad .$$

Consequently, a figure of 6% was expected in the omega region where a figure of $8.7 \pm 0.9\%$ was measured.

Another but much smaller effect was observed and that was where a pion appeared to double and give two adjacent pion counts. This was probably due to a gamma ray doubling and the shower spreading backwards to the inner charged as well as forwards. A measurement of $0.75 \pm 0.2\%$ was obtained in $3\pi_s n$ with the requirement that two pions were coplanar with the third adjacent to one of them.

It was also possible for a pion to appear as an adjacent δ and gamma signal. This was studied in $2\pi n$ events and a figure of $2.4 \pm 0.3\%$ obtained. An analysis of $2\pi n$ events in the omega data runs gave $2.8 \pm 0.6\%$ for the process which was probably due to an off-axis event where the pion almost passed between two counters. Misalignment of counters would have caused the same effect.

5.5 The Delta Ray Effects

As already discussed, various effects detected in the analysis of the data obtained for the omega meson were attributable to the passage of delta rays into the decay counter system. These were the π_δ process, the random δ

Delta rays were caused by the passage of a charged particle through matter, when an electron could be removed from a neutral atom. Numerous

delta rays could be produced of varying energies and ultimate directions[4][12].

One of the sources of delta rays was from the passage of beam pions through the hydrogen target. If such a delta ray was produced on the axis of the target and travelled out normally, it would have passed through 32.5 mm of liquid hydrogen and $\frac{1}{16}$ inch of aluminium vacuum flask. This was equivalent to 0.8 gm cm^{-2}. The delta rays were, in fact, produced at some angle to the beam and then suffered multiple scattering through large angles[4]. It was not obvious what allowance to make for the angles at which the delta ray would pass out of the target, but it seemed reasonable to assume a mean angle of 45^{o} to give an order of magnitude. Consequently, the delta ray would then have passed through 1.1 gm cm^{-2}. To do this, it would require a kinetic energy of more than 2 MeV[21]. If a counter threshold of 0.3 MeV was assumed, requiring a penetration of about 0.2 cm into the inner charged counter before a particle could be detected, this implied that a minimum energy of 2.3 MeV was required. If the mean path length of the beam pion in the hydrogen was 15 cm before an event took place, the probability of a delta ray of this energy being produced was 6% per incident pion of 1 GeV/c momentum. The delta rays from this source were randomly distributed about the decay counter system.

Pions produced in an event were also capable of producing delta rays, either in the liquid hydrogen of the target, the aluminium of the vacuum flask or the air between the target and the decay counters. If it is assumed that, on average, a delta ray produced in the hydrogen target was produced about half way out and that the pion itself was at an angle of 60^{o} to the beam, then the delta ray would have, on average, followed the path of the pion, thus travelling at 30^{o} to the normal to the axis. It would thus have travelled through about 16 mm of hydrogen at an angle of

30^{0} whichwas about 0.7 gm cm^{-2}. This required a kinetic energy of about 1.8 MeV in order to be detected in the inner charged counters, or a probability per 500 MeV/c secondary pion of 6.3% for 150 mm path length in hydrogen. For a path length of 32.5 sec 30^{0}, that is 37.5 mm of hydrogen, the probability was 1.6% per pion.

A delta ray passing through the vacuum flask at an angle of 30^{0}, having been produced half way through the aluminium on average, would pass through 0.14 gm cm^{-2} including 0.04 gm cm^{-2} of air. The kinetic energy required would then have been a total of 0.8 MeV giving a probability of producing a delta ray of about 18% per 150 mm of hydrogen for a 500 MeV/c secondary pion. The aluminium had only half as many electrons per nucleon as the hydrogen and so it was only half as effective in producing delta rays. Therefore, the 0.20 gm cm^{-2} of aluminium flask was equivalent to only 0.10 gm cm^{-2} of hydrogen or 1.4 cm, corresponding to a probability of producing a delta ray of 1.7% per 500 MeV/c secondary pion.

Finally, a pion at 60^{0} to the beam had a path length of about 37 cm in air which was equivalent to 0.044 gm cm^{-2}. Again, this was about half as effective as hydrogen and so was equivalent to 0.022 gm cm^{-2} of hydrogen or 0.31 mm. A delta ray produced about half way through to the charged counters would pass through only 0.022 gm cm^{-2} of hydrogen and would require a kinetic energy of approximately 0.32 MeV giving a probability of about 50% per 500 MeV/c secondary pion per 150 mm of hydrogen and so corresponded to a probability of 1.0% per secondary pion.

Consequently, the total probability of delta rays from any source was $6 + 4.3n\%$ where n was the total number of secondary pions present. If these delta rays were all randomly distributed, the chance of obtaining a non-adjacent delta was $\frac{14}{20}$ of 14.6% or 10.2%. This figure was based on a beam momentum of 1 GeV/c and a secondary pion of 500 MeV/c. The

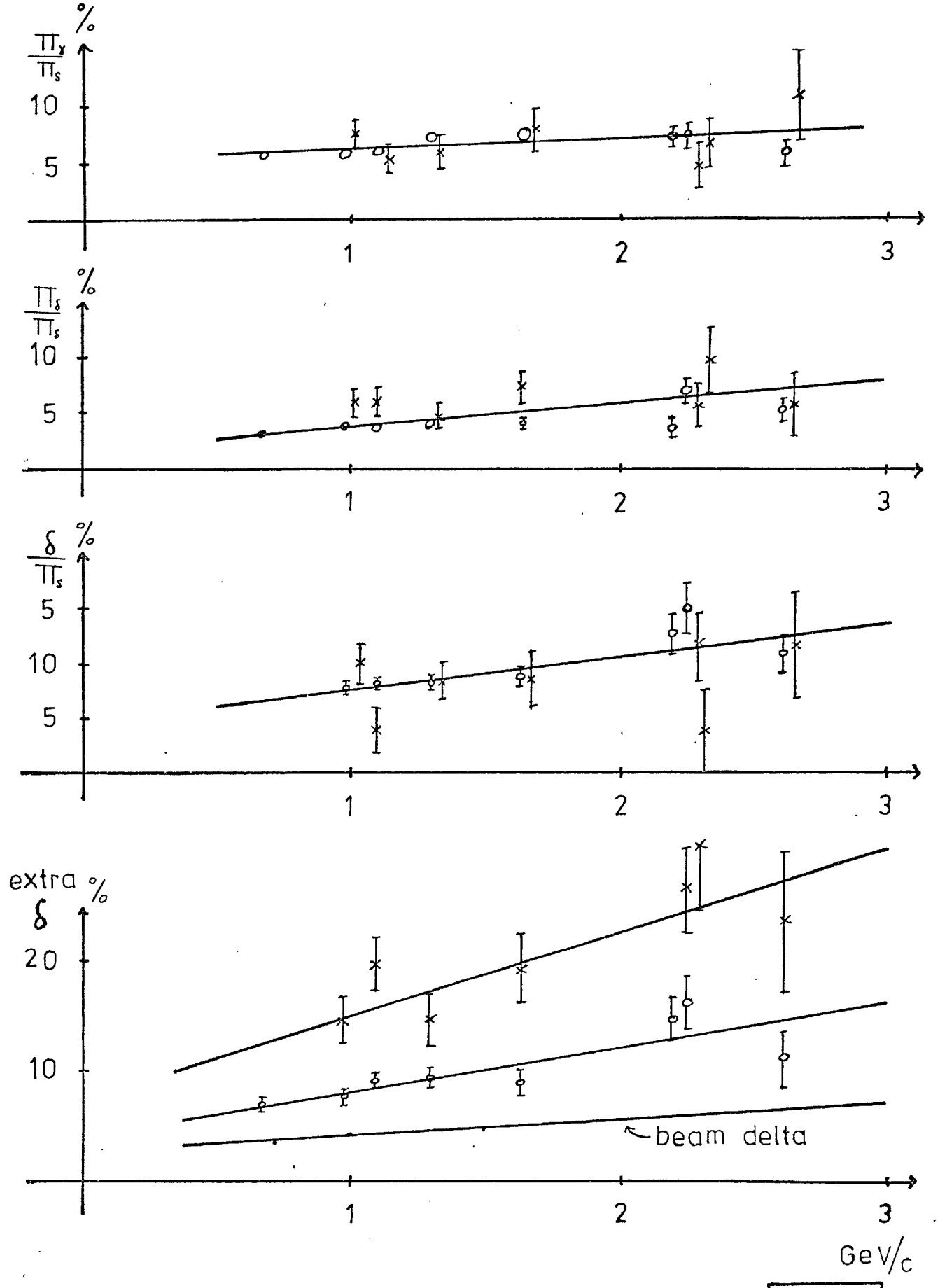
%
$\frac{\pi_\gamma}{\pi_s}$
10
5
1
2
3
%
$\frac{\pi_\delta}{\pi_s}$
10
5
1
2
3
$\frac{\delta}{\pi_s}$ %
5
10
5
1
2
3
extra %
δ
20
10
beam delta
1
2
3
GeV/c
2πn
π⁻π°p

Figure 5.3

experimental figure was $8.7 \pm 0.9\%$ for a random delta in the omega region. Beam deltas were measured as 4% not the predicted 6%. There would, of course, be a tendency for the deltas from secondary pions to be biased towards the pion's counter of entry.

5.6 Conclusions

As a result of the study of omega, together with n, $2\pi\bar{n}$ and $\pi^-\pi^0$ p, in the main experiment, it was clear that there were many effects of importance to the analysis other than gamma efficiency and gamma doubles. However, as the bulk of these effects involved pion behaviour and the number of pions present in an event was defined to be even for neutron time of flight, say, the main problem was still to count the number of gammas present.

The data obtained by all four types of event were consistent and a table of the effects present is given below. About 20% of the $\omega \to \pi^+\pi^-\pi^0$ signal actually appeared in the $2\pi_s\ 2\gamma_s$ channel.

Process	Magnitude
gamma effects	
$\gamma_s \rightarrow \Pi_s$	$12 \pm 1\%$ per gamma in the cylinders
	$26 \pm 4\%$ per gamma in the lids
gamma cross over	$2.5 \pm 0.5\%$ per gamma
random extra gamma	5% per event
$\gamma \rightarrow \gamma_s + \delta_{adjacent}$	3 - 4% per gamma
pion effects	
pion cross over	$2.0 \pm 0.3\%$ per pion
$\Pi \rightarrow \delta$	$0.067 + 0.011\ p\Pi$ per pion
$\Pi \rightarrow \Pi\gamma$	$0.045 + 0.01\ p\Pi$ per pion
$\Pi \rightarrow \Pi\delta$	$0.019 + 0.009\ p\Pi$ per pion
extra delta from secondary pion	$0.0146 + 0.029\ p\Pi$ per pion
extra delta from beam pion	$0.025 + 0.015\ p_{beam}$ per event
$\Pi \rightarrow \Pi_s + \Pi_s$ adjacent	$0.75 \pm 0.2\%$ per pion
$\Pi \rightarrow \gamma_s + \delta_{adjacent}$	$2.4 \pm 0.3\%$ per pion
pion undetected	3% per pion
$\Pi \rightarrow \gamma_s$	$2.0 \pm 0.3\%$ per pion

CHAPTER VI

THE BRANCHING RATIOS OF THE OMEGA MESON

6.1 Introduction

After using the omega meson to examine the performance of the equipment, together with other processes, the omega itself was studied with a view to measuring its branching ratios into the prominent decay modes of $\pi^0\gamma$ and $\pi^+\pi^-\pi^0$, together with a search for the $\pi^0\pi^0\gamma$ mode. Although the charged mode was well established, conflicting measurements of the neutral modes had been put forth in the literature. Whereas the neutral mode had generally been accepted as mainly $\pi^0\gamma$, some evidence had been put forward that it consisted very largely of $\pi^0\pi^0\gamma$. This experiment was able to identify the gammas in the neutral decay and hence add to the direct information on this question.

6.2 The Basic Problems

The first step was to make sure that the resonance was, in fact, the omega meson and so its mass and width were measured. For a timing particle of mass M_n and momentum P_n at a laboratory angle of θ_L to the beam axis, where its time of flight was t_n as against the time taken for the gammas to reach the neutron counters, t_o :

$$t_n^2 = t_o^2 \sec^2 \theta_L \left(1 + \frac{M_n^2}{P_n^2} \right) .$$

Thus,

$$P_n = \frac{M_n \, t_o \sec \theta_L}{\left[t_n^2 - t_o^2 \sec^2 \theta_L \right]^{\frac{1}{2}}} .$$

Let M_π M_p M_n and M_x be the masses of the beam pion, the target proton, the timing neutron and the resonance respectively. If the beam momentum and energy were P_π and E_π and the neutron energy was E_n, then :

$$M_X^2 = M_\pi^2 + M_p^2 + M_n^2 + 2E_\pi M_p + 2P_\pi P_n \cos\theta_L - 2(E_\pi + M_p)E_n \quad .$$

The omega mass was found from the time of flight corresponding to the peak value of the timing spectrum in the omega region using these equations and a value of 785 ± 5 MeV/c^2 was obtained. The times of flight corresponding to the half heights on either side of the peak were similarly converted into mass values and this gave a width for the omega peak. Allowing for a timing error of about 0.8 ns standard deviation, the experimental mass resolution, $13\frac{1}{2}$ MeV/c^2, of the apparatus was taken into account and a width of 12 ± 3 MeV/c^2 obtained. The best world values were 783.9 ± 0.3 MeV/c^2 (32) and 10.0 ± 0.6 MeV/c^2 (32) for the mass and width respectively. Consequently, there was no doubt that the peak corresponded to the omega meson.

The time of flight spectrum for omega was obtained at 1153 MeV/c. The background to the omega signal could be removed by subtracting a similar spectrum obtained below the omega threshold of 1090 MeV/c and so 1018 and 1044 MeV/c data were used for this purpose. The assumption made here was that the only difference between the above and below threshold data was the omega signal itself. For this to be true, there had to be no other resonance within the region of the omega timing gate at all three momenta. Also, the non-resonant background was assumed to be constant in shape and abundance.

The only known resonances close to the gate chosen, 6-12 ns, were η and ρ in $\pi^- p \to X^0 n$, and Σ and Λ in $\pi^- p \to X^0 K^0$. The rho was very wide and peaked at 5, $8\frac{1}{2}$ and 9 ns at 1153, 1044 and 1018 MeV/c respectively. It also decayed almost entirely into two charged pions and was not able to decay into two neutral pions. Consequently, it did not influence the channels used to examine omega. Eta is discussed in detail in Section(6.3) whilst Σ and Λ are discussed in Section(6.4)

The main non-resonant background was from two pions. It was found

that the remaining non-resonant background varied very little over the momentum range considered here. The two charged pion background was not able to enter the $2\pi_s 2\gamma_s$ channel used to measure $\omega \to \pi^+\pi^-\pi^o$ but the background due to two neutral pions was able to affect the detection of the neutral omega modes. This is discussed in more detail in Section(6.5). The two pion background did vary in abundance but varied very little in shape. Because of the different yields, it was not possible to use the below threshold subtraction technique in the analysis of the neutral decay modes.

The background subtraction method used for neutrals depended upon a knowledge of the amounts of background present which were capable of entering the detection channels. If these could be measured, they could then be subtracted from the signal data, leaving only the omega. The assumption was made that the Monte Carlo program was able to simulate the various background spectra and then, once the cross sections of the processes had been established, the fraction entering the decay selection channels could be predicted. Two processes were dealt with in this way, the eta and the two pion non-resonant background. Any remaining background after these had been removed was estimated by drawing a straight line between the parts of the time of flight spectra immediately on either side of the timing gate. Such background was found to be small and nearly flat.

A search was made for these backgrounds in their preferred decay channels and a cross section established. This then avoided any uncertainties involved in using numbers found elsewhere and feeding in such factors as neutron counter efficiency, the angular acceptance of the neutron counters and the production angular distribution of the processes themselves.

The three techniques used in this work were, then, varying the beam momentum to obtain above and below threshold data, measuring the cross

sections of other relevant processes present in different channels and selecting the preferred decay channels of the various effects concerned.

For the measurement of branching ratios, it would have been useful to have a figure for the total yield into omega for all decay channels. This was not possible, however, as the 2π non-resonant background was so large and rapidly varying that there was too great an uncertainty involved in estimating the background level. The difference between the below and above threshold data was too sensitive to the small difference in shape of the 2π non-resonant background and the large difference in cross section. Consequently, the omega signal present in the $\pi^+\pi^-\pi^0$ mode was measured and compared with that in the $\pi^0\gamma$ mode.

The errors involved in these measurements were found internally, from a consideration of $\frac{2\pi_s\,\gamma_s}{2\pi_s 2\gamma_s}$, where the gammas were obviously the correct energy for the $\pi^+\pi^-\pi^0$ mode, and from $\eta \to 2\gamma$, where the gammas were of a similar energy to those in the $\omega \to \pi^0\gamma$ mode, at the same centre of mass momentum. The pion contribution to the error was estimated from a comparison of the pion effects predicted at the omega momentum and those actually found there.

6.3 The Contribution of Eta to the Background

The eta meson was able to affect the background subtraction by its presence at 6 ns on the edge of the timing gate at 1018 and 1044 MeV/c, even though it was at $4\frac{1}{2}$ ns at 1153 MeV/c, much earlier than the omega meson. As the main decay modes of eta were $\pi^+\pi^-\pi^0$, 2γ and $3\pi^0$, it was able to enter the omega selection channels. However, only one event of η per 100 Mπ entered the timing gate of the $2\pi_s 2\gamma_s$ selection channel, compared with 115 events of ω per 100 Mπ and so this was negligible. (Section 6.6). On the other hand, about 8 events of η per 100 Mπ entered the timing gate of the $3\gamma_s$ selection channel, compared with 15 events of ω per 100 Mπ and so this was an important background effect. (Section 6.7).

The abundant $2\pi^0$ non-resonant background (Section 6.5) was falling

very rapidly in the time of flight spectrum and about 20% of this was in the $2\gamma_s$ channel. Therefore, the $\eta \rightarrow 2\gamma$ decay mode was not easily observed in the $2\gamma_s$ channel. The $\eta \rightarrow \pi^+\pi^-\pi^0$ decay mode was also not readily observed in the $2\pi_s 2\gamma_s$ channel as discussed above. As 23% and 11% of the $2\pi^0$ non-resonant background entered the $3\gamma_s$ and $4\gamma_s$ channels respectively, compared with 13% and 15% of the $3\pi^0$ decay mode of η, the $5\gamma_s$ mode was used to measure the η cross section. Only 8% of the $3\pi^0$ decay mode entered this channel but there was also less than $\frac{1}{2}$% of the $2\pi^0$ background.

The number of eta events measured at 1153, 1044 and 1018 MeV/c were 3, 5.6 and 4.8 per 100 Mπ respectively. Assuming the 8% figure obtained from the DSP and a branching ratio of 30.0%[32] for this decay mode, these events corresponded to 133 $\pm$ 44, 247 $\pm$ 68 and 212 $\pm$ 64 events of η to all channels per 100 Mπ. No momentum correlation was observable from these figures and so a mean of 197 $\pm$ 34 η events per 100 Mπ was assumed in this momentum region. After allowance was made for $2\pi^0$ events in the η region in $5\gamma_s$ a figure of 195 $\pm$ 34 etas was obtained, which corresponded to a cross section for $\pi^- p \rightarrow n\eta$ of 0.50 $\pm$ 0.10 mb. The cross section calculation assumed a neutron counter efficiency of $\frac{1}{3}$, and a neutron counter acceptance of about 10^{-2} from the DSP assuming isotropic production of the eta meson. The momentum at which η was investigated here was well past the peak yield of the meson at 693 MeV/c[22]. Between threshold at 680 MeV/c and this peak value, the cross section for η production was found to be given by 17 p^*[23]. The value obtained here for the cross section compared favourably with the published values at these higher momenta[24]. (Fig. 6.1).

6.4 The Σ^0 and Λ^0 Problem

These two particles were produced in conjunction with K^0 [25][26][27], the timing particle only being detected if it was K^0_L. Their thresholds

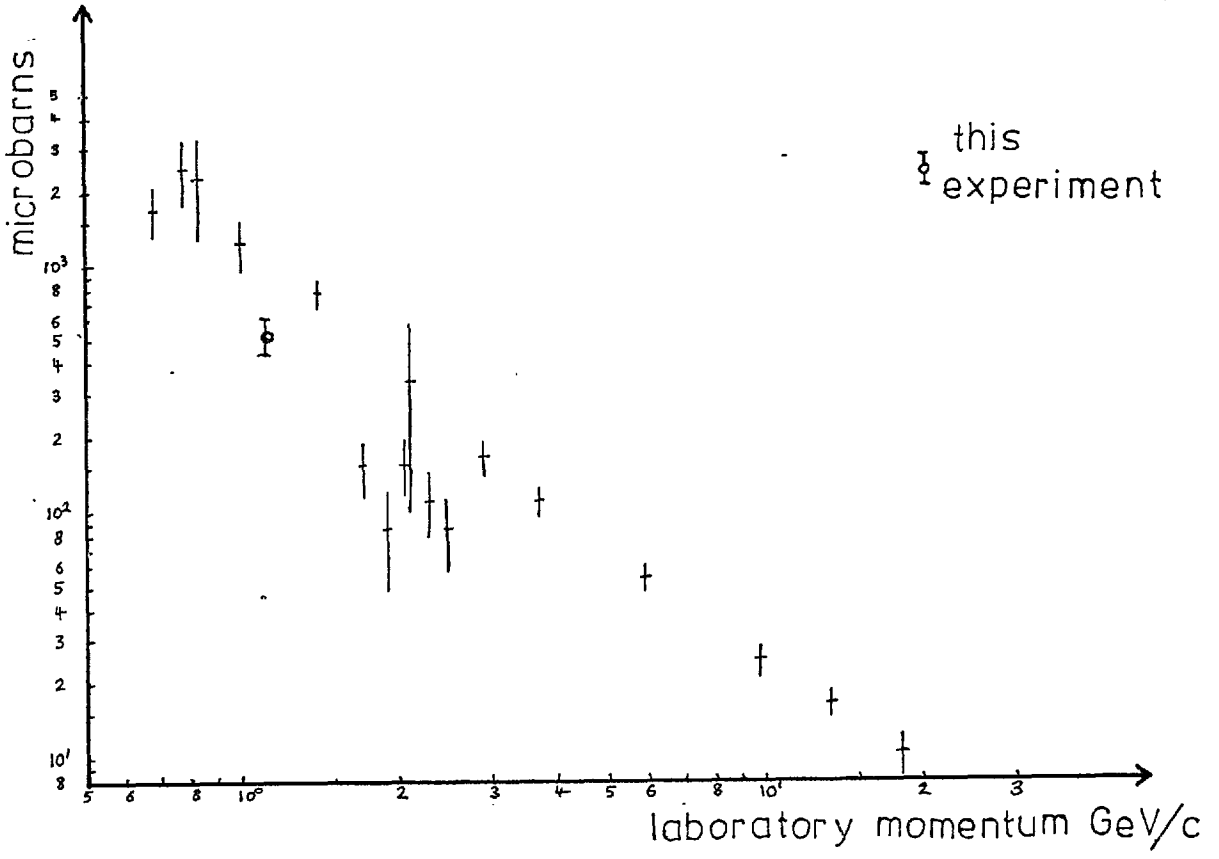

Figure 6.1

Eta Cross Section

were at 898 MeV/c and 1035 MeV/c respectively. At 1153 MeV/c, the Λ peaked at $3\frac{1}{2}$ ns and the Σ at 5 ns compared with the ω at 9 ns. The Λ peaked at 5 to $5\frac{1}{2}$ ns at 1044 and 1018 MeV/c, whereas the Σ, which was present at 1044 but not 1018 MeV/c, peaked at $11\frac{1}{2}$ ns.

The lambda meson was outside the timing gate for omega. Also, as it decayed into $p\pi^-$ (64%) and $n\pi^0$ (36%) and the proton or neutron passed through the lid hole, it did not constitute any problem in the analysis.

Σ decayed almost entirely to $\Lambda^0\gamma$ and then to $p\pi^-\gamma$ or $n\pi^0\gamma$. Most of the neutrons or protons entered the lid hole. The DSP program predicted that only $2\frac{1}{2}$% of them entered the lid counters. Taking the amount of material present to be about one seventh of an interaction length, the amount of neutrons interacting was about 3%. Consequently, the Σ would have been detected in the $\pi_s\gamma_s$ or $3\gamma_s$ decay channels. Only the $3\gamma_s$ mode was able to interfere with the detection of ω. The $\pi_s\gamma_s$ mode was lost in the $2\pi^\pm$ non-resonant background.

Taking into account the relative yields of Σ and ω[25][27][28], their branching ratios, the neutron counter acceptance and efficiency for K^0_L and n, the amount of Σ present in $3\gamma_s$ at 1044 MeV/c would have been less than a fifth of the omega present at 1153 MeV/c. There was no observable sigma in $3\gamma_s$ at 1044 MeV/c. This could have been due to incorrect figures for gamma efficiency and doubles in the DSP but this had been carefully checked in the $\pi 7\gamma$ experiments at low and high energies and then for omega and eta resonances as well as $\pi^+\pi^-n$ and $\pi^-\pi^0p$ with the decay detection system in situ. The alternative explanation was that Σ was not produced isotropically. This experiment was very sensitive to any anisotropy in production.

As the 1018 and 1044 MeV/c data were averaged, any sigma signal present at 1044 MeV/c would have been halved, anyway.

6.5 The Contribution of $2\pi^0$ to the Background

This was the most crucial background effect to the neutral decay modes

due to its abundance and shape, the latter varying only a little over the momentum region concerned (Fig. 6.2). The $2\pi^0$ moved only slightly, from $5\frac{1}{2}$ ns at 1153 MeV/c to $6\frac{1}{2}$ ns at 1018 MeV/c, whilst the full width at half height varied from 5 ns to 4 ns over the same range. There were no $2\pi^0$ resonances to make the $2\pi^0$ non-resonant background difficult to measure, so selecting the $4\gamma_s$ channel, the number of events at five different momenta were measured per 100 Mπ. These are shown below, together with an estimate of the total $2\pi^0$ present assuming a decay selection efficiency of 0.107 ± 0.010 into $4\gamma_s$.

pπ	$2\pi^0$ in 4γs	Total $2\pi^0$
1153	34.7 ± 3.3	324 ± 62
1125	47.2 ± 6.9	442 ± 106
1097	45.3 ± 6.7	423 ± 102
1044	57.3 ± 7.6	538 ± 118
1018	73.0 ± 8.5	683 ± 144

Spectra were also available at 1018 and 1044 MeV/c in the $3\gamma_s$ channel and so this was compared with the data above. There was $22.6 \pm 1.6\%$ of $2\pi^0$ in the $3\gamma_s$ channel and this gave a total of 760 ± 111 and 657 ± 98 events per 100 Mπ, respectively.

For subsequent use, the number of total $2\pi^0$ events per 100 Mπ was found from the graph of the data above, as shown in (Fig. 6.3).

Estimates were made of the cross section of the $2\pi^0$ non-resonant background at 1018, 1044, 1097, 1125 and 1153 MeV/c, assuming isotropic production, a neutron counter efficiency of one third and a neutron counter acceptance of 1.6×10^{-2} from the DSP. Values of 1120 ± 220, 930 ± 190, 660 ± 130, 690 ± 140 and 500 ± 100 μb were obtained respectively. The cross

Figure 6.2

$2\pi^0$ Non - Resonant Background

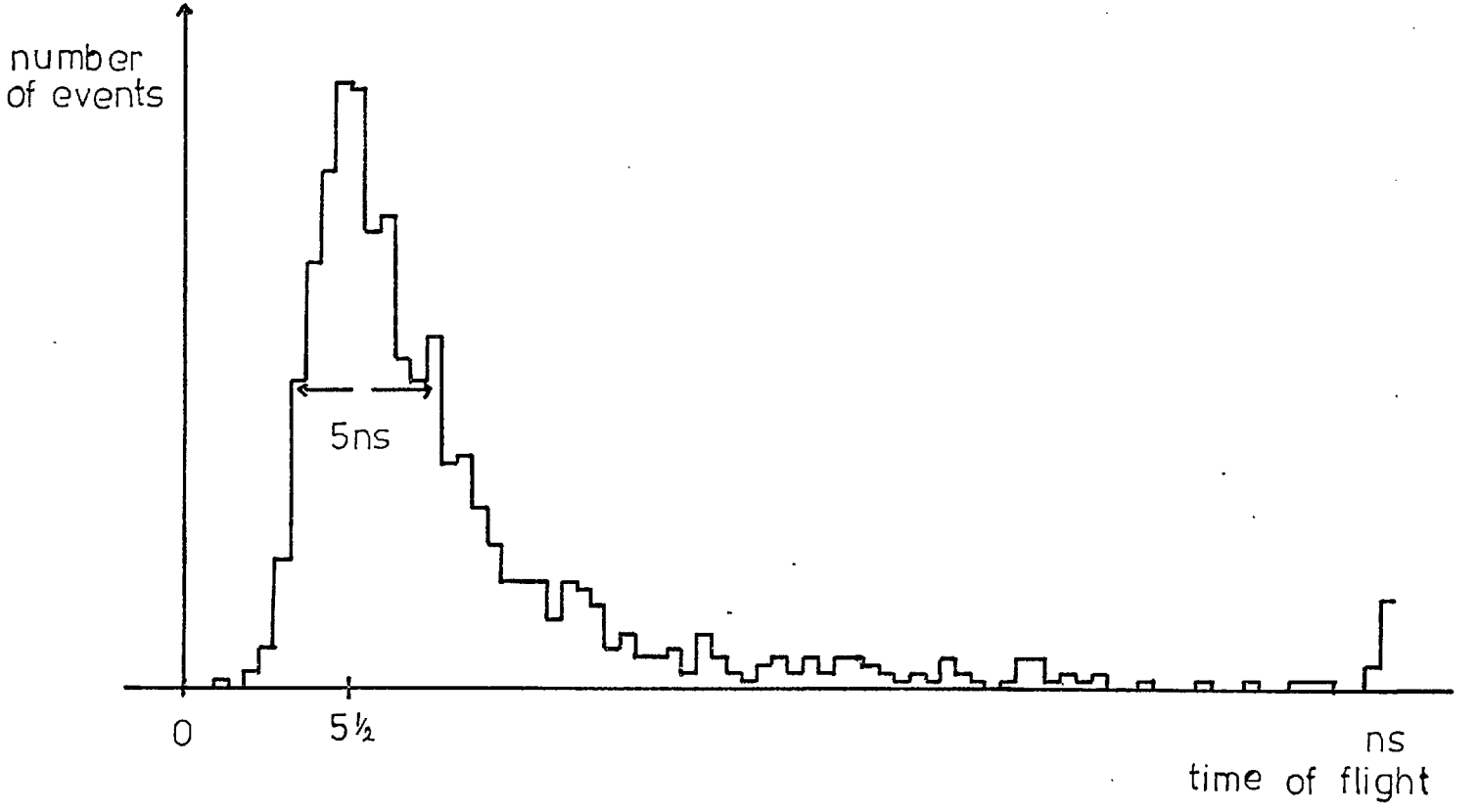

Figure 6.3

$2\pi^o$ Events

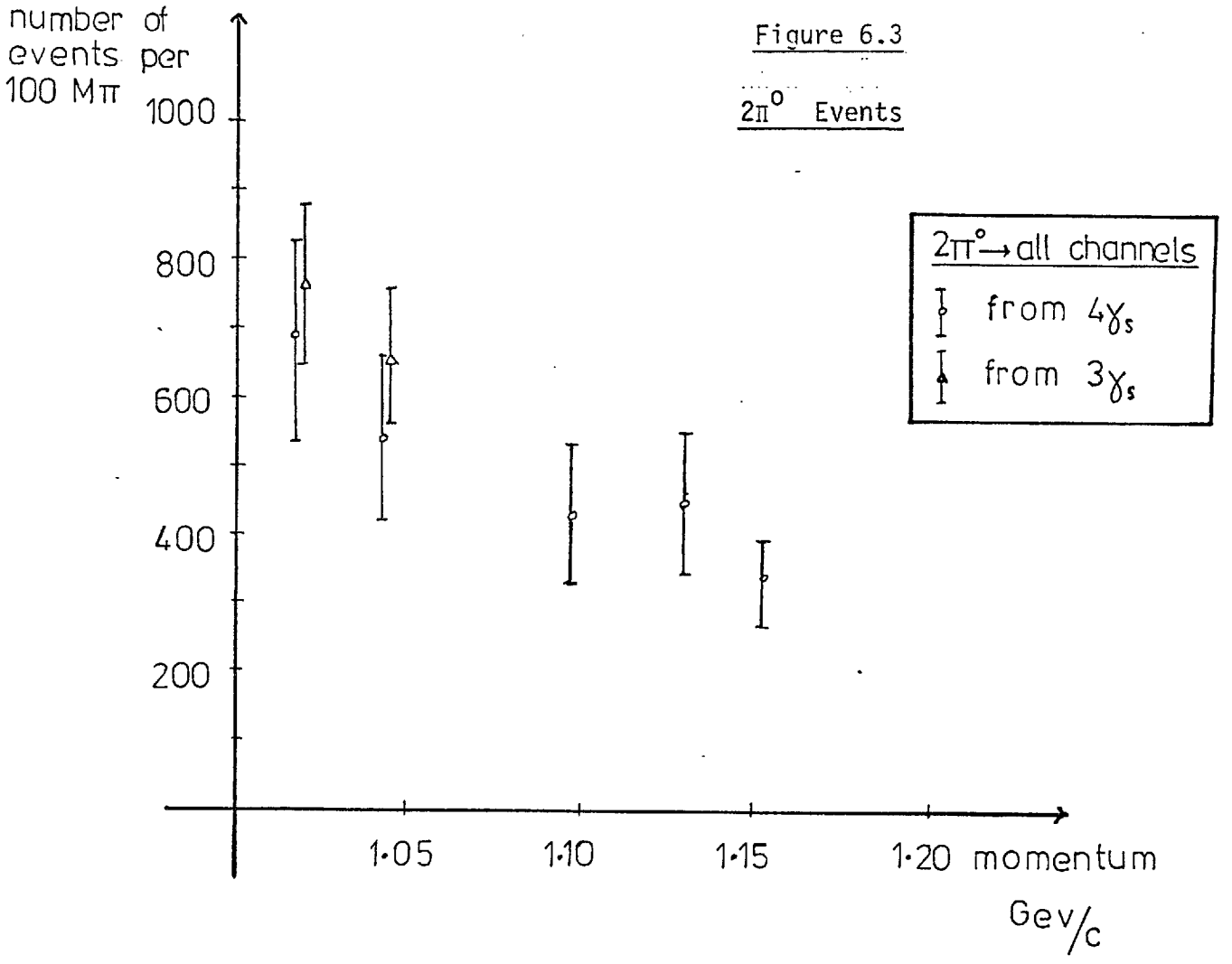

section was falling by a factor of about two over this region as was the published data in this region. Values obtained elsewhere were 3580 ± 700[29], 3100[30], 3060 ± 280[31], 1820 ± 260[31], 2030 ± 400[29] and 1450 ± 180[31] μb at 994, 1000, 1005, 1106, 1244 and 1249 MeV/c respectively. (Fig. 6.4). The cross sections obtained here were smaller than the published data given. It was assumed that this could have been due to anisotropy in the production process.

6.6 A Study of the $\pi^+\pi^-\pi^0$ Mode

This decay mode of omega was observed in the $2\pi_s 2\gamma_s$ channel at 1153 MeV/c. Accidental background was removed from both the signal and the background subtraction data by examining the time of flight spectrum at negative times, that is, before the arrival of the gamma peak. The 1018 and 1044 MeV/c data were averaged and then normalised to 100 Mπ, as was the signal data. The signal data before and after background subtraction are shown in Figs. (6.5) and (6.6). As there were less than 2.7 events of η and $2\pi^0$ combined per 100 Mπ, this was regarded as negligible. To remove the remaining background, mainly $\pi^+\pi^-\pi^0$ non-resonant background of which there was about 1 mb[24], a straight line was drawn between the parts of the time of flight spectra immediately on either side of the timing gate.

The number of omega events detected per 100 Mπ in the $2\pi_s 2\gamma_s$ channel was 115 ± 9 at 1153 MeV/c. The decay selection efficiency of $20 \pm 3\%$ from the DSP gave a predicted number of 600 ± 80 $\pi^+\pi^-\pi^0$ omega events per 100 Mπ.

6.7 The $\pi^0\gamma$ Mode

Although the previous background subtraction method would have been preferred, it was found impracticable to do this. This decay mode of the omega meson was investigated in the $3\gamma_s$ channel. There was a considerable amount of $2\pi^0$ non-resonant background present and it was clear that the difference between the yields at the various momenta was too great for the

Figure 6.4

$2\pi^0$ Cross Section

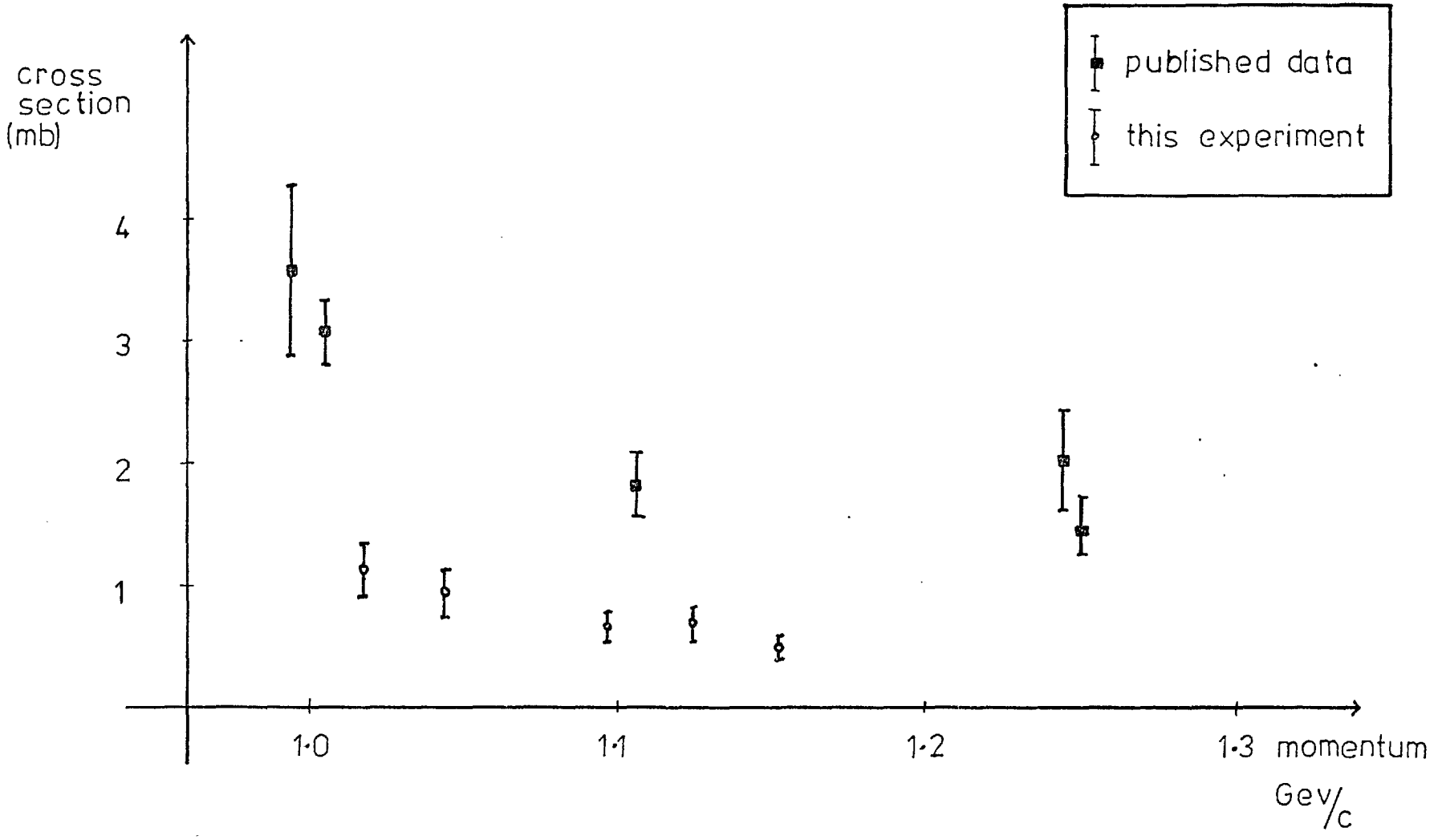

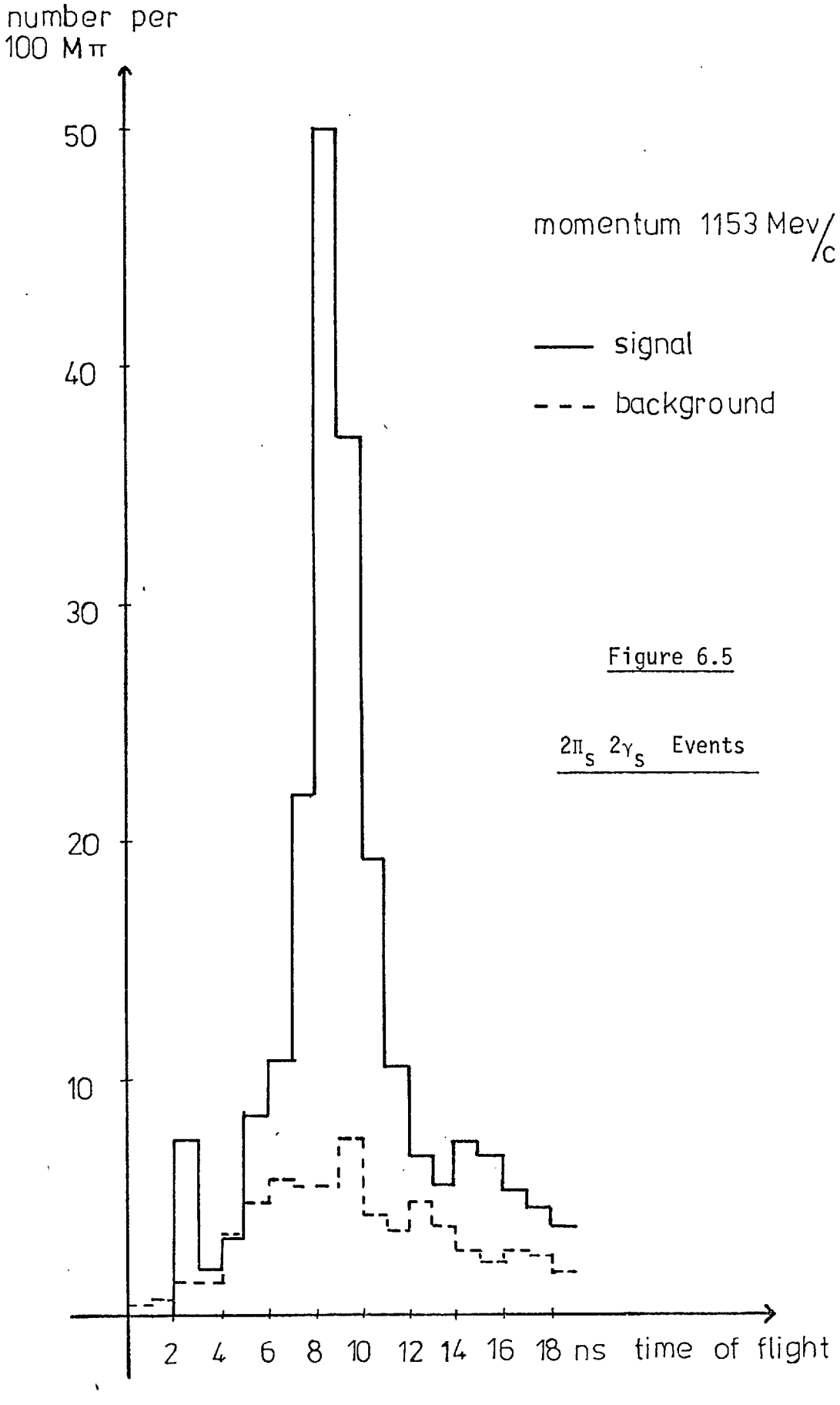

Figure 6.5

$2\Pi_s$ $2\gamma_s$ Events

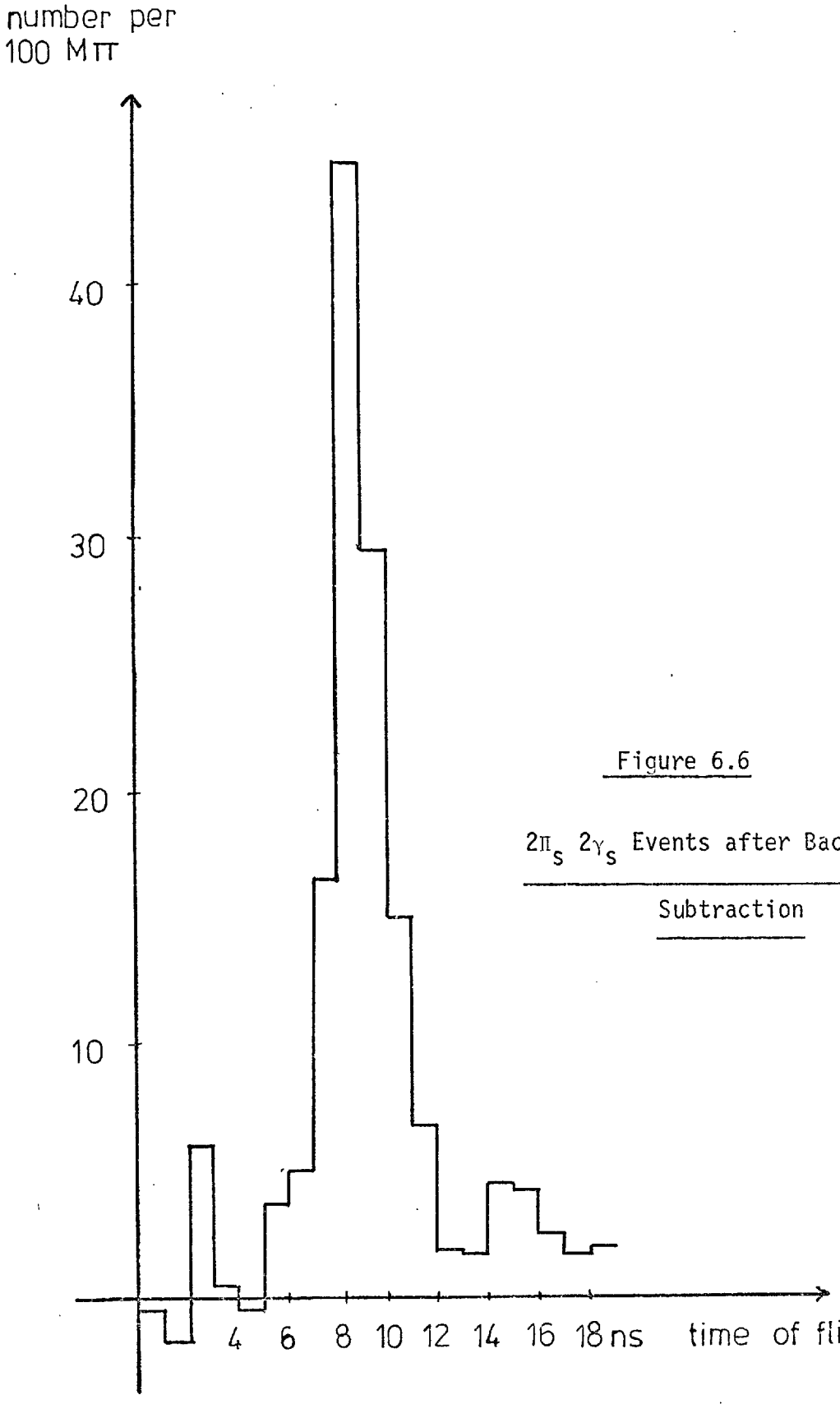

Figure 6.6

$2\pi_s$ $2\gamma_s$ Events after Background Subtraction

below threshold data to be used in the previous manner.

After the time of flight spectrum had been corrected for accidental background and normalised to 100 MΠ, DSP simulations of the spectra for η and $2\Pi^0$ phase space were combined and superimposed on the experimental data, as shown in Fig. (6.7). Also shown in this figure is the signal left after subtraction. It was then assumed that the remaining background could be subtracted out by drawing a straight line through the events on either side of the omega gate. The number of omega events seen in $3\gamma_s$ per 100 MΠ at 1153 MeV/c was 15 ± 5. The decay selection efficiency was estimated from the DSP to be $25 \pm 3\%$. This gave a predicted total of $\Pi^0\gamma$ omega events of 60 ± 20 per 100 MΠ.

6.8 The Search for $\Pi^0\Pi^0\gamma$

For the same reason as in the previous section, the background was not estimated using the below threshold data. At 1153 MeV/c, data were available in the $4\gamma_s$ and $5\gamma_s$ channels.

No measureable background was observed in $5\gamma_s$ after the subtraction of accidental background, η and $2\Pi^0$ non-resonant background. Within the timing gate, there were then 1.3 ± 0.6 events per 100 MΠ.

It was possible for the $\Pi^0\gamma$ decay mode to contaminate the $4\gamma_s$ channel of the $\Pi^0\Pi^0\gamma$ mode. From the DSP, the quantity of $\Pi^0\gamma$ present was calculated to be just 1.0 event per 100 MΠ. After subtracting the accidental background from the $4\gamma_s$ spectrum, the amount of η and $2\Pi^0$ was subtracted out using the DSP and the estimated cross sections of the two effects. Once again, there was no significant background remaining as shown in Fig. (6.8). Within the timing gate, there were -0.4 ± 0.2 events per 100 MΠ.

Taking a weighted mean of the two measurements, the amount of $\Pi^0\Pi^0\gamma$ seen in $4\gamma_s$ and $5\gamma_s$ at 1153 MeV/c was -0.23 ± 0.19. The decay selection efficiency was $25 \pm 7\%$ which led to a predicted number of -0.9 ± 0.8 events

Figure 6.7

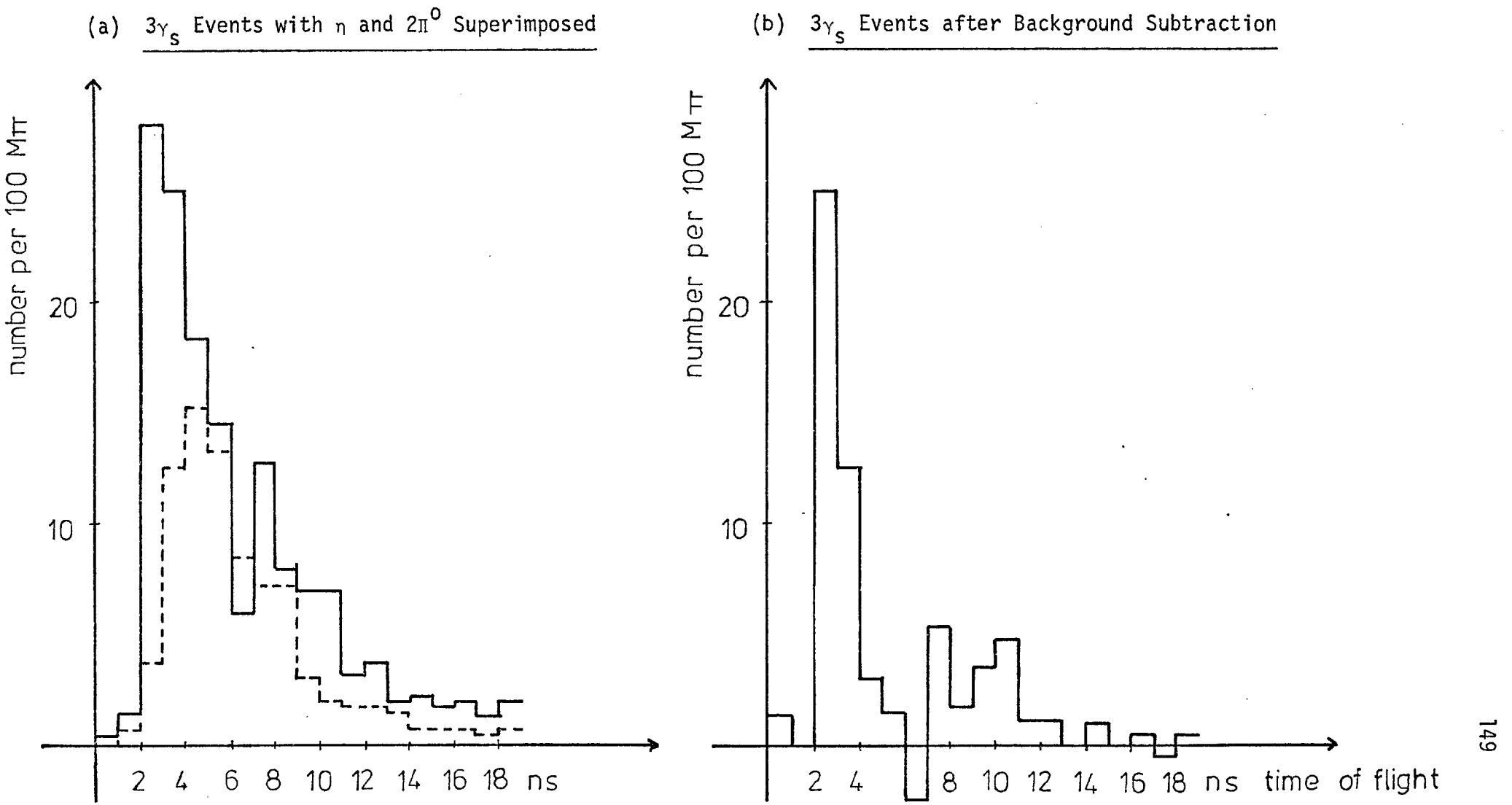
(a) $3\gamma_s$ Events with η and $2\pi^0$ Superimposed
(b) $3\gamma_s$ Events after Background Subtraction
number per 100 MeV
20
10
2 4 6 8 10 12 14 16 18 ns
2 4 8 10 12 14 16 18 ns time of flight

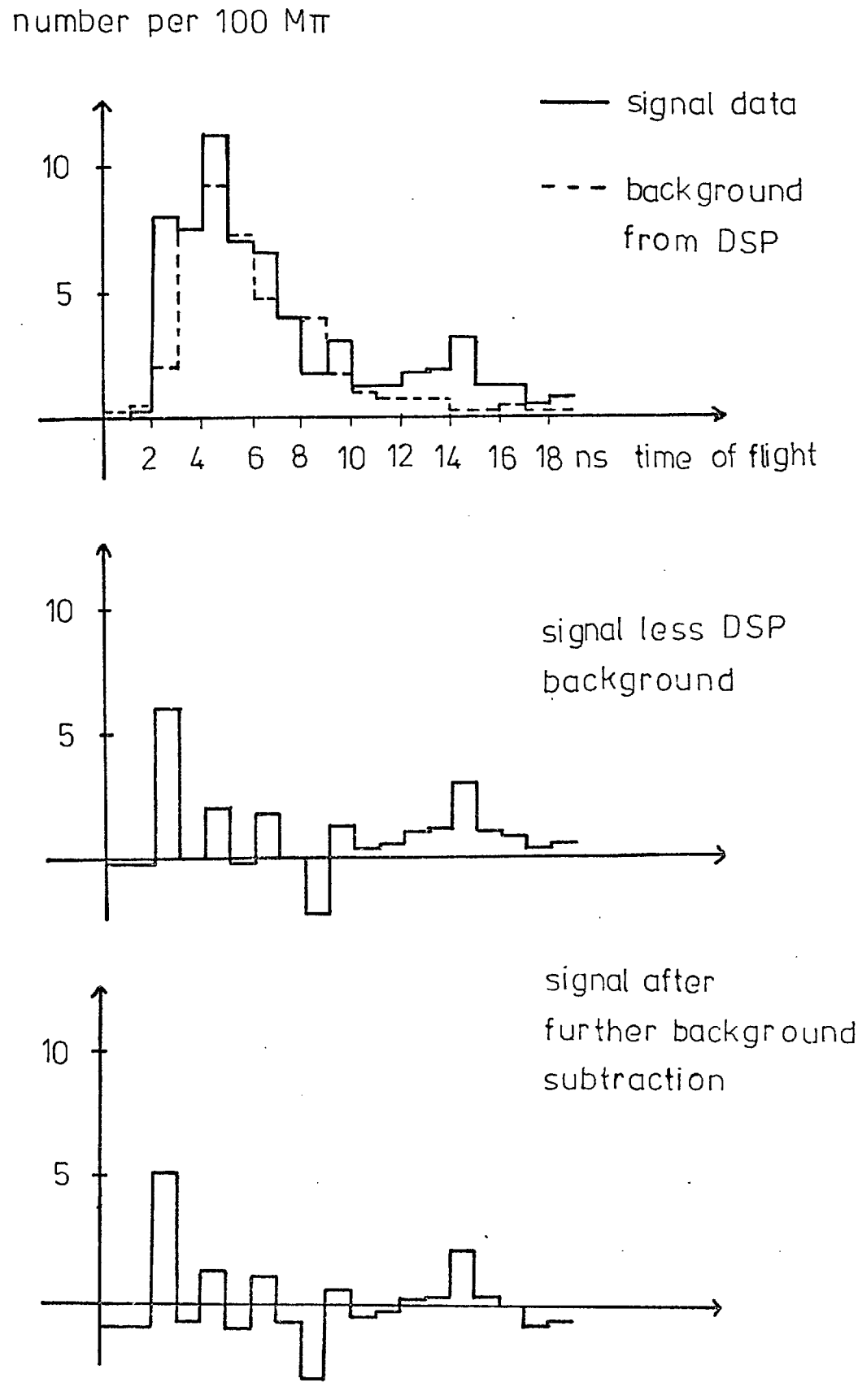

Figure 6.8

$\Pi^0\Pi^0\gamma$ Events in the $5\gamma_s$ and $4\gamma_s$ Channels

per 100 MΠ.

It was possible for another predicted decay mode of omega, that is $\eta\gamma$, to enter these two channels. This would, therefore, have reduced the actual amount of any signal seen that might have been attributed to the $\Pi^0\Pi^0\gamma$ mode. The upper limit of $\omega \rightarrow \Pi^0\Pi^0\gamma$ was then 0.7 events per 100 MΠ.

6.9 Conclusions

Making the assumption that the omega meson decayed only into the two modes $\Pi^+\Pi^-\Pi^0$ and $\Pi^0\gamma$, the respective branching ratios were $90.8 \pm 7.7\%$ and $9.2 \pm 2.9\%$ from the present experiment. Assuming only these two decay modes, the total amount of omega seen was 660 ± 100 events per 100 MΠ. This was equivalent to a cross section of 780 ± 120 μb, which is shown on a cross section versus p* graph from various other omega experiments in Fig. (6.9).

The best world values[32] for the decay of the omega meson were :

$\Pi^+\Pi^-\Pi^0$	89.7 ± 4.0 %
$\Pi^0\gamma$	9.0 ± 1.0 %
$\Pi^+\Pi^-\gamma$	< 5 %
$\Pi^0\Pi^0\gamma$	< 1 %
η + neutrals	< 1.5%
$\Pi^+\Pi^-$	1.2 ± 0.3 %
$\mu^+\mu^-$	< 0.02%
$\Pi^0\mu^+\mu^-$	< 0.2%

In this experiment, an upper limit of 0.7 events of $\omega \rightarrow \Pi^0\Pi^0\gamma$ were observed which gave an upper limit of 1.0%. If the value of 1.2% was assumed for the $\Pi^+\Pi^-$ decay mode, the branching ratios of the principal decay modes would then have been 89.8% and 9.1%.

The good agreement between the branching ratios of the two principal

Figure 6.9

Omega Cross Sections

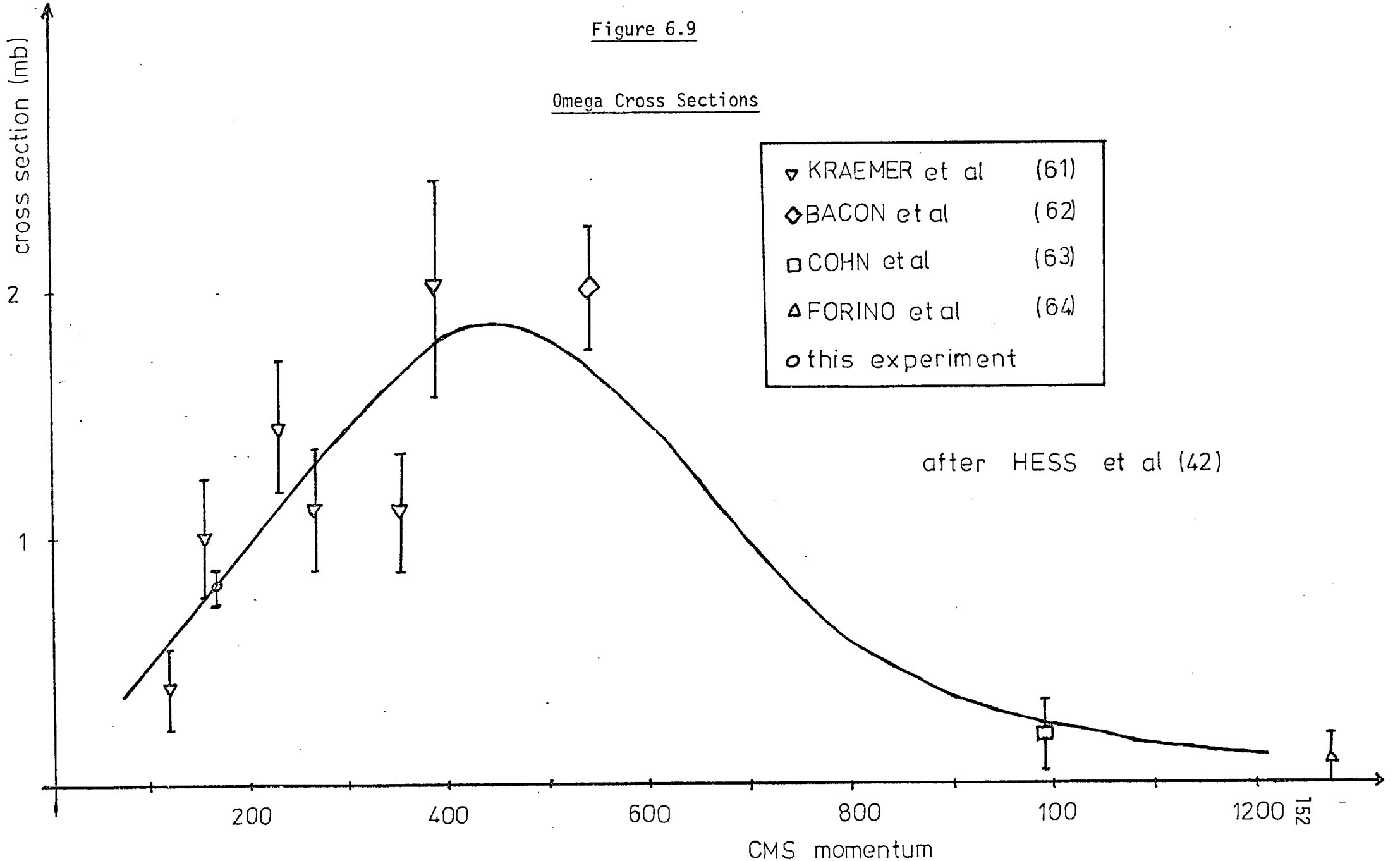

decay modes of omega and the best world values was a clear indication of the reliability of the decay detection system used and a justification of the experimental tests of the equipment and their interpretation and implementation into the decay simulation program.

The two main decay modes of omega have been studied many times. The more recent measurements obtained are shown in the table in Fig. (6.10).

The decay of omega into just two charged pions has caused problems in measurement due to omega-rho interference. No information could be added to the literature[55-60] from the present work. Various upper and lower limits have been assessed by experimenters and the best world value is given above.

A large number of measurements of the ratio of neutrals to $\pi^+\pi^-\pi^0$ have been made, the best world value being 10.43 ± 0.91[32] together with measurements of neutrals to total omega. These measurements have concentrated on experiments that did not count the gammas. Jacquet et al[52] measured $\pi^0\gamma/\ \pi^+\pi^-\pi^0$ and obtained $13.0 \pm 4.0\%$ and Deinet et al[41] measured $\pi^0\gamma$/neutrals as >81%. Consequently, there was some interest in the percentage of the neutral decay mode found to be due to other sources. Barmin et al[37] obtained an upper limit of 10% for $\pi^0\pi^0\gamma/\pi^0\gamma$, Deinet et al 19% for $\pi^0\pi^0\gamma$/neutrals and Jacquet et al[38] 8% for $\pi^0\pi^0\gamma/\pi^+\pi^-\pi^0$. A measurement by Strugalski et al[39] cast some doubt on the situation when they obtained the branching ratio of $\pi^0\pi^0\gamma$ to $\pi^0\gamma$ of $45 \pm 33\%$ and $\eta\gamma$ to $\pi^0\gamma$ of $58 \pm 30\%$. This raised the possibility that the branching ratio of omega to $\pi^0\gamma$ was less than 5%.

This experiment was able to identify the individual gammas present. The fact that an upper limit of 1.0% was found for the $\pi^0\pi^0\gamma$ decay mode of omega as against an observed branching ratio of $9.0 \pm 1.0\%$ for $\pi^0\gamma$ reinforced the belief that the neutral decay of omega was very largely $\pi^0\gamma$.

Figure 6.10

Table of Experimental Results for Omega

Author	Ref	Date	Experimental Result		
ARMENTEROS	44	1963	neutrals/$\pi^+\pi^-\pi^0$	=	17 ± 4 %
BUSCHBECK	45	1963		=	11 ± 2 %
KRAEMER	46	1964		=	8 ± 3 %
MILLER	47	1965		=	13.0 ± 3.5%
JAMES	48	1966		=	$6 \begin{smallmatrix}+5\\-2\end{smallmatrix}$ %
FLATTÉ	40	1966		=	9.7 ± 1.6%
ALFF	49	1966		=	9.9 ± 4 %
DI GIUGNO	51	1966		=	13.4 ± 2.6 %
BARASH	50	1967		=	10 ± 3 %
FELDMAN	53	1967	neutrals/total	=	12.4 ± 2.1 %
BOLLINI	43	1968		=	8.4 ± 1.5 %
DEINET	41	1969		=	7.9 ± 1.9 %
BOYD	36	1968	$\pi^+\pi^-\pi^0$/total	=	0.840 ± 0.016 %
BARMIN	28	1963	$\pi^0\gamma/\pi^+\pi^-\pi^0$	>	12.5 ± 2.4 %
JACQUET	52	1969		=	13 ± 4 %
DEINET	41	1969	$\pi^0\gamma$ /neutrals	>	81 %
JACQUET	38	1969	$\pi^0\pi^0\gamma/\ \pi^+\pi^-\pi^0$	<	8 %
STRUGALSKI	39	1969	$\pi^0\pi^0\gamma/\ \pi^0\gamma$	=	45 ± 33 %
BARMIN	37	1969	$\pi\ \pi$	<	10 %
DEINET	41	1969	$\pi^0\pi^0\gamma$ /neutrals	<	19 %
FLATTÉ	40	1966	$\eta\gamma/\pi^+\pi^-\pi^0$	<	1.7 %
JACQUET	38	1969		<	4.5 %
DEINET	41	1969	$\eta\gamma$ /neutrals	<	24 %
STRUGALSKI	39	1969	$\eta\gamma \rightarrow 3\gamma/\pi^0\gamma$	=	22 ± 11 %
FLATTÉ	40	1966	$\eta\pi^0/\pi^+\pi^-\pi^0$	<	1.7 %

ACKNOWLEDGEMENTS

I wish to thank Professor C.C. Butler for the opportunity of carrying out research as a member of the High Energy Nuclear Physics group at Imperial College of Science and Technology.

I would also like to acknowledge the early yet considerable encouragement and help given to me by the late Mr. A. Newth and also Dr. J. Walters. I am most grateful indeed to my supervisor, Dr. D.M. Binnie, for his encouragement and guidance throughout.

Many thanks are also due to my colleagues : Dr. A.R. Faruqi, Dr. D.A. Garbutt, Dr. W.G. Jones, Dr. M. Lewis, Mr. P.J. Nicholson, Dr. P.N. Upadhyay and Dr. J.G. Wilson at Imperial College; Dr. I.F. Burton, Dr. M.M. Haque, Dr. J.G. McEwen and their colleagues at the University of Southampton and Mr. R.J. Gray at the Rutherford Laboratory. I would especially like to thank my colleague, Mr. A. Duane of Imperial College, for his especially valuable assistance and many valuable discussions.

I am also indebted to the very considerable technical skill of Mr. D. Miller, Mr. R.F. Hobbs and Mr. D.J. Scholes, who constructed the decay system with great care and skill. Thanks are also due to the staff of the Rutherford Laboratory for their assistance throughout. I am also very grateful for the technical help of Mrs. Henneforth (née Koch) in much of the analysis of the thesis. I am deeply indebted to Miss Linda Jones for her patience and skill in typing this thesis.

For financial support during the period 1965 to 1968, I have to thank the Science Research Council.

REFERENCES

1. GOLDSCHMIDT-CLERMONT, CERN, D. PH.II, Physics, 67-32 (1967).
2. J. YARWOOD, Atomic Physics (1958).
3. W. HEITLER, The Quantum Theory of Radiation (1954).
4. B. ROSSI, High Energy Particles (1952).
5. H.A. BETHE and W. HEITLER, Proc. Roy. Soc. A146, 83 (1934).
6. J.A. WHEELER and W.E. LAMB , Phys. Rev. 55, 858 (1939).
7. K.M. WATSON, Phys. Rev. 72, 1060 (1947).
8. A. BORSELLINO, Helv. Phys. Acta 20, 136 (1947).
9. V. VOTRUBA, Phys. Rev. 73, 1468 (1948).
10. B. ROSSI and K. GREISEN, Rev. Mod. Phys. 13, 240 (1941).
11. M. STEARNS, Phys. Rev. 76, 836 (1949).
12. W.E. BURCHAM, Nuclear Physics (1963).
13. S.C. CURRAN, Luminescence and the Scintillation Counter (1953).
14. A.R. FARUQI, private communication.
15. D.C. MASON, Ph.D. Thesis (1968).
16. E.N. LURCH, Fundamentals of Electronics (1963).
17. W.S.C. WILLIAMS, An Introduction to Elementary Particles (1961).
18. R.F. MOZLEY and F.C. SHOEMAKER, Rev. Sci. Instrum., 23, 569 (1952).
19. R.M. EISBERG, Fundamentals of Modern Physics (1961).
20. D.J.X. MONTGOMERY, Cosmic Ray Physics (1949).
21. L. KATZ and A.S. PENFOLD, Rev. Mod. Phys., 24, 28 (1952).
22. W.G. JONES, Ph.D. Thesis (1966).
23. W.G. JONES, D.M. BINNIE, A. DUANE, J.P. HORSEY, D.C. MASON, J.A. NEWTH, I.U. RAHMAN, J. WALTERS, N. HORWITZ, P. PALIT, Phys. Lett. 23, 597 (1966).
24. E. FLAMINIO, J.D. HANSEN, D.R.O. MORRISON, N. TOVEY, Cern/Hera 70 - 7 (1970).
25. M.M. HAQUE and G. McEWEN, private communication.

26. L. BERTANZA, P.L. CONNOLLY, B.B. CULWICK, F.R. EISLER, T. MORRIS, R. PALMER, A. PRODELL, N.P. SAMIOS, Phys. Rev.Lett. 8, 332 (1962).

27. J.A. ANDERSON, F.S. CRAWFORD, J.C. DOYLE, Phys. Rev. 152, 1139 (1966).

28. V.V. BARMIN, A.G. DOLGOLENKO, Yu. S. KRESTINOV, A.G. MESHKOVSKY, Yu. P. NIKITIN, V.A. SHEBANOV, Phys. Lett. 6, 279 (1963).

29. BRISSON, 45, Aix-En-Provence Internation Conference on Elementary Particles (1963).

30. PETER, University of California, Berkeley, 11576 (1964).

31. C.B. CHIU, R.D. EANDI, A.C. HELMHOLZ, R.W. KENNEDY, B.J. MOYER, J.A. POIRIER, W.B. RICHARDS, R.J. CENCE, V.Z. PETERSON, N.K. SEHGAL, V.J. STENGER, Phys. Rev. 156, 1415 (1967).

32. A. RITTENBERG, A. BARBARO-GALTIERI, T. LASINSKI, A. ROSENFELD, T. TRIPPE, M. ROOS, C. BRICMAN, P. SÖDING, N. BARASH-SCHMIDT, C. WOHL, Rev. Mod. Phys. 43, 2, II (1971).

33. T. BINFORD, M. GOOD, V. LIND, D. STERN, R. KRAUSS, E. DETTMAN, Phys. Rev. 183, 1134 (1969).

34. O. VAN DYCK, R. BLUMENTHAL, S. FRANKEL, V. HIGHLAND, J. NAGY, T. SLOAN, M. TAKATS, W. WALES, R. WERBECK, Phys. Rev. Lett. 23, 50 (1969).

35. J. KEREN, Phys. Rev. 133, 8457 (1964).

36. J. BOYD, A. ERWIN, W. WALKER, E. WEST, Phys. Rev. 166, 1458 (1968).

37. V. BARMIN, A. DOLGOLENKO, Yu. S. KRESTNIKOV, A. MESHKOVSKY, Yu. P. NIKITIN, V. SHEBANOV, Sov. Phys. Jetp. 18, 5, 1289 (1964).

38. F. JACQUET, U. NGUYEN-KHAC, A. HAATUFT, A. HALSTEINSLID, Nuovo Cim., 63A, 743 (1969).

39. Z. STRUGALSKI, I. CHUVILO, I. IVANOVSKAYA, Z. JABLONSKI, T. KANAREK, L. OKHRIMENKO, E. FENYVES, T. GEMESY, S. KRASNOVSKY, G. PINTER, Phys. Lett., 29B, 8, 532 (1969).

40. S. FLATTÉ, D. HUWE, J. MURRAY, J. BUTTON-SHAFER, F. SOLMITZ, M. STEVENSON, C. WOHL, Phys. Rev. 145, 1050 (1966).

41. W. DEINET, A. MENZIONE, H. MÜLLER, H. STAUDENMAIER, S. BUNIATOV, D. SCHMITT, Phys. Lett. 30B, 426 (1969).

42. R.I. HESS, O.I. DAHL, L.M. HARDY, J. KIRZ, D.H. MILLER, Phys. Rev. Lett. 17, 1109 (1966).

43. D. BOLLINI, A. BUHLER-BROGLIN, P. DALPIAZ, T. MASSAM, F. NAVACH, F. NAVARRIA, M. SCHNEEGANS, A. ZICHICHI, Nuovo Cim. 56A, 531 (1968).

44. R. ARMENTEROS, D. EDWARDS, T. JACOBSEN, A. SHAPIRA, J. VANDERMEULEN, CH. D'ANDLAU, A. ASTIER, P. BAILLON, H. BRIAND, J. COHEN-GANOUNA, C. DEFOIX, J. SIAUD, C. CHESQUIÈRE, P. RIVET, Proc. Int. Conf. on Elementary Particles, Sienna, 1, 296 (1963).

45. B. BUSCHBECK-CZAPP, I. WALEK, W. COOPER, A. FRIDMAN, E. MALAMUD, G. OTTER, E. GELSEMA, A. TENNER, Proc. Int. Conf. on Elementary Particles, Sienna, 1, 166 (1963).

46. R. KRAEMER, L. MADANSKY, M. MEER, M. NUSSBAUM, A. PEVSNER, C. RICHARDSON, R. STRAND, R. ZDANIS, T. FIELDS, S. ORENSTEIT, T. TOOTIG, Phys. Rev. 136B, 496 (1964).

47. D. MILLER, Ph.D. Thesis (1965).

48. F. JAMES, H. KRAYBILL, Phys. Rev. 142, 896, (1966).

49. C. ALFF-STEINBERGER, D. BERLEY, D. COLLEY, N. GELFAND, U. NAUENBERG, D. MILLER, J. SCHULTZ, J. STEINBERGER, T. TAN, H. BRUGGER, P. KRAMER, R. PLANO, Phys. Rev. 145, 1072 (1966).

50. N. BARASH, L. KIRSCH, D. MILLER, T. TAN, Phys. Rev. 156, 1399 (1967).

51. G. DI GIUGNO, I. PERUZZI, G. TROISE, F. VANOLI, M. GIORGI, P. SCHIAVON, V. SILVESTRINI, Nuovo Cim. 44A, 1272 (1966).

52. F. JACQUET, V. NGUYEN-KHAC, C. BAGLIN, A. BEZAGUET, B. DEGRANGE, R. KURZ, P. MUSSETT, A. HAATUFT, A. HALSTEINLID, J. OLSEN, Int. Conf. on Elementary Particles, Heidelberg (1967).

53. M. FELDMANN, W. FRATI, R. GLEESON, J. HALPERN, M. NUSSBAUM, S. RICHERT, Phys. Rev. 159, 1219 (1967).

54. R. BIZZARRI, L. MONTANET, S. NILSSON, C.H. D'ANDLAU, J. COHEN-GANOUNA, Nucl. Phys. B27, 140 (1970).

55. G. GOLDHABER, W. BUTLER, D. COYNE, B. HALL, J. MACNAUGHTON, G. TRILLING, Phys. Rev. Lett. 23, 1351 (1969).

56. W. ALLISON, W. COOPER, T. FIELDS, D. RHINES, Phys. Rev. Lett. 24, 618 (1970).

57. P. BIGGS, R. CLIFFT, E. GABATHULER, P. KITCHING, R. RAND, Phys. Rev. Lett. 24, 1201 (1970).

58. S. HAGOPIAN, V. HAGOPIAN, E. BOGART, W. SELOVE, Phys. Rev. Lett. 25, 1050, (1970).

59. S.M. FLATTÉ, Phys. Rev. D, 1, 1 (1970).

60. R. BIZZARRI, G. CIAPETTI, U. DORE, M. GASPERO, P. GUIDONI, I. LAAKSO, F. MARZANO, G.C. MONETI, L. GRAY, P. HAGERTY, T. KALOGEROPOULOS, Phys. Rev. Lett. 25, 1385 (1970).

61. R. KRAEMER, L. MADANSKY, M. MEER, M. NUSSBAUM, A. PEVSNER, C. RICHARDSON, R. STRAND, R. ZDANIS, T. FIELDS, S. ORENSTEIN, T. TOOHIG, Phys. Rev. 136B, 496 (1964).

62. T. BACON, Proc. Conf. on Resonant Particles, Athens, 129 (1965).

63. H.O. COHN, R.D. McCULLOCH, W.M. BUGG, G.T. CONDO, Nucl. Phys. B1, 57 (1967).

64. A. FORINO, R. GESSAROLI, L. LENDINARA, C. QUARENI, A. QUARENI-VIGNUDELLI, N. ARMENISE, B. GHIDINI, M. DELLA CORTÉ, G. DICAPORIACO, J. LABERRIGUE-FROLOW, N.H. KHANH, J. QUINQUART, M. SENÉ, W. FICKINGER, O. GOUSSU, Phys. Lett. 19, 68 (1965).